Replicative aging impedes stress-induced assembly of a key human protein disaggregase

Authors: Yasith Mathangasinghe[1]†, Niels Alberts[1,2]†, Carlos J. Rosado[3], Dezerae Cox[4], Natalie L. Payne[1], Angelique R. Ormsby[4], Keziban Merve Alp[5], Roman Sakson[6], Sanjeev Uthishtran[7], Thomas Ruppert[8], Senthil Arumugam[7,9,10], Danny M. Hatters[4], Harm H. Kampinga[2] and Nadinath B. Nillegoda[1,11]*

Affiliations

[1]Australian Regenerative Medicine Institute, Monash University, Clayton, Victoria, Australia.

[2]Department of Biomedical Sciences of Cells & Systems, University Medical Center Groningen (UMCG) and University of Groningen (RuG), Groningen, The Netherlands.

[3]Department of Diabetes, Central Clinical School, Monash University, Melbourne, Victoria, Australia.

[4]Department of Biochemistry and Pharmacology, Bio21 Molecular Science and Biotechnology Institute, The University of Melbourne, Melbourne, Victoria, Australia.

[5]Max Delbrück Center for Molecular Medicine in the Helmholtz Association, Berlin, Germany.

[6]Leibniz-Institut für Analytische Wissenschaften-ISAS-e.V., Dortmund, Germany.

[7]Monash Biomedicine Discovery Institute, Monash University, Melbourne, Victoria, Australia.

[8]Core facility for Mass Spectrometry and Proteomics, Zentrum für Molekulare Biologie der Universität Heidelberg, Heidelberg, Germany.

[9]European Molecular Biological Laboratory Australia (EMBL Australia), Monash

27 University, Melbourne, Victoria, Australia

28 [10]Australian Research Council Centre of Excellence for Advanced Molecular

29 Imaging, Monash University, Clayton, Victoria, Australia

30 [11]Centre for Dementia and Brain Repair at the Australian Regenerative Medicine

31 Institute, Monash University, Melbourne, Victoria, Australia

32

33 † These authors contributed equally to this work

34 *Corresponding author. Email: nadinath.nillegoda@monash.edu

35

Abstract

The collapse of protein homeostasis manifests itself in a toxic protein aggregation cascade, which is associated with degenerative diseases and aging. To solubilize aggregates, dedicated protein disaggregases exist in unicellular organisms, but these have no nuclear/cytosolic orthologs in metazoa. Alternative metazoan disaggregation machines have been described, but how these are operated and regulated *in vivo* remained unknown. We show that protein disaggregases are functionally diversified in human cells to efficiently target different types of stress-induced aggregates in sequential and temporally distinct phases. In particular, we show the selective assembly of an Hsp70-DNAJA1-DNAJB1 trimeric disaggregase that forms during late phase of stress recovery., *i.e.*, after VCP-dependent solubilization of non-native proteins that accumulate in cellular condensates such as nucleoli or stress granules. When activated, the trimeric disaggregase provides resistance to stress toxicity and contributes to amyloid disposal. Strikingly, this disaggregase collapses early in cells undergoing replicative aging with important underlining pathophysiological consequences.

Keywords

Protein disaggregation, cellular aging, senescence, heat shock, Hsp70, J-domain proteins, VCP, amyloid

Main

The collapse of protein homeostasis and the increase in protein aggregation are closely associated with aging and many age-related diseases.[1,2] Healthy cells maintain protein homeostasis by an elaborate protein quality control (PQC) network that supports the proper flux of protein biogenesis (protein synthesis, folding, transport) to protein degradation. Thereby, protein function is ensured, and the accumulation of potentially toxic misfolded or aggregated proteins is prevented. However, these PQC pathways can be overwhelmed by acute

62 or chronic proteotoxic stresses, resulting in the accumulation of toxic protein aggregates that
63 could trigger cell death. Cells have evolved survival mechanisms to reverse such deleterious
64 effects of protein aggregation through protein disaggregation function.[3,4] Previous studies show
65 that the disruption of protein disaggregation function significantly decreases cell fitness and
66 organismal lifespan.[5-8]
67
68 The machinery that performs aggregate solubilization is well understood in unicellular
69 organisms (e.g., bacteria and fungi),[9] where AAA+ ATPases of the Hsp100 class of chaperones
70 (e.g., bacterial ClpB; yeast Hsp104) use a threading mechanism to untangle and release
71 aggregate-trapped polypeptides.[9-11] Metazoans lack cytosolic/nuclear Hsp100 disaggregases
72 and instead appear to have evolved aggregate solubilization machines based on Hsp70.[12]
73 Evidence for metazoan protein disaggregation is provided by proof-of-principle biochemical
74 studies showing the disassembly of artificially formed protein aggregates by reconstituted
75 disaggregases with different Hsp70s and J-domain proteins (JDP).[12-15] *In vivo* evidence is,
76 however, limited to observational data showing the disappearance of aggregated proteins,[7,16]
77 reactivation of stress-insolubilized model proteins,[17,18] and large-scale proteomics studies that
78 monitored proteome solubility dynamics after proteotoxic stress insults.[19,20] Although the
79 induction of molecular chaperones including various Hsp70s and JDPs and the state of
80 thermotolerance correlate with stress-induced aggregate disappearance,[7,21] direct visualization
81 of the assembly of functional Hsp70-based disaggregase complexes in metazoan cells has not
82 been achieved. This aspect is challenging due to the unavailability of approaches that
83 disentangle the effects of Hsp70 machineries that prevent protein aggregation (e.g., holdase
84 and foldase) from possible disaggregase function.
85
86 Here, we used a protein-protein interaction-based method to track the complete assembly of a
87 major disaggregase consisting of a trimeric Hsp70-DNAJA1-DNAJB1 complex on

88 endogenous protein aggregates, which, for the first time, allowed us to dissect how aggregate
89 solubilization is activated and regulated during repair of human cells after proteotoxic stress in
90 space and time. Strikingly, the assembly of this trimeric disaggregase occurs in the late phase
91 of stress recovery, sequential to and dependent on the resolubilization of stress-unfolded
92 proteins from biomolecular condensates (nucleoli and stress granules). Resolubilization of
93 condensates during the early phase of stress recovery is dependent on the action of another
94 mammalian disaggregase, the AAA+ ATPase Valosin-Containing Protein (VCP).[22-24] The two
95 distinct disaggregases act on substrates with different solubility properties. Importantly, the
96 late-acting Hsp70-DNAJA1-DNAJB1 trimeric disaggregase is crucial to stress tolerance and
97 enhances the capacity of the cell to dispose of amyloid-type aggregates. Importantly, we show
98 that activation of this Hsp70 disaggregase is severely hampered in human cells that undergo
99 replicative aging, which correlates with increased occurrences of pathological protein
100 aggregation. These findings establish previously unresolved critical crossing points for protein
101 disaggregation, cell repair, and senescence.
102

103 **Heat shock triggers selective assembly of the Hsp70-DNAJA1-DNAJB1 trimeric**
104 **chaperone complex**

105 Previously, we tested the ability of four human class A and B JDP proteins in ten different
106 configurations to assist Hsp70 (HSPA8) in solubilizing preformed aggregates of firefly
107 luciferase biochemically (Supplementary Data Fig. 1a).[12] A synergistic increase in
108 disaggregation and refolding of aggregated luciferase was observed only for those JDP
109 members that could form interclass JDP complexes with Hsp70 (Supplementary Data Fig. 1b),
110 consistent with previous findings.[12] The Hsp110 cochaperone, which functions primarily as a
111 nucleotide exchange factor (NEF) for Hsp70, was added to reactions to power protein
112 disaggregation efficiency.[25]
113

114 Next, we optimized and used the *in situ* proximity ligation assay (PLA)[14,26] to trace the
115 assembly of trimeric Hsp70 disaggregases in human cells (Fig. 1a). After signal amplification,
116 six intra- and interclass JDP assemblies could be detected in unstressed (U) HeLa cells, albeit
117 at low frequencies (yellow, false-colored puncta; Fig. 1b; Supplementary Data Fig. 2a).
118 Controls consisting of only one of the JDP-specific primary antibodies did not generate
119 fluorescent puncta (Supplementary Data Fig. 2b). The specificity of the interaction was further
120 confirmed by depleting the JDP members using RNAi, which strongly decreased the PLA
121 signal (Supplementary Data Fig. 2c, d). To induce protein aggregation, we next applied a
122 proteotoxic stress using a 60 min heat shock (HS) at 43°C (Supplementary Data Fig. 2e). This
123 led to a significant increase in the assembly of the DNAJA1-DNAJB1 scaffolds, exclusively
124 (Fig. 1b; Supplementary Data Fig. 2a). We also observed an increase in the interaction between
125 Hsp70 and the two JDPs on a very similar time scale (Fig. 1c). A mutant of DNAJB1
126 ($DNAJB1^{RRR}$; RRR denotes D4R, E69R, and E70R) that we previously identified as defective
127 in interacting with class A JDPs for disaggregase function *in vitro*,[12] but fully active in assisting
128 other functions of Hsp70 (e.g., refolding of heat-denatured luciferase[12] and capable of shuttling
129 into and out of nucleoli during resolution of heat-denatured proteins (Supplementary Data Fig.
130 3a)),[27-29] showed a strong decrease in PLA foci formation (Supplementary Data Fig. 3b). A
131 similar observation was made for a DNAJB1 mutant with a disrupted HPD motif
132 ($DNAJB1^{H32Q}$) that cannot bind to Hsp70 (Supplementary Data Fig. 3c).[30] Together these data
133 indicate that PLA captures direct interactions between specific JDPs and Hsp70s that appear to
134 assemble a trimeric chaperone complex in cells with the same configuration as the
135 biochemically identified Hsp70-DNAJA1-DNAJB1 disaggregase complex (Supplementary
136 Data Fig. 1b). Disassembly of this trimeric chaperone complex to the basal levels occurred
137 within 24h after HS (Fig. 1b, c). Disassembly was delayed in cells that were simultaneously
138 depleted of all three Hsp110-type NEFs that were previously described to specifically increase
139 the efficacy of protein disaggregation, *in vitro*.[25] Depleting other types of NEFs such as BAG1

140 and HSPBP1 had no effect (Supplementary Data Fig. 4a, b). This further suggests that the
141 activity of Hsp70-DNAJA1-DNAJB1 complex is related to disaggregase function in cells. The
142 scaffold was also assembled upon relatively mild temperature elevations that resemble mild-
143 moderate fever (37 °C to 39 °C) although to a lesser degree and shorter induction time (Fig.
144 1d; Supplementary Data Fig. 4c), supporting its physiological relevance.
145

146 **The late induction of Hsp70-DNAJA1-DNAJB1 disaggregase is geared to specifically**
147 **target a distinct population of aggregates in human cells**

148 The delayed induction of the Hsp70-DNAJA1-DNAJB1 trimeric complex during stress
149 recovery (which peaked approximately at 6h post-HS) (Fig. 1b) was puzzling because heat-
150 induced aggregate formation (measured as the appearance of denatured protein containing foci
151 or insoluble detergent protein material) occurs almost immediately in cells. Many of these
152 initial aggregating proteins are associated with or sequestered in biomolecular condensates
153 such as nucleoli and stress granules (SG).[27-29,31] Furthermore, the majority of detergent-
154 insoluble material and condensates were found to disappear before the first 6 hours after HS
155 (Supplementary Data Fig. 5a,b)[27,28,31,32], *i.e.*, before the trimeric Hsp70-DNAJA1-DNAJB1
156 complex peaks in its assembly. Thus, the late induction of this complex might be functionally
157 unrelated to the disassembly of these aggregated/ condensated proteins induced by HS.
158 Therefore, we hypothesized that this trimeric Hsp70 disaggregase might be performing a
159 unique task, perhaps targeting a different population of aggregated protein species, different
160 from condensates that escape the early clearance phase. To detect whether such escaping
161 aggregated species exist in human cells, we expressed the catalytically inactive yeast Hsp104
162 (E285Q, E687Q Double Walker B) tagged with GFP ($Hsp104^{DWB}$-GFP) which decorates
163 stress-induced aggregates.[33] $Hsp104^{DWB}$-GFP showed a diffuse fluorescent GFP signal in
164 unstressed cells (cyan, false-colored; Fig. 1e; Supplementary Data Fig. 6a). Immediately after
165 HS, fluorescent puncta (white arrows), denoting aggregates, emerged predominantly in the

166 cytosol (Supplementary Data Fig. 6a). Notably, no enrichment of Hsp104^{DWB}-GFP positive
167 puncta was detected in nucleoli containing stress-induced condensates immediately after HS.
168 At 6h after HS recovery, the number of Hsp104^{DWB}-GFP positive aggregates increased in
169 number and became more compact in appearance in cells. However, 24h after stress recovery,
170 these aggregates were completely resolved (Fig. 1e; Supplementary Data Fig. 6a). The
171 prevalence of Hsp104^{DWB}-GFP positive aggregates was consistent with the timing of the
172 assembly and disassembly of the Hsp70-DNAJA1-DNAJB1 complexes. To further test
173 whether Hsp104^{DWB}-GFP positive aggregates were targeted by the Hsp70-DNAJA1-DNAJB1
174 trimeric complex, we used VER-155008, a specific adenosine-derived small molecule inhibitor
175 of Hsp70.[34] VER-155008 significantly inhibited disaggregase activity mediated by Hsp70-
176 DNAJA1-DNAJB1, *in vitro* (Supplementary Data Fig. 6b). The addition of VER-155008 to
177 cells immediately after HS has been shown to block the early recovery of insoluble proteins
178 accumulated in nucleoli.[27,28] Therefore, to allow the completion of this recovery and
179 specifically inhibit the activity of the Hsp70-DNAJA1-DNAJB1 trimeric complex, we added
180 VER-155008 5h after HS. Treatment with VER-155008 completely blocked the disappearance
181 of Hsp104^{DWB}-GFP positive aggregates (Fig. 1e; Supplementary Data Fig. 6a). In line,
182 DNAJA1-DNAJB1 scaffolds also persisted up to 24h after HS (Supplementary Data Fig. 6a).
183 The presence of VER-155008 caused the PLA signal from DNAJA1 and DNAJB1 complex
184 formation (Fig. 1f) to strongly overlap with Hsp104^{DWB}-GFP positive foci (Mander's overlap
185 correlation coefficient (r) = 0.984), which is consistent with JDP scaffolds forming on
186 aggregate surfaces to drive the assembly of this trimeric Hsp70 disaggregase during protein
187 disaggregation. Washing out VER-155008 12h after HS led to re-initiation of Hsp104^{DWB}-GFP
188 positive aggregate resolution (Supplementary Data Fig. 7a, b). These results indicate that the
189 disassembly of Hsp104^{DWB}-GFP positive aggregates requires Hsp70 activity. The resolution of
190 the aggregates in the washed cells VER-155008 coincided with the disassembly of the
191 DNAJA1-DNAJB1 scaffolds (Supplementary Data Fig. 7c), suggesting that they help recruit

192 active Hsp70 to form disaggregases on the aggregates. To further test this hypothesis, we
193 expressed wildtype yeast Hsp104, which cooperates with the mammalian Hsp70 system to
194 form very potent disaggregases *in vitro* (Supplementary Data Fig. 8a) and *in vivo*,[35] in HeLa
195 cells. The frequency of DNAJA1-DNAJB1 scaffolds was strongly reduced in cells expressing
196 Hsp104-GFP 6h after HS (Supplementary Data Fig. 8b) due to a rapid decrease in aggregate
197 load (see below section; Supplementary Data Fig. 8c), indicating a functional redundancy
198 between Hsp104 and the trimeric Hsp70 disaggregase systems. Furthermore, the data
199 suggested that the presence of aggregates could also be a trigger for the assembly of DNAJA1-
200 DNAJB1 scaffolds.
201
202 Next, we used DNAJB1 mutants defective in assembling the trimeric complex to assess
203 whether JDP scaffolding is required to solubilize HS-induced Hsp104^{DWB}-GFP positive
204 aggregates. The *in vitro* disaggregation of heat aggregated luciferase was significantly reduced
205 in reactions containing DNAJB1^{RRR} and DNAJA1 (Supplementary Data Fig. 9a). Accordingly,
206 ectopically expressed DNAJB1^{RRR} in *DNAJB1* knocked out (KO) HEK 293 cells (confirmed
207 by immunoblotting; Fig. 1g) was unable to solubilize Hsp104^{DWB}-GFP positive aggregates
208 induced by HS compared to wild type DNAJB1 (Fig. 1h-j; Supplementary Data Fig. 9b-d). A
209 similar result was observed with DNAJB1$^{H32Q,\ D34N}$ (DNAJB1^{QPN}), which is defective in
210 binding to Hsp70. However, DNAJB1^{QPN} readily complexed with endogenous DNAJA1 after
211 HS (Fig. 1g, k), but these JDP scaffolds could not support disaggregation, presumably due to
212 the decreased ability to recruit Hsp70, and as a consequence prevented efficient aggregate
213 resolution in recovering cells (Fig. 1k, Supplementary Data Fig. 9c). Together, these findings
214 support that the Hsp70-DNAJA1-DNAJB1 trimeric complex represents a real, functional
215 disaggregase in mammalian cells, tentatively crucial for solubilizing a population of stress-
216 induced aggregates that are distinct from those accumulated in condensates.
217

218 To investigate whether the DNAJA1-DNAJB1 scaffold is interchangeable with other class A
219 and B members as observed in biochemically reconstituted systems (Supplementary Data Fig.
220 1),[12] we knocked down DNAJA1 or DNAJB1 in HeLa cells using RNAi, which, as expected,
221 decreased the assembly of the JDP scaffold after HS. However, knocking down DNAJA1 or
222 DNAJB1 did not result in the remaining unpaired partner complexing with other JDPs (e.g.,
223 DNAJB1 with DNAJA2 or DNAJA1 with DNAJB4) in cells (Supplementary Data Fig. 10a).
224 Thus, regardless of the expression and HS induction of other JDP paralogs (Supplementary
225 Data Fig. 10b) in mutual subcellular locations (Supplementary Data Fig. 11), this particular
226 Hsp70 disaggregase is cogged to assemble with DNAJA1 and DNAJB1 during the late phase
227 of stress recovery in human cells. In line with this, DNAJB1 activity could not be fully restored
228 in *DNAJB1* KO cells by overexpressing other JDPs tested (Supplementary Data Fig. 9e). These
229 data highlight the strict dependency on DNAJB1 for the functionality of this disaggregase. The
230 observations also indicate that single JDP-containing disaggregases described
231 biochemically[14,36-39] are ineffective in solubilizing this persisting fraction of heat-induced
232 aggregates in human cells.
233
234 To identify the protein composition of the aggregates targeted by Hsp70-DNAJA1-DNAJB1
235 disaggregase in HeLa cells, we applied a two-phase fractionation approach coupled to a
236 proteomic workflow (Supplementary Data Fig. 12a).[19] Data were agnostically clustered into
237 four different response patterns by k-means clustering (see Methods; Supplementary Data
238 Table 1). The proteins in cluster (iii) showed a pattern of aggregation and recovery that was
239 consistent with being potential substrates for this disaggregase activity. Specifically, they
240 appeared to show impaired solubility recovery after treatment with VER-155008 between 6
241 and 12 hours (Supplementary Data Fig. 12b, c). Approximately half of the hits in this cluster
242 included RNA-associated proteins (Supplementary Data Table 1). Two proteins in cluster (iii),
243 Heterogeneous nuclear ribonucleoprotein K (HNRNPK; solubility profile in Fig. 2a) and

244 Adenosylhomocysteinase (AHCY; solubility profile in Fig. 2b), were selected for further
245 analysis. Both HNRNPK and AHCY formed puncta that persisted at 6h after HS in HeLa cells,
246 but they were completely solubilized and redistributed to original subcellular locations at 12h
247 after stress recovery (Fig. 2c, d). The addition of VER-155008 (Fig. 2c, d; Supplementary Data
248 Fig. 12d) as well as the knocking down of DNAJA1 or DNAJB1 (Fig. 2e) prevented this
249 resolubilization. Fluorescent recovery after photobleaching (FRAP) analysis showed that the
250 HNRNPK puncta were immobile, suggesting tight protein packing in these aggregates
251 (Supplementary Data Fig. 12e). The formation of these HS-induced immobile HNRNPK
252 puncta was completely suppressed after expressing the yeast Hsp104 disaggregase
253 (Supplementary Data Fig. 8c). This explains the reduced assembly of the trimeric disaggregase
254 after HS in cells ectopically expressing Hsp104 (Supplementary Data Fig. 8b).
255
256 **Cellular heterogeneity in aggregate solubilization by sequentially activated Hsp70-**
257 **DNAJA1-DNAJB1 and VCP-based disaggregase systems**
258 The assembly and disassembly kinetics of the Hsp70-DNAJA1-DNAJB1 disaggregase and the
259 disaggregation of HNRNPK and AHCY are highly distinct from the recovery of protein
260 aggregates that accumulate in biomolecular condensates after HS. Though HNRNPK and TIA-
261 1 are both RNA-binding proteins, they sequestered into spatially distinct aggregates
262 (HNRNPK; cyan) and SGs (TIA-1; yellow) in the cytosol after HS (Fig. 2f). Compared to
263 HNRNPK aggregates, the disassembly of the TIA-1 SGs occurred rapidly within 6h after HS
264 and did not rely on Hsp70-DNAJA1-DNAJB1 disaggregase activity, as evident from VER-
265 155008 treatment and JDP knockdown experiments (Fig. 2f, g; Supplementary Data Fig. 13),
266 suggesting that these SGs are processed through a distinct nonoverlapping disaggregase
267 activity. We also noted the presence of a fraction of highly ubiquitinylated proteins that
268 immediately insolubilized, but rapidly resolved before 6h into recovery from HS
269 (Supplementary data Fig 5a, right panel). Recent findings show that AAA+ ATPase VCP (p97)

270 is not only recruited to ubiquitylated substrates, but is also required for their disaggregation in
271 cooperation with the ubiquitin proteasome machinery.[22-24] Furthermore, VCP was found to be
272 involved in SG clearance in mammalian cells.[40] To test whether VCP targets the heat-induced
273 Ub+ insolubilize protein fraction, we depleted the AAA+ ATPase using RNAi, which indeed
274 resulted in a considerable delay in resolving the Ub+ aggregated proteins (Fig. 3a) and TIA-1
275 SGs (Fig. 3b, c). Surprisingly, however, VCP depletion also delayed the solubilization of
276 HNRNPK and Hsp104^{DWB}-GFP positive aggregates (Fig. 3b, c; Supplementary Data Fig. 14a)
277 that largely lacked an Ub signature (Supplementary Data Fig. 14b). In line, the disassembly of
278 the Hsp70-DNAJA1-DNAJB1 disaggregase was also delayed after VCP knockdown
279 (Supplementary Data Fig. 14c). To test whether loss of VCP directly affected the action of
280 Hsp70 disaggregase or whether VCP itself also facilitated the resolution of non-condensate-
281 associated Hsp104^{DWB}-GFP positive aggregates, we treated cells with the VCP inhibitor NMS-
282 873[41] at 0h or 5h after HS. Adding NMS-873 at 0h post-HS triggered the same phenotype as
283 that of depleting VCP. However, blocking VCP function using a low (1 μM) or high (10 μM)
284 dose of NMS-873 5h after HS, *i.e.* after clearing of Ub+ aggregates, did not affect Hsp104^{DWB}-
285 GFP positive aggregate solubilization (Fig. 3d; Supplementary Data Fig. 14d). Consequently,
286 under this condition, the Hsp70-DNAJA1-DNAJB1 disaggregase disassembled back to basal
287 levels at 24h after HS (Fig. 3e). Inversely, increasing VCP levels did not affect the activation
288 of the Hsp70-DNAJA1-DNAJB1 disaggregase during stress recovery (Supplementary Data
289 Fig. 15), which is in stark contrast to observations made under overexpression of the yeast
290 Hsp104 disaggregase (Supplementary Data Fig. 8). These observations suggest that the
291 function of trimeric Hsp70 disaggregase cannot be compensated for by stimulating the function
292 of VCP in human cells. Together, these data describe for the first time how protein
293 disaggregation activity is organized into two phases (early and late) in living human cells
294 undergoing stress recovery. The stress-induced trimeric complex Hsp70-DNAJA1-DNAJB1
295 forms a crucial part of an integrated network of at least two distinct disaggregase systems that

296 function sequentially and in a non-redundant manner to target different populations of heat-
297 induced aggregated substrates.
298
299 **Regulation of Hsp70-DNAJA1-DNAJB1 disaggregase**
300 Next, we asked how the kinetics of these sequentially acting disaggregases are regulated by
301 stress signaling. VCP, which acts at the early phase of aggregate solubilization, is not induced
302 by proteotoxic stresses (Fig. 3a, left panel)[42] and knocking down its levels prior to heat stress
303 affects the disassembly of Ub+ aggregates/SGs (Fig. 3a,b). On the contrary, the Hsp70-
304 DNAJA1-DNAJB1 disaggregase, which shows low abundance in unstressed cells, is massively
305 induced after HS, indicating that this disaggregase is highly regulated. In HeLa cells, the peak
306 assembly of the DNAJA1-DNAJB1 scaffold (Fig. 1b), which initiates the assembly process
307 and provides specificity for this PQC machine, coincided with the highest expression of the
308 disaggregase components in protein (Supplementary Data Fig. 16a), but not mRNA levels
309 (Supplementary Data Fig. 16b). Induction of machine components after stress suggests that the
310 heat shock response (HSR) might modulate the formation of this disaggregase in repairing
311 cells. Knocking down the HSF-1 transcription factor, the central regulator of the HSR, inhibited
312 the synthesis of disaggregase components and reduced the assembly of the disaggregase
313 (Supplementary Data Fig. 16c) and subsequent resolution of its substrates (Supplementary Data
314 Fig. 16d; Supplementary Data Fig. 17a). In contrast, HSF-1 knockdown had no effect on the
315 VCP-dependent disassembly of TIA-1 SGs (Supplementary Data Fig. 17a) again highlighting
316 the nonoverlapping disaggregase activities of the two systems. Similar to HSF-1 depletion,
317 treatment of cells with the translational inhibitor cycloheximide (CHX) immediately after HS
318 also blocked the assembly of Hsp70-DNAJA1-DNAJB1 disaggregase (Supplementary Data
319 Fig. 17b). In contrast, HSF-1 depletion or CHX treatment did not affect the HS-induced
320 localization dynamics of pre-HS synthesized Hsp70s and JDPs (Supplementary Data Fig. 18;
321 Supplementary Data Fig. 19) coinciding with the extraction of denatured/aggregated proteins

322 from nucleoli SGs immediately after HS.[27-29] This implies that the late phase, but not the early
323 phase of aggregate solubilization is under tight transcriptional regulation. This regulation also
324 allows the assembly of spatially and temporally separated Hsp70 machines through pre- and
325 post-HS synthesized DNAJA1 and DNAJB1 molecules. In essence, this serves as a strategy to
326 efficiently organize different chaperone machines that cater to various cellular needs on a
327 priority basis, for example, to promote rapid recovery of proteins associated with translational
328 machinery crucial for immediate stress adaptation[43-46] followed by resolving persistent
329 aggregated protein junk to reduce downstream cytotoxicity.
330

331 **Physiological relevance of Hsp70-DNAJA1-DNAJB1 disaggregase: heat resistance,**
332 **replicative aging, and pathological protein aggregation**

333 To address the physiological relevance of the Hsp70-DNAJA1-DNAJB1 disaggregase, we first
334 evaluated the impact of its assembly on the fitness of human cells recovering from heat stress
335 using the lactate dehydrogenase (LDH)-Glo-based cytotoxicity assay (Supplementary Data
336 Fig. 20a). Again, VER-155008 was added after the completion of rapid recovery of heat-
337 denatured proteins from nucleoli immediately after HS.[29] The Hsp70-DNAJA1-DNAJB1
338 disaggregase activity inhibited HeLa cells (Supplementary Data Fig. 20b) showed increased
339 heat toxicity compared to control cells treated with DMSO (Supplementary Data Fig. 20c).
340 This shows that the resolution of aggregates escaping early clearance contributes significantly
341 to the cellular tolerance of acute proteotoxic stress.
342

343 To address whether the trimeric Hsp70-DNAJA1-DNAJB1 disaggregase also plays a role in
344 chronic stress conditions resulting from aging and age-related diseases, we first assessed its
345 assembly in six lines of primary dermal fibroblasts (HDF) derived from humans with ages
346 ranging from 21 to 75 years. We did not observe a substantial chronological age-driven
347 variation in the inducibility of Hsp70-DNAJA1-DNAJB1 disaggregase after HS in all

348 fibroblast lines tested (Fig. 4a; Supplementary Data Fig. 21a). Similar to immortalized HeLa
349 cells, primary dermal fibroblasts also only induced the DNAJA1-DNAJB1 scaffold after HS
350 (Supplementary Data Fig. 21b), underscoring that this assembly, with the same kinetics and
351 specific components, is also active in normal human diploid cells.
352
353 Recent work shows that during chronological aging, senescent cells resulting from replicative
354 aging accumulate progressively in various mammalian tissues.[47-49] Therefore, we evaluated
355 whether replicative aging has an effect on activating the Hsp70 disaggregase. Three of the
356 human dermal fibroblast lines (derived from 21-, 55-, and 75-year-old donors) were subjected
357 to replicative aging by *ex vivo* passaging (P) of cells up to 18 times (Fig. 4b, see Methods).
358 Senescence was detected using lysate-based SPiDER-Gal activity assay and direct cell staining
359 for senescence-specific β-galactosidases levels. Compared to non-senescent P 6 cells, cells in
360 P 12 showed a rise in the senescent signal, which increased further in P 18 cells in all lines,
361 regardless of the chronological age of the donor (Fig. 4c; Supplementary Data Fig. 21c, d).
362 Strikingly, the stress-induced assembly of Hsp70-DNAJA1-DNAJB1 disaggregase observed
363 in cells at P 3 or P 6 was completely absent in cells at P 12 and P 18 (Fig. 4d). Importantly, no
364 notable differences were observed in the heat inducibility of disaggregase components between
365 P 6 and P 12 cells (Fig. 4e). Consistently, HSR, which is reported to collapse in cells at late
366 senescence with permanent cell cycle arrest,[50,51] was still fully intact in still replicating P 12
367 cells, as indicated by robust induction of the HSF-1 dependent HSPA6 chaperone[52]
368 (Supplementary data Fig. 22a). This finding argues that additional pathways beyond the HSR
369 are required for the assembly of the Hsp70-DNAJA1-DNAJB1 disaggregase. Furthermore, as
370 in P 6 cells, P 12 cells also showed similar levels of heat-induced i) nuclear shuttling of ATF-
371 6 to activate the unfolded protein response of the endoplasmic reticulum (UPR_{ER})
372 (Supplementary Data Fig. 22b), and ii) proteasome activity (Supplementary Data Fig. 22c) that
373 decline in human cells at late senescence.[53] We also did not observe any decrease in VCP levels

374 in fibroblasts in P 6 vs P 12 (Supplementary Data Fig. 22a). Together, these intriguing findings
375 indicate that Hsp70-DNAJA1-DNAJB1 disaggregase is a PQC component that declines very
376 rapidly with replicative aging. The early decline of this disaggregase activity has functional
377 consequences as P 12 fibroblasts showed an inability to resolve heat-induced protein
378 aggregates (Supplementary Data Fig. 23a, b), showed reduced fitness after HS (Fig. 4f), and
379 contained aggregated proteins even under non-stressed conditions (Supplementary Data Fig.
380 23b), a hallmark of aging cells.
381
382 Replicative aging, which drives chronic senescence, has been implicated in the etiopathology
383 of several neurodegenerative diseases.[47] Therefore, we evaluated how impairment of this
384 Hsp70 disaggregase during replicative aging affects the aggregation of pathological proteins
385 associated with Huntington's disease (HD). Appearance of intracellular Huntingtin protein
386 (Htt) exon 1 containing expanded polyglutamine (polyQ) amyloid aggregates drives
387 neurotoxicity in HD.[2] These aggregates form in cells independent of proteotoxic stresses such
388 as HS (Supplementary Data Fig. 24a). Our findings showed that priming of Hsp70-DNAJA1-
389 DNAJB1 disaggregase assembly through HS reduced the accumulation of polyQ aggregates
390 (HttQ46-mEmGFP) in a Hsp70, DNAJA1, and DNAJB1 dependent manner in HeLa cells
391 (Supplementary information 1, Supplementary Data Fig. 24). Unlike HeLa cells, Htt46Q-
392 mEmGFP was largely soluble with only a mild aggregation phenotype in unstressed dermal
393 fibroblasts at P 6 and P 12 (Fig. 4g). However, after HS, the soluble Htt46Q-mEmGFP formed
394 into prominent aggregates (punctated cyan fluorescent signal, 6h after HS) in both P 6 and P
395 12 cells, which is in line with an acute overloading of the PQC pathways that prevents the
396 initiation of polyQ aggregation in stressed cells. Strikingly, these polyQ aggregates
397 subsequently disappeared in P 6, but not P 12 fibroblasts (Fig. 4g) that can activate the trimeric
398 Hsp70 disaggregase. These proof-of-principle findings unravel a critical breakdown of
399 amyloidogenesis suppression in cells undergoing senescence. Together, our data reveal that the

400 *in vivo* assembly of this Hsp70-DNAJA1-DNAJB1 trimeric chaperone complex vitally
401 contributes to cellular resistance to stress and declines rapidly during replicative aging with
402 putative relevance to disease-related amyloidosis.
403
404 **Discussion**
405 The critical role of recovery of aggregated proteins through Hsp100-based disaggregation
406 activity in unicellular organisms such as bacteria and yeast after heat stress has been widely
407 accepted.[54-56] Whilst metazoa lack cytosolic/nuclear Hsp100 disaggregases,[10] a number of
408 recent studies suggested that these organisms possess several functionally equivalent protein
409 disaggregase systems composed of different proteins with chaperone or chaperone-like
410 properties (e.g. Hsp70, VCP, and DAXX).[12,23,57] Importantly, however, it was not understood
411 how these different protein disaggregase systems are assembled (if at all) and regulated
412 similarly or differently in time and space in live cells exposed to protein aggregation stresses.
413 It was also not understood how these disaggregase systems are organized (if at all) in cells
414 during cell repair. Here, we describe for the first time how proteotoxic stress induces the
415 selective assembly of an *in vitro* identified Hsp70-based disaggregase with a specific DNAJA1
416 and DNAJB1 containing JDP scaffold in primary and immortalized human cells. We show that
417 this trimeric disaggregase operates in the late phase of aggregate solubilization sequentially to
418 the action of a VCP-based disaggregase. The early phase of aggregate solubilization is
419 predominated by the activity of VCP-based disaggregase. VCP largely depends on a Ub signal
420 to recognize its aggregates/SG components, but could also function independently of Ub to
421 disassemble some protein complexes.[58] Following the initial aggregate solubilization phase,
422 the trimeric Hsp70 disaggregase assembles on remaining aggregates. The data suggest that the
423 Hsp70 disaggregase is particularly effective in "mopping up" tightly packed solid-like
424 cytotoxic protein aggregates that were not sequestered into condensates (e.g., SG or nucleoli)
425 and hence escaped the early phase of clearance. Although the late phase depends on the

426 completion of the early phase, it does not require VCP. In terms of the fate of disaggregated
427 polypeptides, there is likely a culmination of protein recovery and degradation during both
428 phases.[59-62]
429
430 The two disaggregase systems affect resistance to cellular stress and appear to be associated
431 with age-associated human diseases. Recent work shows the ability of VCP to target tau
432 amyloids associated with Alzheimer's disease.[23] Genetic defects in VCP activity were found
433 to cause inclusion body myopathy associated with Paget's disease of the bone and front-
434 temporal dementia (FTD).[63] Additionally, VCP activity was reported to be important for
435 clearing stress granules,[40] and mutations in VCP alter SG dynamics closely linked to ALS and
436 FTD pathologies.[62] Our data show that assembly of the Hsp70-DNAJA1-DNAJB1
437 disaggregase also leads to resistance against acute (heat) stresses. Once induced, this trimeric
438 disaggregase is capable of targeting pathological amyloids (e.g., HttpolyQ amyloids associated
439 with HD).
440
441 Importantly, we show that the ability to assemble the Hsp70-DNAJA1-DNAJB1 disaggregase
442 is highly impaired during replicative aging that causes chronic senescence. Mechanistically,
443 the breakdown of this disaggregase activity is due to the inability to effectively assemble the
444 DNAJA1-DNAJB1 JDP scaffold. Importantly, our results revealed that the assembly of Hsp70-
445 DNAJA1-DNAJB1 disaggregase is impaired even before human cells undergoing replicative
446 aging lose several proteotoxic signaling routes, such as the HSR and the UPR_{ER}, which have
447 often been considered to precede the collapse of protein homeostasis upon aging.[53,64] This early
448 collapse could explain the accumulation of difficult-to-resolve aggregates in unstressed cells
449 (Supplementary Data Fig. 23b) and may act as a trigger that contributes to (rather than being
450 the result of) senescence, and thereby rapidly prevent damaged cells from propagation.
451 Interestingly, compared to human cells, non-metazoans such as budding yeast, modulate

452 protein disaggregation function entirely differently during replicative aging. Instead, yeast cells
453 that undergo senescence significantly enhance protein disaggregation function by inducing
454 Hsp104 disaggregase levels to counteract proteostasis defects[65] suggesting that stress-induced
455 protein disaggregation activity is wired differently in aging unicellular and multicellular
456 organisms.
457
458 The implications related to the inactivation of this PQC machine during replicative aging could
459 be significant. As we show, the assembly of this disaggregase already occurs at fever-like
460 temperatures (Fig. 1d). In cells already expressing a high load of aggregation-prone proteins,
461 this mild stress can trigger amyloidogenesis, as here exemplified in polyQ-expressing dermal
462 fibroblasts (Fig. 4g). If Hsp70-DNAJA1-DNAJB1 disaggregase activity is reduced, as we see
463 in cells undergoing replicative aging, these amyloids will not resolve and could lead to disease
464 progression. This may also contribute to the faster decline rates observed for processes
465 associated with aging in HD models and HD patients.[66] Collectively, our data show how
466 metazoa have evolved an intricate network of protein disaggregase machines that perform
467 different sequential tasks, all required to ensure cell resilience to acute and chronic stresses,
468 relevant to mammalian cellular aging and organismal health span.
469
470 **Figure Legends**
471 **Figure 1. The Hsp70-DNAJA1-DNAJB1 trimeric complex forms a heat-induced protein**
472 **disaggregase which targets aggregates that escape early clearance**. **a,** Detection of Hsp70-
473 JDP and JDP-JDP interactions during the assembly of Hsp70-DNAJA1-DNAJB1 trimeric
474 complex *in situ* through proximity ligation assay (PLA). Captured protein-protein interactions
475 generate fluorescent puncta (yellow) after signal amplification by rolling circle PCR.
476 Fluorescently labeled oligonucleotides hybridize with an amplified DNA bundle to enhance
477 the proximity signal. **b,** Top: Detection of multiple JDP^{A}-JDP^{B} scaffolds that support *in vitro*

478 Hsp70 disaggregase activity in unstressed (U) and heat shocked (HS, red) HeLa cells using
479 PLA. Upon HS, cells show selective induction of the DNAJA1-DNAJB1 scaffold (PLA
480 fluorescent signal, yellow). Nuclei stained with DAPI (magenta). HS was performed at 43 ° C
481 for 1h; Stress recovery at 37 ° C for 0h, 6h and 24h. Scale bar 20 µm (n = 3). Images are
482 maximum intensity projections (all channels). Bottom: Quantification of PLA signal from (data
483 are mean +/- s.e.m.; see supplementary methods for details). **c,** Top: PLA-based detection of
484 DNAJA1-Hsp70 and DNAJB1-Hsp70 interactions during the formation of Hsp70-DNAJA1-
485 DNAJB1 trimeric complex. The Hsp70 antibody used in PLA recognizes both constitutively
486 expressed Hsc70 (HAPA8) and the stress-induced Hsp70 paralog (HSPA1A). Scale bar 20 µm
487 (n = 3). Bottom: Quantification of PLA signal (data are mean +/- s.e.m.). **d,** Assembly of
488 DNAJA1-DNAJB1 scaffold at 39 ˚C *vs* 42 ˚C for 2h that mimic mild-moderate and high fever,
489 respectively. Quantification of PLA signals (data are mean +/- s.e.m.). **e,** Resolution of heat-
490 induced aggregates in cells +/- Hsp70 inhibitor VER-155008. Top: HS triggered the formation
491 and solubilization of Hsp104^{DWB}-GFP positive aggregates (cyan; punctated fluorescent signal
492 pointed by white arrows) in HeLa cells. U denotes unstressed cells. Heat shock (HS) in red.
493 Scale bar 20 µm (n = 3). Bottom: Visualization of assembly and disassembly of Hsp70
494 disaggregase through formation of the JDP scaffold (PLA; yellow) in HeLa cells recovering
495 from heat shock (HS). Nuclei in magenta. Scale bar 20 µm (n = 3). The inhibitor was added to
496 cells 5h after HS. Scale bar 20 µm (n = 3). DMSO, vehicle control for VER-155008.
497 **f,** Assembly of DNAJA1-DNAJB1 scaffolds (PLA, yellow, see Methods) on Hsp104^{DWB}-GFP
498 positive heat-induced aggregates (cyan) during HS recovery (37 ° C for 12h) in HeLa cells.
499 Inset shows zoomed in region of interest. Cells were treated with cycloheximide (CHX) at 3.5h
500 and VER-155008 at 5.5h after HS. Mander's coefficient (r) = 0.984 (s.e.m. = 0.004). Manders'
501 overlap correlation coefficients were calculated using thresholded images (n=5). Nuclei in
502 magenta. Scale bar 20 µm. **g,** Immunoblot showing expression levels of wild type DNAJB1-
503 HA, DNAJB1^{RRR}-HA and Hsp70-binding defective DNAJB1^{QPN}-HA (H32Q+D34N) mutant

504 in *DNAJB1* knocked out (KO) HEK 293 cells. **h-k,** Defective assembly of Hsp70-DNAJA1-
505 DNAJB1 disaggregase results in persistence of heat-induced aggregates in cells. Top:
506 Visualization of solubilization of Hsp104^{DWB}-GFP positive heat-induced aggregates during HS
507 recovery in *DNAJB1* KO HEK 293 cells ectopically expressing (**h**) empty vector (control), (**i**)
508 wild type DNAJB1-HA, (**j**) DNAJB1^{RRR}-HA, and (**k**) DNAJB1^{QPN}-HA. Bottom:
509 (Dis)assembly dynamics of DNAJA1-DNAJB1 scaffold by PLA (yellow) in *DNAJB1* KO
510 HEK 293 cells ectopically expressing (**h**) empty vector (control), (**i**) wild type DNAJB1-HA,
511 (**j**) DNAJB1^{RRR}-HA, and (**k**) DNAJB1^{QPN}-HA. U denotes unstressed cells. Scale bar 20 µm (n
512 = 3).
513
514 **Figure 2. Endogenous substrates of the Hsp70-DNAJA1-DNAJB1 disaggregase. a-d,**
515 Solubilization of heat aggregated HNRNPK and AHCY (SAHH) requires the induction of
516 Hsp70-DNAJA1-DNAJB1 disaggregase. **a,** Solubility profile of HNRNPK: Graphs show
517 representative traces for ΔpSup in the presence of DMSO (left panel) or VER-155008 (center
518 panel), and the corresponding ΔΔpSup (right panel) (n = 3). See methods for the two-phase
519 fractionation approach coupled to a proteomic workflow used to identify aggregated substrates
520 recovered by Hsp70- disaggregase activity. **b,** As in (**a**), for AHCY (n = 3). **c,** Solubilization
521 of heat aggregated HNRNPK in HeLa cells visualized using immunocytochemistry
522 (HNRNPK, cyan; DAPI stained nuclei, magenta). Hsp70 is inhibited with VER-155008 added
523 5h after HS. Cycloheximide (CHX) was added to inhibit protein synthesis at 5h after HS. White
524 arrows indicate heat-aggregated HNRNPK. Aggregate solubilization is indicated by the
525 disappearance of the punctated fluorescence signal and the appearance of a diffused signal.
526 DMSO, vehicle control for VER-155008. Heat shock (HS) in red. U denotes unstressed cells.
527 Scale bar 20 µm (n = 3). **d,** As in (**c**), for AHCY (n = 3). **e,** Disruption of DNAJA1-DNAJB1
528 JDP scaffold formation prevents solubilization of heat-aggregated HNRNPK. Left:
529 Immunoblot showing JDP knockdown efficiencies in HeLa cells. Right: Persistence of heat

530 aggregated HNRNPK in DNAJA1 and DNAJB1 depleted HeLa cells. The non-targeting
531 control siRNA (siScrambled) is used as the control for RNAi. Scale bar 20 µm (n = 3). **f,** Stress-
532 induced Hsp70 disaggregase targets different aggregate types in cells. Top: Hsp70-depended
533 solubilization of HNRNPK aggregates (cyan) *vs* TIA-1-GFP containing SGs (yellow) in HeLa
534 cells recovering from heat stress. The addition of VER-155008 at 0h after HS blocks resolution
535 of HNRNPK aggregates, but not TIA-1 SGs. The inset depicts zoomed-out cells. Scale bar 20
536 µm. **g,** Quantification of TIA-1 SGs and HNRNPK aggregates (n = 3, data are mean +/- s.e.m.
537 * adjusted p-value < 0.05, one-way ANOVA LSD post hoc test).
538
539 **Figure 3. VCP and Hsp70-DNAJA1-DNAJB1 disaggregases operate sequentially and**
540 **nonredundantly in cells recovering from heat stress. a,** Disaggregase activity exerted by
541 VCP facilitates rapid resolution of heat-induced ubiquitin (Ub) positive protein aggregates. 1%
542 NP-40 insoluble aggregates were isolated at indicated time points during heat stress recovery
543 using a two-phase fractionation approach and probed with antibody against ubiquitin (n = 3).
544 Immunoblots show depletion of VCP delays the disaggregation and clearance of Ub positive
545 protein aggregates in HeLa cells. VCP protein levels show knockdown efficiency. GAPDH,
546 loading control. **b,** Solubilization of heat-induced HNRNPK aggregates (cyan) and TIA-1-GFP
547 containing SGs (yellow) are affected in VCP depleted HeLa cells. The inset depicts zoomed-
548 out cells. The non-targeting control siRNA (siScrambled) is used as the control for RNAi (same
549 from Supplementary Data Fig. 13). Nuclei stained with DAPI (magenta). Scale bar 20 µm. **c,**
550 Quantification of TIA-1 SGs and HNRNPK aggregates (n = 3, data are mean +/- s.e.m. *
551 adjusted p-value < 0.05, ** adjusted p-value < 0.01, ns - not significant, one-way ANOVA
552 LSD post hoc test). **d,** Blocking VCP disaggregase activity with inhibitor NMS-873 (1 µM,
553 low dose) after 5h post-HS does not inhibit the resolution of $Hsp104^{DWB}$-GFP positive
554 aggregates by Hsp70 disaggregase. On the contrary, the addition of NMS-873 at 0h post-HS
555 results in a phenotype similar to the depletion of VCP. DMSO, vehicle control for the inhibitor

556 (n = 2). Nuclei stained with DAPI (magenta). **e,** Disassembly of DNAJA1-DNAJB1 scaffold
557 is delayed in HeLa cells treated with NMS-873 at 0h post-HS, but not at 5h post-HS (PLA
558 signal, yellow). Nuclei stained with DAPI (magenta). Heat shock (HS) in red. U denotes
559 unstressed cells. Scale bar 20 µm (n = 3).
560
561 **Figure 4. Pathophysiological consequences of the collapse of Hsp70-DNAJA1-DNAJB1**
562 **disaggregase in cells undergoing replicative aging. a,** Chronological age has no effect on
563 Hsp70-DNAJA1-DNAJB1 disaggregase activation in human cells. The PLA signal (yellow)
564 shows the induction of Hsp70-DNAJA1-DNAJB1 disaggregase in heat-stressed primary
565 human dermal fibroblasts derived from 21-year-old (21-y), 55-y and 75-y human subjects.
566 Nuclei stained with DAPI (magenta). U denotes unstressed cells. Heat shock (HS) in red. Scale
567 bar 20 µm (n = 3). **b,** Experimental scheme showing replicative aging of human dermal
568 fibroblasts. P denotes cell passage (see Methods). **c,** Cells at P = 12 and 18 show a considerable
569 increase in the marker of senescence. Cellular senescence correlates with the increased levels
570 of senescence specific β-galactosidase activity in replicating fibroblasts. **d,** HS-induced
571 assembly of Hsp70 disaggregase collapses in cells undergoing replicative aging. The level of
572 induction of Hsp70 disaggregase assemblies after HS in human dermal fibroblasts at P = 6, 12
573 and 18 using PLA. Scale bar 20 µm (n = 3). **e,** Immunoblot analysis of the induction of
574 components of the disaggregase machine after HS (n = 3). **f,** Cells defective in activating
575 Hsp70-DNAJA1-DNAJB1 disaggregase due to aging (replicative) show reduced cellular
576 fitness after HS. Level of cytotoxicity measured with Ultra-Glo rLuciferase-based cytotoxicity
577 assay in unstressed (blue) and HS recovering (red) human dermal fibroblasts at P 6 and P 12
578 cells. Error bars depicted as s.e.m. (n = 3). **g,** Human dermal fibroblasts at P 12 lose the ability
579 to solubilize Htt46Q-GFP aggregates (cyan) by assembling Hsp70-DNAJA1-DNAJB1
580 disaggregase. Cycloheximide (CHX) was added to prevent protein synthesis. Scale bar 20 µm
581 (n = 3).

584 **Methods**

585 **Plasmids**

586 Exon 1 carrying C-terminally tagged HttQ25-EmGFP and HttQ46-EmGFP were generated in
587 the mammalian expression vector pTREX (Invitrogen). VCP (wt)-EGFP (Addgene, catalog
588 number: 23971), pFRT/TO eGFP TIA1 (Addgene, catalog number: 106094) and pCMV3-
589 GFP-hnRNPK (LSBio, catalog number: LS-N40093) were purchased. pcDNA5/FRT/TO
590 HttQ119-eGFP was previously generated.[67] pEGFP-N1 Hsp104 and pEGFP-N1 Hsp104 ^{E285Q,}
591 ^{E687Q} were kind gifts from Bernd Bukau, Ph.D. (Heidelberg University). The generation of
592 Hsp70 (HSPA8), Hsp110 (HSPH2), DNAJA1, DNAJA2, DNAJB1, DNAJB4, and mutant
593 variants tagged with 6xHis-Smt3 in the vector pCA528 for recombinant expression and
594 purification was previously described.[12,25] Standard recombinant DNA techniques described
595 by Sambrook et al.[68] combined with standard site-directed mutagenesis with Phusion Plus DNA
596 Polymerase (Thermo Fisher Scientific) were used to generate V5-DNAJA1, V5-DNAJA2, V5-
597 DNAJB1, V5-DNAJB4, V5-DNAJB1^{H32Q}, DNAJB1-HA, DNAJB1^{D4R,E69R,E70R}-HA,
598 DNAJB1^{H32Q,D34N}-HA in pcDNA5/FRT/TO mammalian expression plasmid (Thermo Fisher
599 Scientific).[69] Gene sequences were verified by sanger sequencing.

600

601 **Protein purification**

602 Human Hsp70, Hsp110, DNAJA1, DNAJA2, DNAJB1, DNAJB4, JDP mutants and firefly
603 luciferase were recombinantly expressed and purified as previously described.[12,25] Briefly, *E.*
604 *coli* strains BL21 (D3E)/ pRARE carrying the corresponding expression vectors were induced
605 for protein expression with 0.5 mM isopropyl-1-thio-D-galactopyranoside (IPTG, Sigma-
606 Aldrich) for three hours at 30 ° C. Cells were lysed in 50 mM HEPES-KOH, pH 7.5, 750 mM
607 KCl, 5 mM $MgCl_2$, protease inhibitor cocktail (Roche), 2 mM phenylmethylsulphonyl fluoride,
608 10% glycerol (for human JDP purifications) or 50 mM HEPES-KOH, pH 7.5, 300 mM KCl, 5
609 mM $MgCl_2$, protease inhibitor cocktail (Roche), 2 mM phenylmethylsulphonyl fluoride, 10%

610 glycerol (for human Hsp70/110 purifications). After centrifugation at 30000 x g (30 min, 4 °
611 C) the resulting supernatants were applied to the Ni-NTA/Ni-IDA matrix and incubated for 60
612 min at 4 ° C. Subsequent washing steps were performed with high salt buffers (50 mM HEPES-
613 KOH, pH 7.5, 750 and 500 mM KCl, 5 mM $MgCl_2$ and 10% glycerol or 50 mM HEPES-KOH,
614 pH 7.5, 300 and 100 mM KCl, 5 mM $MgCl_2$ and 10% glycerol for human JDP and Hsp70/110
615 purifications, respectively). In the case of Hsp70/110 purification, an additional wash step was
616 included with ATP buffer (50 mM HEPES-KOH, pH 7.5, 100 mM KCl, 5 mM $MgCl_2$, 5 mM
617 ATP). Protein elution was performed with 300 mM imidazole in the corresponding low salt
618 buffers. Dialysis was performed overnight at 4 ° C in the presence of 4 µg of the 6xHis tagged
619 Ulp1 per mg of substrate protein for proteolytic cleavage of the 6xHis-Smt3 tag. The 6xHis-
620 Smt3 tag and Ulp1 were removed by incubating the dialyzed proteins in a Ni-NTA/ Ni-IDA
621 matrix for 60 min at 4 ° C. Pyruvate kinase was purchased from Sigma-Aldrich. Proteins were
622 further purified using Superdex 200 (GE Healthcare).
623
624 **Luciferase disaggregation assay**
625 Luciferase disaggregation assays were performed as previously described.[14] Briefly, 20 nM
626 firefly luciferase was incubated at 45 ° C for 15 minutes in HKM buffer (50 mM Hepes-KOH
627 pH 7.5, 50 mM KCl, 5 mM $MgCl_2$, 2 mM DTT, 2 mM ATP pH 7.0, 10 µM BSA) to generate
628 thermally denatured luciferase. Protein disaggregation was initiated by adding 1 µM HSPA8,
629 100 nM HSPH2, 250 nM JDP/mutant variants (total) and an ATP regenerating system (3 mM
630 phosphoenolpyruvate (PEP) and 20 ng/µl pyruvate kinase) to the preformed luciferase
631 aggregates followed by shifting the reaction to 30 ° C. 1 µM of recombinant yeast Hsp104
632 (kind gift from Yuki Oguchi, Ph.D.) was added to generate the bichaperone disaggregation
633 system. Luciferase activity was measured at the indicated time points with a Lumat tube
634 luminometer (Berthold Technologies) by transferring 1 µL of the sample to 100 µL of assay
635 buffer (25 mM Glycylglycin, pH 7.4, 5 mM ATP pH 7, 100 mM KCl, 15 mM $MgCl_2$) mixed

636 with 100 µL of 0.25 mM luciferin. The Hsp70 inhibitor VER-155008 (Sigma, SML0271) was
637 added at a working concentration of 5 µM.
638
639 **Cell culture**
640 Human adenocarcinoma epithelial cell line HeLa (ATCC CRM-CCL-2) and human embryonic
641 kidney HEK 293 cells (ATCC CRL-3216) were obtained from the American Type Culture
642 Collection. HEK 293 *JB1* KO cells were kindly provided by Christian Hansen, Ph.D. (Lund
643 University). These cell lines were cultured in DMEM (Gibco, Thermo Fisher Scientific, catalog
644 number: 10569044) supplemented with 10% (v/v) heat inactivated fetal bovine serum (FBS:
645 Gibco catalog number: 10082147), 1x L-alanine-L-glutamine dipeptide (Gibco Glutamax 100x
646 catalog number: 35050061), 10 mM sodium pyruvate (Gibco catalog number: 11360070) and
647 100 U/ml penicillin/streptomycin (Gibco 1x 104 U/ml catalog number: 15140122) at 37 ° C in
648 5% CO_2. Human dermal fibroblasts were isolated and grown from 6 mm skin punch biopsies
649 as previously described.[70] Dermal fibroblasts were cultured on 0.1% gelatin (Sigma catalog
650 number: G1890) treated wells using fibroblast media consisting of DMEM (Gibco catalog
651 number: 10569044), 10% FBS, 0.1 mM MEM non-essential amino acids solution (Gibco
652 catalog number: 11140050), 100 U/ml penicillin/streptomycin, 0.1mM 2-Mercaptoethanol,
653 (Gibco catalog number: 21985023). Cell passaging: 0.25 million dermal fibroblasts were
654 seeded in a 10 cm culture plate until cell confluency reached 70%. This was defined as a
655 passage (P), and the process was repeated to generate replicatively aged cell lines. Mycoplasma
656 contamination of cells was tested and ruled out with the LookOut Mycoplasma Detection kit
657 (Sigma-Aldrich; catalog number: MP0035).
658
659 **Heat shock and drug treatments**
660 Heat shock was performed by exposing HeLa cells to 43 ° C for 1 hour in a water bath or
661 otherwise indicated. A 42 ° C, 2 hours heat shock in an incubator was applied to HEK 293 and

662 human dermal fibroblasts. Following heat shock, cells were returned to 37 ° C for stress
663 recovery. Temperature measurements for heat shock conditions in the water bath and incubator
664 were determined using a VOLTCRAFT K101 digital thermometer (Conrad). Hsp70 inhibitor
665 VER-155008 (Sigma, catalog number: SML0271) was used at a working concentration of 5
666 µM (*in vitro*) or 50 µM (in cells) or otherwise stated. Protein synthesis was inhibited by adding
667 cycloheximide (CHX) (Sigma, catalog number: 01810) at a final concentration of 100 µg/mL.
668 NMS-873 (Sigma, catalog number: SML 1182) was used for VCP inhibition at a final
669 concentration of 1 or 10 µM.
670
671 ***In situ* proximity ligation assay (PLA)**
672 PLA was performed as previously described.[14,26]. Cells were washed 2x with PBS, fixed with
673 4% paraformaldehyde in PBS, and the proximity ligation assay was performed according to
674 the DUOLINK manufacturer's guideline for mammalian cells (Sigma-Aldrich). DNA was
675 stained with DAPI-containing mounting medium (Sigma-Aldrich, catalog number:
676 DUO82040). The staining, imaging, processing, and analysis conditions were kept consistent
677 for each experiment.
678
679 **Immunocytochemistry and staining**
680 Cells were cultured on soda lime glass diagnostic slides masked with epoxy resin (Marienfield-
681 superior, catalog number: 1216530) until 70-80% confluence. Cells were washed 2x with PBS,
682 fixed with 4% paraformaldehyde in PBS for 10 minutes, and washed 2x again with PBS. Cells
683 were permeabilized with 0.2% Triton X-100 in PBS for 10 minutes. After permeabilization,
684 cells were washed 2x with PBS and blocked for 10 minutes in PBS containing 0.5% bovine
685 serum albumin and 0.15% Glycine (PBS+ buffer). Primary antibodies were diluted in PBS+
686 buffer and incubated for 1.5 hours at room temperature (RT) or overnight at 4 ° C. After
687 incubation, cells were washed 4x with PBS+ buffer. Secondary antibodies were diluted in

688 PBS+ buffer and incubated for 1.5 hours at RT, followed by 2x washes in the same buffer.
689 DNA was stained with DAPI-containing mounting medium (Sigma-Aldrich, catalog number:
690 DUO82040) or Hoechst staining (Thermo Scientific, catalog number: 62249) according to the
691 manufacturer's guidelines.
692
693 **Transfections and siRNA knockdowns**
694 Plasmid transfections were performed according to standard protocols using Lipofectamine
695 2000 or 3000 (Thermo Fisher Scientific). siRNA transfections were carried out according to
696 standard protocols using DharmaFECT one transfection reagent (Dharmacon, DHA-T-2001).
697 HeLa cells were transfected with 25-50 nM of Dharmacon onTarget Plus smartpool siRNA
698 against DNAJA1 (Dharmacon, L-019617-00), DNAJA2 (Dharmacon, L-012104–01),
699 DNAJB1 (Dharmacon, L-012735–01), DNAJB4 (Dharmacon, L-015678-01), HSF-1
700 (Dharmacon, L-012109-02), BAG1 (Dharmacon, L-003871-00), HSPBP1 (Dharmacon, L-
701 016607-00), HSPH1 (Dharmacon, L-004972-00), HSPA4 (Dharmacon, L-012636-00),
702 HSPA4L (Dharmacon, L-017633-00), VCP (Dharmacon, L-008727-00), or scrambled non-
703 targeting siRNA (Dharmacon, D-001810–10) for 48 hours. The knockdown efficiencies were
704 verified by immunoblotting using specific antibodies.
705
706 **Confocal microscopy**
707 LSM 780 and LSM 980 laser scanning confocal systems on inverted stands with diode 405 nm,
708 argon 488 nm, and DPSS 561 nm lasers (Carl Zeiss, Germany) were used for microscopy. The
709 images were taken with the Plan-Apochromat 40x/1.4 oil objective (Carl Zeiss) and identical
710 acquisition settings with a pinhole of approximately 1 AU. Maximum projection images were
711 generated from acquired z-stacks. Linear adjustments of brightness and contrast were
712 performed to the same degree within each experiment. The DAPI, PLA, and GFP signals were

713 pseudo-colored in magenta, yellow, and cyan. Fluorescence intensity profile plots (line scans)
714 were generated on the raw images using the RGB Profiler plugin in Fiji.
715
716 **PLA quantification**
717 The PLA signal was quantified using custom code (https://github.com/Sanudish/Punctate-
718 Detection.git) in MATLAB R2021a using functions from the Image Processing Toolbox, and
719 Statistics and Machine Learning Toolbox. Briefly, the brightest slice of each volume,
720 determined by the cumulative intensity of the slice, was extracted to perform the quantification.
721 The nuclei-stained channel of the images was first processed with a median filter followed by
722 a maximum filter, both of which utilized a 4x4 kernel. The user input-based percentile
723 thresholding was then applied to the processed images. The connected nuclei were then further
724 segmented through the implementation of a Watershed transformation. To refine nuclei
725 segmentation, user inputs for the degree of connectivity and area were utilized. The output
726 enabled quantification of the number of cells per image. Next, for extraction of puncta,
727 logarithmic frequency histograms of the intensity profiles were plotted to generate a
728 normalized user input range between -1 and 1 to threshold out puncta. To improve the
729 segmentation of the puncta from noise, area thresholding was implemented. The resulting
730 number of puncta, and their characteristics were measured. The product of the average punctate
731 mean intensity per cell and the number of punctate structures per cell was calculated to obtain
732 the PLA raw parameter. The final induction of Hsp70 and JDP assemblies were reported as a
733 PLA fold change to an unstressed condition.
734
735 **Colocalization between PLA signal and Hsp104^{DWB}-GFP positive heat-induced foci**
736 Hela cells expressing Hsp104^{DWB}-GFP were heat shocked at 42 ° C for 2h and allowed to
737 recovery at 37 ° C for 12h. Cells were treated with cycloheximide (CHX) at 3.5h and VER-
738 155008 at 5.5h after HS. Super-resolution images were acquired using LSM 980 Airyscan

739 super-resolution module (Carl Zeiss, Germany). Raw images were processed using the Zen
740 Blue software's Airyscan Processing function in 3D mode. Colocalization analysis between
741 PLA signal and Hsp104^{DWB}-GFP foci was conducted using Fiji
742 plugin Just Another Colocalization Plugin (JACoP).[71] Manders' overlap correlation
743 coefficients were calculated using thresholded images (n=5).
744
745 **Aggregate quantification**
746 Endogenous protein aggregates and TIA-1 biomolecular condensates in HeLa cells were
747 quantified using a Fiji macro termed AggreCount as previously described.[72] Briefly, the
748 aggregates were extracted by processing images with gamma enhancement, mean background
749 reduction, and a user-based threshold. The contrast enhancement of the nuclei enabled
750 segmentation of nuclei regions, which were then utilized to generate a composite image with
751 the preprocessed image. The signal-enhanced composite image enables the detection of local
752 maxima of cell regions. Implementing the watershed algorithm, a Voronoi diagram was
753 generated and the proportion of cells with aggregates was measured. The fold change was
754 determined by calculating the difference of each parameter in the stress recovery conditions
755 and the unstressed condition. When segmenting hnRNPK aggregates, the threshold diameter
756 of inclusions was set at 1 µm to avoid intranuclear inhomogeneities being falsely detected as
757 aggregates. The aggregates in HEK 293 cells were calculated manually as previously
758 described[73] because AggreCount segmentation was less efficient.
759
760 **Fluorescence Recovery After Photobleaching**
761 HeLa cells expressing GFP tagged hnRNPK were exposed to 43 ° C for 1 hour in a water bath
762 and returned to 37 ° C for 1 hour. FRAP was performed on heat-induced hnRNPK aggregates
763 using an LSM 780 laser scanning confocal system on inverted stands at 37 ° C with argon 488
764 nm laser (Carl Zeiss, Germany). The images were taken with the Plan-Apochromat 40x/1.4 oil

765 objective (Carl Zeiss). Aggregates were photobleached using 100% FRAP laser power for 10
766 ms. Images were obtained every 500 ms to observe fluorescence recovery up to 40 s. Images
767 were analyzed using easyFRAP.[74] Recovery curves were normalized to background
768 fluorescence for subtracting noise, and adjacent non-bleached aggregates for fluorescence
769 intensity fluctuations. Average and standard errors were calculated from seven individual
770 traces.
771
772 **Immunoblotting**
773 Immunoblot analysis was performed using standard methodologies.[14] Briefly, cells were lysed
774 in RIPA buffer with a protease inhibitor cocktail (Roche cOmplete - EDTA free, catalog
775 number: 05056489001) and sonicated (3x cycles, each cycle at 5 seconds and 50% amplitude)
776 in a Branson SFX150 Digital Sonifier (Emerson). Protein concentrations were determined
777 using the bicinchoninic acid protein assay kit (PierceTM, BCA, catalog numbers: Reagent-A:
778 23228, Reagent-B: 23224). Protein samples were stabilized with 1x sample buffer and boiled
779 for 5 minutes at 95 ° C. For SDS-PAGE, 25 µg total protein was loaded into 4% stacking gel
780 and resolved through 12% running gel. Protein transfer to a PVDF membrane was performed
781 using a Bio-Rad transfer tank (Mini Trans-Blot Cell). Anti-rabbit (800CW; C90220-05) and
782 anti-mouse (680RD; C90219-05) antibodies from LI-COR Biosciences were used as secondary
783 antibodies. The detection was carried out with an Odyssey Immunoblotting Imaging System
784 (LI-COR).
785
786 **Supernatant-pellet assay**
787 HeLa cells were grown in 100 mm cell culture plates. Before lysis, cells were washed 1x with
788 ice-cold PBS, scraped, and collected with 500 µl of ice-cold PBS. Cells were collected at 600
789 x g for 5 minutes at 4 ˚ C. Cell pellets were resuspended in lysis buffer containing 25 mM
790 HEPES, 75 mM NaCl, 1 mM $MgCl_2$, 1% NP-40, 75 U/ml Benzonase (EMD Millipore) and

791 Protease Inhibitors cocktail (Roche) and lysed by vortexing for 20 seconds and subsequently
792 for 5 seconds every 10 minutes over the course of 1 hour. Protein quantification was performed
793 using the DC-protein assay (Bio-Rad) and the samples were equalized. 10% of the total protein
794 lysate was transferred to a fresh Eppendorf tube and boiled in Laemmli buffer (60 mM Tris pH
795 6.8, 2% SDS, 10% glycerol, 5% β-mercaptoethanol). From the remaining lysate, the pellet
796 fractions were isolated by centrifuging the samples at 20,817 x g for 30 minutes at 4 ˚ C and
797 removing the supernatant. The pellet fractions were washed and resuspended in urea buffer
798 (8M Urea, 50 mM Tris pH 7.4, 2% SDS, 50 mM DTT). The resuspended samples were shaken
799 at 1000 rpm in a heating block at 60 ˚ C for 1 hour and subsequently at 1000 rpm in RT,
800 overnight, and boiled prior to SDS-PAGE.
801
802 **qRT-PCR**
803 HeLa cells were washed with ice cold PBS, scraped in TRIzol reagent (Invitrogen) and
804 incubated at RT for 5 minutes. Chloroform was added to cell lysates, vortexed for 15 seconds
805 and incubated for 2-3 minutes before centrifugation at 18,000 x g for 15 minutes at 4 ˚ C. The
806 aqueous phase was transferred to a tube without DNAase/RNAase, isopropanol was added and
807 incubated in RT for 10 minutes. RNA was precipitated by centrifugation at 18,000 x g for 10
808 minutes at 4 ˚ C. The supernatants were removed, 75% ethanol was added to the pellets, and
809 the samples were centrifugated at 18,000 x g for 5 minutes at 4 ˚C. The supernatants were
810 removed and the pellets were resuspended in DNA/RNAase-free H_2O. DNAases were removed
811 with the Turbo DNAase free kit (Invitrogen) according to the manufacturer's instructions.
812 cDNA synthesis was performed using M-MLV reverse transcriptase (Invitrogen) according to
813 the manufacturer's instructions. The primers used in the PCR step were previously described.[75]
814
815 **LDH-Glo cytotoxicity assay**

816 Heat shock-induced cytotoxicity was determined using the LDH-Glo cytotoxicity assay
817 (Promega, catalog number: J2380) according to the manufacturer's guidelines. Briefly, HeLa
818 cells and human dermal fibroblasts were cultured in a 6-well plate at 37 ˚ C. Heat shock was
819 performed at 43 ˚ C in a water bath for 1 hour and returned to the 37 ˚ C incubator for recovery.
820 VER-155008 (5 μM) and cycloheximide (100 μg/mL) treatments were performed 2.5 hours
821 after heat shock. 5 μL samples from the cell culture media were collected at indicated time
822 points during heat shock recovery, and immediately mixed with 95 μL of LDH storage buffer
823 and kept at 4 ˚ C. The LDH-Glo cytotoxicity assay was performed using a plate reader
824 (CLARIOstar^{Plus}, BMG Labtech).
825
826 **Cellular senescence detection assay**
827 Cellular senescence was assessed using fluorescence- and immunocytochemistry-based assays.
828 The fluorescence-based assay was performed with the Cellular Senescence Plate Assay Kit-
829 SPiDER-βGal (Dogindo, catalog number: 05-05) according to the manufacturer's guidelines.
830 Fluorescence intensity was measured using a plate reader (CLARIOstar^{Plus}, BMG Labtech;
831 Excitation: 535 nm/ emission: 580 nm). SA-β-Gal activity was normalized to cell count
832 determined using a hemocytometer. The immunocytochemistry-based assay was performed
833 with Senescence β-Galactosidase Staining Kit (Cell Signaling Technology, catalog number:
834 9860) according to the manufacturer's guidelines. DIC images were obtained on a Leica DMi8
835 system using Plan-Apochromat 40x/1.4 oil objective. The percentage of cells positive with β-
836 Galactosidase signal was quantified manually.
837
838 **Proteasome activity assay**
839 The chymotrypsin-like activity of the 20S proteasome was assessed using a commercially
840 available fluorometric proteasome activity assay kit (Abcam, catalog number: ab107921)
841 according to the manufacturer's guidelines. Fluorescence intensity was measured using a plate

842 reader (CLARIOstar^{Plus}, BMG Labtech; Excitation: 350 nm/ emission: 440 nm). The readout
843 was normalized to the protein concentrations of the lysate samples determined using the
844 bicinchoninic acid protein assay kit (PierceTM, BCA, catalog numbers: Reagent-A: 23228,
845 Reagent-B: 23224).
846
847 **Multiple reaction monitoring mass spectrometry**
848 HeLa cells were cultured in 150 mm cell culture plates until 70-80% confluence. Light samples
849 were grown as previously described. To generate a heavy internal standard, cells were grown
850 in arginine and lysine-depleted DMEM (Thermo Fisher Scientific) supplemented with 100
851 mg/L L-arginine-HCl, $^{13}C_6$, $^{15}N_4$ (Thermo Fisher Scientific) and 100 mg/L L-Lysine-2HCl
852 $^{13}C_6$, $^{15}N_2$ (Thermo Fisher Scientific). The cells were grown in the heavy medium for 6 passages
853 until the incorporation of heavy amino acids was at least 95%. To ensure that all proteins of
854 interest were detectable, a heavy standard was generated from lysates of unstressed and heat
855 shocked cells for 1 hour at 43 ˚ C. Before lysis, cells were washed with ice-cold PBS and
856 detached by scraping with 1 ml of ice-cold PBS. Cells were pelleted at 500 x g for 5 minutes
857 at 4 ˚ C and the supernatant was discarded. Cell pellets were snap frozen in liquid nitrogen and
858 stored at -80 ˚ C or processed immediately. Cell pellets were resuspended in Benzonase
859 containing urea buffer (6 M Urea, 50 mM Tris pH = 7.5, 2 mM $MgCl_2$, 50 mM DTT, 0.25 U
860 μL^{-1} Benzonase) and lysed for 10 minutes at RT. The lysate was centrifuged at 5,000 x g for
861 10 minutes in RT. The supernatant was transferred to a fresh tube. Protein quantification was
862 performed using the DC Protein Assay (Bio-Rad).
863
864 Light samples and heavy internal standards were mixed in a 1:1 (w/w) ratio and 100 µg of total
865 protein was precipitated using a mixture of methanol and chloroform according to a published
866 protocol [76]. For in-solution digestion, precipitated protein pellets were resolved in 50 µL of
867 urea buffer (8 M Urea, Carl Roth, 100 mM NaCl, Applichem, in 50 mM triethylammonium

868 bicarbonate (TEAB), pH 8.5, Sigma-Aldrich). To reduce disulfide bridges, the sample was
869 incubated with 10 mM 1,4-dithiothreitol (Sigma-Aldrich) for 30 min at RT, constantly agitated
870 at 350 rpm. Next, alkylation was performed with 30 mM iodacetamide (Sigma-Aldrich) in
871 100 mM TEAB buffer for 30 min at RT in the dark. Sample predigestion was performed by
872 adding 2.5 µg Lysyl Endopeptidase® (Wako Chemicals) and incubating for 4 hours at 28 °C
873 and 350 rpm agitation. After diluting the urea concentration to 2 M by adding 50 mM TEAB
874 buffer, 1 µg of trypsin (Thermo Fisher Scientific) was added and the samples were incubated
875 for 16 hours at 28 °C and 350 rpm agitation. The digestion process was stopped by reducing
876 pH < 2 by adding trifluoroacetic acid (TFA, Sigma-Aldrich) to a final concentration of 0.4 –
877 0.8% (v/v). The samples were centrifuged for 10 min at 20,000 x g in RT and the supernatant
878 was desalted using SepPak C18 cartridges (500 mg; Waters) and the Waters Extraction
879 Manifold. The SepPak C18 cartridges were equilibrated by adding 3 ml of 100% acetonitrile
880 (ACN), then 3 ml of 50% ACN / 0.1% TFA and finally 3 ml of 0.1% TFA. Digested peptide
881 samples were loaded onto SepPak cartridges and washed with 3 ml of 0.1% TFA. Finally, the
882 samples were eluted into fresh LoBind tubes using 1 ml of 50% ACN / 0.1% TFA. The samples
883 were dried in a vacuum centrifuge and stored at -20 ° C until LC-MRM analysis. Before LC-
884 MRM analysis, the peptides were resolubilized in 10 µL of 20% ACN / 0.1% (v/v) TFA and
885 incubated for 5 min in RT, then diluted 10-fold with 0.1% TFA to obtain a final concentration
886 of 2% ACN. 5 µg of tryptic digest including a set of 11 synthetic peptides for indexed retention
887 time scheduling[77] were analyzed per LC-MRM injection. The samples were measured in a
888 randomized order using a nanoACQUITY UPLC System (Waters) online-coupled to an ESI-
889 QTrap 5500 via a NanoSpray III Source (both Sciex). The UPLC was equipped with a trapping
890 column (Waters, Symmetry C18; 2 cm length, 180 µm inner diameter, 5 µm C18 particle size,
891 100 Å pore size) and an analytical column (Waters, M-Class Peptide BEH C18; 25 cm length,
892 75 µm inner diameter, 1.7 µm C18 particle size, 130 Å pore size). The peptides were trapped
893 for 7 min at a flow rate of 10 µL min^{-1} with 99.4% of buffer A (1% v/v ACN, 0.1% v/v FA)

894 and 0.6% of buffer B (89.9% v/v ACN, 0.1% v/v FA) and separated at the analytical column
895 temperature of 60°C, with a flow rate of 300 nl min^{-1} and a 37 min linear gradient of buffer B
896 in buffer A from 3 to 37% B, followed by washing and reconditioning of the column to 3% B.
897 Uncoated precut emitters (Silica Tip, 20 µm inner diameter, 10 µm tip inner diameter, New
898 Objectives, Woburn, MA) were used and a voltage of approximately 2.6 kV was applied for
899 electrospray ionization. QTrap 5500 was operated in scheduled mode at Unit resolution for Q1
900 and Q3 with 180 sec MRM detection window width and 2.5 sec target scan time. Peptide
901 retention times for scheduling were previously determined using commercial synthetic peptide
902 standards (JPT).
903
904 **LC-MRM data and statistical analysis**
905 The MRM data was first manually reviewed using Skyline 64-bit version 20.1. Data sets were
906 imported into Skyline, and signal quality was assessed using the Peak Areas and Retention
907 Time visualization features. We ensured via the Results Grid that all reference dot-product
908 (rdotp) correlations for ratios of the observed transition intensities between the corresponding
909 light and heavy precursor pairs were equal to or above 0.9. Then, all data were exported from
910 Skyline and imported into R version 4.0.3 (2020-10-10) "Bunny-Wunnies Freak Out" for
911 further analysis using a custom script. Briefly, all quantitative transitions were summed up
912 across proteins, and log2 light/heavy ratios were computed to account for technical variance.
913 In addition, all samples were normalized to their respective tubulin alpha-1A protein level to
914 account for biological variance. Then, pairwise group comparisons were performed using linear
915 regression models between protein ratios of different conditions and the unstressed control.
916 The slope of the linear regression corresponded to the fold change between the respective
917 condition and the control and was plotted together with its respective standard error.
918

919 **Identification of aggregated proteins recovered by Hsp70 disaggregase activity (post 6h**
920 **heat shock)**
921 Briefly, HeLa cells were heat-shocked followed by sustained recovery over 12h. We chose
922 recovery time points that encompass the evolution and resolution (i.e. 6h and 12h post-HS) of
923 aggregates that appeared to be the main target of Hsp70-DNAJA1-DNAJB1. To quantify
924 cellular proteins that change solubility at different harvest time points, we used isobaric
925 labeling (Tandem mass tag; TMT), a method that allows for multiplexing of samples collected
926 at different time points in a recovery course into a single experiment (Supplementary Data Fig.
927 12a). The gist of TMT is that peptides are labeled with one of several distinct agents of the
928 same mass, but cleave into distinct reporter ions during mass spectrometry fragmentation. The
929 workflow included a parallel examination of stress recovery in which Hsp70-DNAJA1-
930 DNAJB1 disaggregase activity was inhibited using VER-155008 to identify potential
931 substrates. The proportion of proteins in the supernatant compared to the total proteome (pSup)
932 was normalized to solubility prior to HS (ΔpSup), and then the effect of VER-155008 was
933 compared to the DMSO control (ΔΔpSup). As expected, we observed a significant decrease in
934 the median pSup at 6h after HS in both DMSO and VER-155008 treated samples
935 (Supplementary Data Fig. 12b; p value < 0.0001, paired Wilcoxon rank test) that supports
936 aggregation throughout the proteome as a result of heat denaturation. After 12 hours of
937 recovery, more than 75% of proteins had recovered their solubility. However, as expected, a
938 subset of proteins recovered differently in the presence of VER-155008, as measured by
939 ΔΔpSup. Proteins with ΔΔpSup > +/ 0.26 (determined by Gaussian thresholding at the 99th
940 percentile of pseudo pre-HS ΔpSup) were considered to have significantly altered solubility
941 due to the presence of VER-155008. Of these proteins, those that were less soluble in the
942 presence of VER-155008 compared to DMSO (ΔΔpSup > 0) at at least one time point were
943 identified as potential clients solubilized by the disaggregase machinery (a total of 51 proteins,
944 Supplementary Data Table 1). We then sought to describe the general behavior of ΔΔpSup

945 among these proteins using unsupervised k-means clustering. The proteins of interest were
946 sorted into four distinct patterns (Supplementary Data Fig. 12c); (i) those that were more
947 soluble at 6h-HS in the presence of VER-155008 compared to the DMSO control, but whose
948 recovery was inhibited compared to the DMSO control at the 12h timepoint, (ii) those that were
949 less soluble at 6h post-HS in the presence of VER155008 but then recovered similarly to the
950 DMSO control at 12h, (iii) those with no difference in solubility due to VER-155008 at 6h
951 post-HS, but whose recovery was inhibited compared to the DMSO control at the 12h
952 timepoint, and (iv) those that were less soluble at both 6h and 12h post-HS in the presence of
953 VER-155008 (Supplementary Data Table 1). Protein degradation and processes such as the
954 recently discovered ubiquitinome reshaping during stress recovery could have in part
955 influenced the generated patterns we observed.[61] Given that the addition of VER-155008 was
956 at 5h post-HS, we postulated that its impact on disaggregation would be most visible at the 12h
957 timepoint. Therefore, we considered proteins with minimal differences in solubility at 6h but
958 inhibited recovery at 12h in the presence of VER-155008 (cluster iii) for validation. **Cell**
959 **fractionation by ultracentrifugation**: HeLa cells were grown in T75 cell culture flasks (Nunc
960 EasYFlask, catalog number: nun156472). Before lysis, cells were washed with 1x ice-cold
961 PBS, scraped and collected with 10 mL of ice-cold PBS. The cells were then pelleted by a mild
962 centrifugation step at 120 x g for 6 minutes at 4 ˚ C twice and the supernatant was discarded.
963 Cell pellets were resuspended in 500 µL of lysis buffer 1 containing 50 mM Tris-HCl pH 7.5,
964 150 mM NaCl, 1% (v/v) IGEPAL CA-630, 10 units/mL DNase I, 1:1,000 protease inhibitor,
965 and Protease Inhibitors cocktail (Roche, catalog number: 11836145001) and lysed by extrusion
966 through a 27-gauge needle for 25 times, followed by a 31-gauge needle for 10 times.
967 Subsequently, EDTA was added to a final concentration of 2 mM. Cell lysate was then divided
968 into two, one for the assessment of total protein and the other pelleted at 100,000 x *g* for 20
969 min at 4 ° C. The resulting supernatant was the collected sample. The volume of total protein
970 and supernatant samples was measured and resuspended in an equal volume of a lysis buffer 2

971 containing lysis buffer 1, 4% sodium dodecyl sulfate (SDS, Thermo Scientific, catalog number:
972 28365) and 4 mM 1,4-dithiothreitol (DTT, Thermo Scientific, catalog number: R0861).
973 Subsequently, the samples were incubated at 95 ° C for 20 minutes. **NanoESI-LC-MS/MS**:
974 Samples were prepared for mass spectrometry as previously detailed.[19] Freeze-dried peptides
975 were resuspended in 80 µl of distilled water and quantified by the BCA assay (Thermo Fisher
976 Scientific) according to the manufacturer's instruction. 20 µl of each sample was diluted into
977 a final volume of 40 µl containing 100 mM TEAB and 30% (v/v) acetonitrile. The samples
978 were then labeled with TMT 11-plex (Thermo Scientific, catalog number: A37725) according
979 to the manufacturer's protocol. The samples were analyzed by nanoESI-LC-MS/MS using an
980 Orbitrap Exploris mass spectrometer (Thermo Scientific) equipped with a nanoflow reversed-
981 phase-HPLC (Ultimate 3000 RSLC, Dionex) fitted with an Acclaim Pepmap nano-trap column
982 (Dionex—C18, 100 Å, 75 µm × 2 cm) and an Acclaim Pepmap RSLC analytical column
983 (Dionex—C18, 100 Å, 75 µm × 50 cm). For each iteration of LC-MS/MS, 0.6 µg of the peptide
984 mix was loaded onto the enrichment (trap) column at an isocratic flow of 5 µl min^{-1} of 2%
985 ACN containing 0.1% (v/v) trifluoroacetic acid for 5 min before the enrichment column was
986 switched in-line with the analytical column. The eluents were 0.1% (v/v) formic acid/5%
987 DMSO (v/v) (solvent A) and 100% ACN/0.1% formic acid/5% DMSO (v/v) (v/v) (solvent B),
988 flowed at 300 nL min^{-1} using a gradient of 3–22% B in 90 min, 22–40% B in 10 min and 40–
989 80% B in 5 min then maintained for 5 min before re-equilibration for 8 min at 3% B prior to
990 the next analysis. All spectra were acquired in positive ionization mode with full scan MS
991 acquired from m/z 300-1600 in the FT mode at a mass resolving power of 120 000, after
992 accumulating to an AGC target value of $3.00e^6$, with a maximum accumulation time of 25 ms.
993 The RunStart EASY-IC lock internal lockmass was used. Data-dependent HCD MS/MS of
994 charge states > 1 was performed using a 3 s scan method, at a normalized AGC target of 75%,
995 automatic injection, a normalized collision energy of 30%, and with spectra acquired at a
996 resolving power of 15000. Dynamic exclusion was used for 20s. **Peptide identification:** The

997 initial analysis of raw mass spectra was carried out using MaxQuant (v 1.6.14.0) against the
998 Swissprot Homo Sapiens database (downloaded 04/03/2020; containing 20350 entries).
999 Searches were conducted with 20 ppm mass tolerance for MS, and 0.2 Da for MS/MS, with
1000 one missed cleavage allowed and match between runs enabled. The MS2 reporter ion was set
1001 to TMT 11-plex and isotopic distribution correction was applied according to the product data
1002 sheet. Variable modifications included methionine oxidation and N-terminal protein
1003 acetylation, while the carbamidomethylcysteine modification was fixed. The false discovery
1004 rate maximum was set to 0.005% at the peptide identification level (actual was 0.005 for each
1005 replicate) and 1% at the protein identification level. All other parameters were left as default.
1006 **Ratio correction and scaling:** Further analysis was performed with custom Python scripts.
1007 The logic was as follows. First, common contaminant proteins were removed, and quantified
1008 proteins were considered as those identified by at least one unique peptide. The ratio of
1009 abundance for each protein in the supernatant as compared to total samples (pSup) was
1010 corrected for differences in total protein amount as quantified via BCA assay described
1011 previously.[19] The relative change in solubility for individual proteins after heat shock (ΔpSup)
1012 was then determined by normalizing to the preheat shock value, such that a protein with no
1013 change in solubility due to heat shock would have a value of 1. The resulting data were then
1014 scaled using a p-value weighted correction.[78] This correction weights the mean ratio of
1015 biological replicates (*n=4*) according to the relative confidence with which it deviates from the
1016 expected value (in this case, 1) as per equation 1:

1017 $$R = \frac{1 - m}{-20^{p}}$$

1018 where *m* corresponds to the mean of the ΔpSup ratios and *p* corresponds to the p-value derived
1019 from a one-sample t-test of the ratios against the expected value under a single timepoint and
1020 treatment regime. Finally, the difference in relative solubility at 6 and 12h post-heat shock
1021 between the DMSO and VER-155008 treated samples (ΔΔpSup) was calculated as $\Delta pSup_{DMSO}$
1022 – $\Delta pSup_{VER}$, such that no difference in relative solubility between the DMSO and VER-155008

1023 treatments would yield a ratio of 0. **Identifying proteins of interest:** To define a ΔΔpSup at
1024 which the changes in solubility could be considered biologically relevant, we first generated a
1025 pseudo-control ΔΔpSup by subtracting per-protein randomized pre-heat shock ratios ($\Delta pSup_{R-}$
1026 $_{Control}$) from the observed pre-heat shock ratios ($\Delta pSup_{Control}$). The resulting frequency
1027 histogram of pseudo-control ΔΔpSup values was then fit to a Gaussian distribution, and by
1028 calculating three times the derived variance parameter (σ) we determined the interval
1029 encompassing 99.7% of the pseudo-control ΔΔpSup values. The boundaries of this interval (in
1030 this case ± 0.26, consistent with previous estimates of ± 0.3 applied to similar data sets[19] were
1031 then used to threshold the ΔΔpSup values at each time point. Proteins that exceeded the
1032 ΔΔpSup threshold at least one time point were collected for additional analyzes. Functional
1033 overrepresentation was tested using PantherGOSlim (http://pantherdb.org), with a Bonferroni-
1034 corrected significance cutoff of $p < 0.05$ against the complete list of proteins identified.
1035 Annotated protein-protein interactions were collected from STRINGdb[79] via Cytoscape (v
1036 3.7.2).[80] Finally, ΔΔpSup traces over time were clustered using k-means as implemented via
1037 the scikit-learn package.[81]
1038
1039 **Statistical Methods**
1040 All quantified experiments were performed at least in triplicate. Data are shown as mean ±
1041 s.e.m. and error bars indicating s.e.m. All statistical analyzes not described elsewhere were
1042 performed on RStudio (Version 1.1.447) or GraphPad Prism 8. One-way between groups
1043 analysis of variance (ANOVA) was conducted for multiple group comparisons. All analyses
1044 were considered statistically significant at $p<0.05$.
1045
1046 **Ethics**

1047 Derivation of human dermal fibroblasts from skin punch biopsies was performed with approval
1048 from the Monash University and Monash Medical Centre Human Ethics Committees (approval
1049 number 10006A).
1050

1051 **Data availability and code availability**

1052 The mass spectrometry proteomics data have been deposited with the ProteomeXchange
1053 Consortium through the PRIDE[82] partner repository with the data set identifier PXD029161.
1054 All analysis scripts are available on request. The multiple reaction monitoring data will be
1055 deposited in the ProteomeXchange Consortium through the Panorama Public[83] partner
1056 repository upon manuscript acceptance and can be reviewed at
1057 https://panoramaweb.org/siDAP.url
1058

1059 **References**

1060 1 Labbadia, J. & Morimoto, R. I. The biology of proteostasis in aging and disease.
1061 *Annu. Rev. Biochem.* **84**, 435-464 (2015).
1062 2 Kampinga, H. H. & Bergink, S. Heat shock proteins as potential targets for protective
1063 strategies in neurodegeneration. *Lancet Neurol.* **15**, 748-759 (2016).
1064 3 Nillegoda, N. B., Wentink, A. S. & Bukau, B. Protein disaggregation in multicellular
1065 organisms. *Trends Biochem. Sci.* **43**, 285-300 (2018).
1066 4 Mogk, A., Bukau, B. & Kampinga, H. H. Cellular handling of protein aggregates by
1067 disaggregation machines. *Mol. Cell* **69**, 214-226 (2018).
1068 5 Sanchez, Y. & Lindquist, S. L. HSP104 required for induced thermotolerance.
1069 *Science* **248**, 1112-1115 (1990).
1070 6 Hong, S.-W. & Vierling, E. Mutants of Arabidopsis thaliana defective in the
1071 acquisition of tolerance to high temperature stress. *Proc. Natl. Acad. Sci. U. S. A.* **97**,
1072 4392-4397 (2000).

1073 7 Kirstein, J. *et al.* In vivo properties of the disaggregase function of J-proteins and
1074 Hsc70 in Caenorhabditis elegans stress and aging. *Aging Cell* **16**, 1414-1424 (2017).
1075 8 Squires, C., Pedersen, S., Ross, B. & Squires, C. ClpB is the Escherichia coli heat
1076 shock protein F84. 1. *J. Bacteriol.* **173**, 4254-4262 (1991).
1077 9 Shorter, J. & Southworth, D. R. Spiraling in control: structures and mechanisms of the
1078 Hsp104 disaggregase. *Cold Spring Harb. Perspect. Biol.* **11**, a034033 (2019).
1079 10 Nillegoda, N. B. & Bukau, B. Metazoan Hsp70-based protein disaggregases:
1080 emergence and mechanisms. *Frontiers in molecular biosciences* **2**, 57 (2015).
1081 11 Haslberger, T. *et al.* Protein disaggregation by the AAA+ chaperone ClpB involves
1082 partial threading of looped polypeptide segments. *Nat. Rev. Mol. Cell Biol* **15**, 641-
1083 650 (2008).
1084 12 Nillegoda, N. B. *et al.* Crucial HSP70 co-chaperone complex unlocks metazoan
1085 protein disaggregation. *Nature* **524**, 247-251 (2015).
1086 13 Yoo, H., Bard, J. A., Pilipenko, E. V. & Drummond, D. A. Chaperones directly and
1087 efficiently disperse stress-triggered biomolecular condensates. *Mol. Cell* **82**, 741-755.
1088 e711 (2022).
1089 14 Nillegoda, N. B. *et al.* Evolution of an intricate J-protein network driving protein
1090 disaggregation in eukaryotes. *Elife* **6**, e24560 (2017).
1091 15 Gonçalves, C. C., Sharon, I., Schmeing, T. M., Ramos, C. H. & Young, J. C. The
1092 chaperone HSPB1 prepares protein aggregates for resolubilization by HSP70. *Sci.*
1093 *Rep.* **11**, 1-16 (2021).
1094 16 Gupta, R. *et al.* Firefly luciferase mutants as sensors of proteome stress. *Nature*
1095 *methods* **8**, 879-884 (2011).
1096 17 Michels, A. A. *et al.* Hsp70 and Hsp40 chaperone activities in the cytoplasm and the
1097 nucleus of mammalian cells. *J. Biol. Chem.* **272**, 33283-33289 (1997).

1098 18 Nollen, E. A., Brunsting, J. F., Roelofsen, H., Weber, L. A. & Kampinga, H. H. In
1099 vivo chaperone activity of heat shock protein 70 and thermotolerance. *Mol. Cell. Biol.*
1100 **19**, 2069-2079 (1999).
1101 19 Sui, X. *et al.* Widespread remodeling of proteome solubility in response to different
1102 protein homeostasis stresses. *Proc. Natl. Acad. Sci. U. S. A.* **117**, 2422-2431 (2020).
1103 20 Määttä, T. A. *et al.* Aggregation and disaggregation features of the human proteome.
1104 *Mol. Syst. Biol.* **16**, e9500 (2020).
1105 21 Kampinga, H. H. Thermotolerance in mammalian cells. Protein denaturation and
1106 aggregation, and stress proteins. *J. Cell Sci.* **104**, 11-17 (1993).
1107 22 Kobayashi, T., Manno, A. & Kakizuka, A. Involvement of valosin-containing protein
1108 (VCP)/p97 in the formation and clearance of abnormal protein aggregates. *Genes*
1109 *Cells* **12**, 889-901 (2007).
1110 23 Saha, I. *et al.* The AAA+ chaperone VCP disaggregates Tau fibrils and generates
1111 aggregate seeds. *BioRxiv* (2022).
1112 24 Darwich, N. F. *et al.* Autosomal dominant VCP hypomorph mutation impairs
1113 disaggregation of PHF-tau. *Science* **370**, eaay8826 (2020).
1114 25 Rampelt, H. *et al.* Metazoan Hsp70 machines use Hsp110 to power protein
1115 disaggregation. *EMBO J.* **31**, 4221-4235 (2012).
1116 26 Alberts, N., Mathangasinghe, Y. & Nillegoda, N. B. In Situ Monitoring of Transiently
1117 Formed Molecular Chaperone Assemblies in Bacteria, Yeast, and Human Cells.
1118 *JoVE*, e60172 (2019).
1119 27 Azkanaz, M. *et al.* Protein quality control in the nucleolus safeguards recovery of
1120 epigenetic regulators after heat shock. *Elife* **8**, e45205 (2019).
1121 28 Frottin, F. *et al.* The nucleolus functions as a phase-separated protein quality control
1122 compartment. *Science* **365**, 342-347 (2019).

1123 29 Nollen, E. A. *et al.* Dynamic changes in the localization of thermally unfolded nuclear
1124 proteins associated with chaperone-dependent protection. *Proc. Natl. Acad. Sci. U. S.*
1125 *A.* **98**, 12038-12043, doi:10.1073/pnas.201112398 (2001).
1126 30 Michels, A. A., Kanon, B., Bensaude, O. & Kampinga, H. H. Heat shock protein
1127 (Hsp) 40 mutants inhibit Hsp70 in mammalian cells. *J. Biol. Chem.* **274**, 36757-36763
1128 (1999).
1129 31 Wallace, E. W. *et al.* Reversible, specific, active aggregates of endogenous proteins
1130 assemble upon heat stress. *Cell* **162**, 1286-1298 (2015).
1131 32 Wang, B. *et al.* ULK1 and ULK2 regulate stress granule disassembly through
1132 phosphorylation and activation of VCP/p97. *Mol. Cell* **74**, 742-757. e748 (2019).
1133 33 Rogers, A. M. & Egan, M. J. Autophagy machinery promotes the chaperone-mediated
1134 formation and compartmentalization of protein aggregates during appressorium
1135 development by the rice blast fungus. *Mol. Biol. Cell* **31**, 2298-2305 (2020).
1136 34 Schlecht, R. *et al.* Functional analysis of Hsp70 inhibitors. *PLoS One* **8**, e78443
1137 (2013).
1138 35 Yasuda, K., Clatterbuck-Soper, S. F., Jackrel, M. E., Shorter, J. & Mili, S. FUS
1139 inclusions disrupt RNA localization by sequestering kinesin-1 and inhibiting
1140 microtubule detyrosination. *J. Cell Biol.* **216**, 1015-1034 (2017).
1141 36 Shorter, J. The mammalian disaggregase machinery: Hsp110 synergizes with Hsp70
1142 and Hsp40 to catalyze protein disaggregation and reactivation in a cell-free system.
1143 *PLoS One* **6**, e26319 (2011).
1144 37 Gao, X. *et al.* Human Hsp70 disaggregase reverses Parkinson's-linked α-synuclein
1145 amyloid fibrils. *Mol. Cell* **59**, 781-793 (2015).
1146 38 Scior, A. *et al.* Complete suppression of Htt fibrilization and disaggregation of Htt
1147 fibrils by a trimeric chaperone complex. *EMBO J.* **37**, 282-299 (2018).

1148 39 Nachman, E. *et al.* Disassembly of Tau fibrils by the human Hsp70 disaggregation
1149 machinery generates small seeding-competent species. *J. Biol. Chem.* **295**, 9676-9690
1150 (2020).
1151 40 Buchan, J. R., Kolaitis, R.-M., Taylor, J. P. & Parker, R. Eukaryotic stress granules
1152 are cleared by autophagy and Cdc48/VCP function. *Cell* **153**, 1461-1474 (2013).
1153 41 Polucci, P. *et al.* Alkylsulfanyl-1, 2, 4-triazoles, a new class of allosteric valosine
1154 containing protein inhibitors. Synthesis and structure–activity relationships. *J. Med.*
1155 *Chem.* **56**, 437-450 (2013).
1156 42 Wang, T. *et al.* Pathogenic mutations in the valosin-containing protein/p97 (VCP) N-
1157 domain inhibit the SUMOylation of VCP and lead to impaired stress response. *J. Biol.*
1158 *Chem.* **291**, 14373-14384 (2016).
1159 43 Ninomiya, K. *et al.* Lnc RNA-dependent nuclear stress bodies promote intron
1160 retention through SR protein phosphorylation. *The EMBO journal* **39**, e102729
1161 (2020).
1162 44 Chen, J. & Stark, L. A. Insights into the relationship between nucleolar stress and the
1163 NF-κB pathway. *Trends Genet.* **35**, 768-780 (2019).
1164 45 Lafontaine, D. L., Riback, J. A., Bascetin, R. & Brangwynne, C. P. The nucleolus as a
1165 multiphase liquid condensate. *Nature Reviews Molecular Cell Biology* **22**, 165-182
1166 (2021).
1167 46 Lafita-Navarro, M. C. & Conacci-Sorrell, M. in *Semin. Cell Dev. Biol.* (Elsevier).
1168 47 Martínez-Cué, C. & Rueda, N. Cellular senescence in neurodegenerative diseases.
1169 *Front. Cell. Neurosci.* **14**, 16 (2020).
1170 48 Covarrubias, A. J. *et al.* Senescent cells promote tissue NAD+ decline during ageing
1171 via the activation of CD38+ macrophages. *Nature metabolism* **2**, 1265-1283 (2020).
1172 49 Pereira, B. I. *et al.* Senescent cells evade immune clearance via HLA-E-mediated NK
1173 and CD8+ T cell inhibition. *Nature communications* **10**, 1-13 (2019).

1174 50 Gutsmann-Conrad, A., Heydari, A. R., You, S. & Richardson, A. The Expression of
1175 Heat Shock Protein 70 Decreases with Cellular Senescencein Vitroand in Cells
1176 Derived from Young and Old Human Subjects. *Exp. Cell Res.* **241**, 404-413 (1998).
1177 51 Fumagalli, M., Rossiello, F., Mondello, C. & d'Adda di Fagagna, F. Stable cellular
1178 senescence is associated with persistent DDR activation. *PLoS One* **9**, e110969
1179 (2014).
1180 52 Ramirez, V. P., Stamatis, M., Shmukler, A. & Aneskievich, B. J. Basal and stress-
1181 inducible expression of HSPA6 in human keratinocytes is regulated by negative and
1182 positive promoter regions. *Cell Stress Chaperones* **20**, 95-107 (2015).
1183 53 Sabath, N. *et al.* Cellular proteostasis decline in human senescence. *Proceedings of*
1184 *the National Academy of Sciences* **117**, 31902-31913 (2020).
1185 54 Weibezahn, J. *et al.* Thermotolerance requires refolding of aggregated proteins by
1186 substrate translocation through the central pore of ClpB. *Cell* **119**, 653-665 (2004).
1187 55 Parsell, D. A., Kowal, A. S., Singer, M. A. & Lindquist, S. Protein disaggregation
1188 mediated by heat-shock protein Hspl04. *Nature* **372**, 475-478 (1994).
1189 56 Glover, J. R. & Lindquist, S. Hsp104, Hsp70, and Hsp40: a novel chaperone system
1190 that rescues previously aggregated proteins. *Cell* **94**, 73-82 (1998).
1191 57 Huang, L. *et al.* DAXX represents a new type of protein-folding enabler. *Nature* **597**,
1192 132-137 (2021).
1193 58 Weith, M. *et al.* Ubiquitin-independent disassembly by a p97 AAA-ATPase complex
1194 drives PP1 holoenzyme formation. *Mol. Cell* **72**, 766-777. e766 (2018).
1195 59 Turakhiya, A. *et al.* ZFAND1 recruits p97 and the 26S proteasome to promote the
1196 clearance of arsenite-induced stress granules. *Mol. Cell* **70**, 906-919. e907 (2018).
1197 60 Tolay, N. & Buchberger, A. Role of the Ubiquitin System in Stress Granule
1198 Metabolism. *Int. J. Mol. Sci.* **23**, 3624 (2022).

1199 61 Maxwell, B. A. *et al.* Ubiquitination is essential for recovery of cellular activities after
1200 heat shock. *Science* **372**, eabc3593 (2021).
1201 62 Gwon, Y. *et al.* Ubiquitination of G3BP1 mediates stress granule disassembly in a
1202 context-specific manner. *Science* **372**, eabf6548 (2021).
1203 63 Watts, G. D. *et al.* Inclusion body myopathy associated with Paget disease of bone
1204 and frontotemporal dementia is caused by mutant valosin-containing protein. *Nat.*
1205 *Genet.* **36**, 377-381 (2004).
1206 64 Labbadia, J. & Morimoto, R. I. Proteostasis and longevity: when does aging really
1207 begin? *F1000Prime Rep.* **6** (2014).
1208 65 Moreno, D. F. *et al.* Proteostasis collapse, a hallmark of aging, hinders the chaperone-
1209 Start network and arrests cells in G1. *Elife* **8**, e48240 (2019).
1210 66 Machiela, E. & Southwell, A. L. Biological aging and the cellular pathogenesis of
1211 Huntington's disease. *Journal of Huntington's disease* **9**, 115-128 (2020).
1212

1213 **Acknowledgements**
1214 We thank Paolo D. L. Rios, Ph.D., and Joachim Berger, Ph.D., and others for scientific
1215 discussions and critical reading of the manuscript. Special acknowledgements go to Oleksandr
1216 Chernyavskiy, Ph.D. (Monash Micro Imaging Facility) and Tim E. Powers, Ph.D. (Monash
1217 eResearch Center) for assistance with microscopy and statistical analysis. We thank Xinran
1218 Cheng, Ph.D., Peck S. Tan, Ph.D., Sophie Kopetschke, and Jeanette F. Brunsting for
1219 experimental/technical support. Some figures were created with BioRender.com.
1220

1221 **Funding**
1222 National Health and Medical Research Council of Australia Investigator Grant APP1197021
1223 to NBN, APP1161803, and APP1154352 to DMH.
1224 Recruitment Grant from Monash University Faculty of Medicine Nursing and Health Sciences

with funding from the State Government of Victoria and the Australian Government to NBN.

Yulgilbar Foundation, Australia to NBN

Australian Research Council of Australia Grant DP170103093 to DMH.

Deutsche Forschungsgemeinschaft Project ID FOR2509 P05 to TR.

Bundesministerium für Bildung und Forschung (BMBF), Ministerium für Kultur und Wissenschaft des Landes Nordrhein-Westfalen (MKW) and Regierender Bürgermeister von Berlin to RS.

We thank Merck PTY LTD Australia for its concessional product pricing for the work.

Authors' contributions

Conceptualization: NBN

Methodology: YM, NA, DC, CJR, RS, KMA and NBN

Software development: SU, YM and SA

Investigation: YM, NA, CJR, DC, NLP, ARO, RS, KMA, and NBN

Formal analysis: YM, NA, CJR, DC, RS, KMA, SU, TR, SA, DMH, HHK and NBN

Original draft writing: NBN

Editing: YM, NA, CJR, DC, RS, KMA, SU, TR, SA, DMH, HHK and NBN

Reviewing: YM, NA, DMH, HHK and NBN

Competing interests

The authors declare no competing interests.

Materials and correspondence

Correspondence and requests for materials should be addressed to

Nadinath.nillegoda@monash.edu

Supplementary Materials

Supplementary Information is available for this paper.

Rights and permissions

Reprints and permissions information is available at www.nature.com/reprints

1258 **Supplementary Data Figure legends**

1259 **Supplementary Data Figure 1. Reactions containing interclass JDP scaffolds show**
1260 **increased protein disaggregation/refolding activity, *in vitro*. a,** Top: Schematic diagram of
1261 Hsp70, JDP and Hsp110 mediated protein disaggregation. JDP scaffolds presumably assemble
1262 on aggregates and recruit Hsp70. Hsp110's primarily function as nucleotide exchange factors
1263 (NEFs) for Hsp70. Bottom left: Domain architectures of class A (green) and class B (blue)
1264 JDPs (depicted as dimers). JD, J-domain; CTD, C-terminal domain; ZFLR, Zink finger like
1265 region; DD, dimerization domain. Bottom right: Intra and interclass JDP complexation which
1266 results in the formation of homo or hetero JDP scaffolds (minimum is a dimer of a dimer) is
1267 driven by intermolecular interactions between JD and CTD.[12] **b,** Left: Luciferase
1268 disaggregation/refolding assay. Heat denaturation triggers misfolding and aggregation of
1269 luciferase. Right: Disaggregation/refolding efficiencies by different JDP scaffolds containing
1270 Hsp70 disaggregases, *in vitro* (n = 3, data are mean + / - s.e.m., * adjusted p-value < 0.05, **
1271 adjusted p-value < 0.01, one-way ANOVA Tukey post hoc test). Hsp110 functions as a NEF.
1272

1273 **Supplementary Data Figure 2. JDP-JDP and JDP-Hsp70 complex formation during**
1274 **disaggregase assembly monitored by PLA in heat shocked human cells. a,** Formation of
1275 intraclass JDP scaffolds between DNAJA1 and DNAJA2, and DNAJB1 and DNAJB4 in HeLa
1276 cells during HS recovery. PLA signal in yellow. DAPI (magenta) staining indicates nuclei. HS
1277 indicated in red. Unstressed cells indicated as U. Scale bar 20 µm (n = 3). **b,** Technical controls
1278 of PLA for antibody specificity. PLA was performed in HeLa cells with single primary
1279 antibodies only. Signal amplification (yellow) was not observed in any of the controls. Scale
1280 bar 20 µm (n = 2). **c,** Immunoblot (IB) showing RNAi knockdown efficiencies for DNAJA1,
1281 DNAJA2, DNAJB1, DNAJB4 in HeLa cells. GAPDH, loading control. **d,** RNAi knockdown-
1282 based controls of PLA for antibody and complexation specificity. RNAi knockdown of single
1283 JDPs decreased JDP^{A}-JDP^{B} and $JDP^{A/B}$-Hsp70 complex formation (yellow puncta) in HeLa

1284 cells. The non-targeting control siRNA (siScrambled) is used as the control for RNAi. Scale
1285 bar 10 µm (n = 2). **e,** Top: The graphs show the temperature changes observed in two HS
1286 regimes (at 42 ˚C 2h in an incubator *vs.* 43 ˚C 1h in a water bath) used in the study. Bottom:
1287 Induction of the DNAJA1-DNAJB1 scaffold (PLA signal, yellow) after applying the two HS
1288 regimes to HeLa cells. Nuclei stained with DAPI (magenta). HS indicated in red. Unstressed
1289 cells indicated as U. Scale bar 20 µm (n = 3).
1290
1291 **Supplementary Data Figure 3. PLA signals capture direct interactions between**
1292 **disaggregase machine components during assembly. a,** DNAJB1^{RRR} can shuttle in and out
1293 of nucleoli immediately after heat shock to support chaperoning function(s) similar to wild type
1294 DNAJB1. The immunocytochemical signal from the HA tag (yellow) shows that both
1295 DNAJB1-HA and the JDP scaffold forming defective mutant DNAJB1^{RRR}-HA rapidly localize
1296 into the nucleoli of HeLa cells immediately after heat shock (HS), and relocate out of the
1297 nucleoli before 6h post-HS. RRR denotes the D4R + E69R + E70R mutations in DNAJB1.
1298 Unstressed cells are denoted as U. Nuclei stained with DAPI (magenta). The nucleoli are
1299 unstained by DAPI and appear as dark spots in the nucleus. Line scans across the nucleoli are
1300 indicated in white. Corresponding line scan plots are shown on the right. **b,** The PLA signal
1301 captures the direct interaction between DNAJA1 and DNAJB1 during the formation of the JDP
1302 scaffold. A decreased PLA signal (yellow) is observed for the interaction between the JDP
1303 scaffold forming defective mutant DNAJB1^{RRR}-HA and endogenous DNAJA1 or DNAJA2.
1304 Nuclei stained with DAPI (magenta). Scale bar 20 µm (n = 2). Immunoblot shows expression
1305 levels of mutant and wild type DNAJB1. **c,** As in (**b**), a similar decrease in the PLA signal is
1306 observed for the interaction between Hsp70 binding defective mutant V5-DNAJB1^{H32Q} and
1307 endogenous Hsp70. Scale bar 20 µm (n = 2). Immunoblot shows expression levels of mutant
1308 and wild type DNAJB1.
1309

1310 **Supplementary Data Figure 4. Hsp110-type nucleotide exchange factors (NEF) impact**
1311 **the disassembly of DNAJA1-DNAJB1 scaffold.** The Hsp110 chaperone family of NEFs
1312 functions redundantly to facilitate the dissociation of ADP from Hsp70 and stimulate the
1313 disaggregation activity. **a,** Mini RNAi screen targeting NEFs from Hsp110 (HSPH1, HSPH2,
1314 and HSPH3), Bag (BAG-1), and HSPB1 (HSPB-1) families in HeLa cells. Single NEF
1315 depletions do not affect the assembly or disassembly of DNAJA1-DNAJB1 scaffold (PLA
1316 signal, yellow) during heat stress recovery (HS, red). Triple knockdown of the Hsp110s, which
1317 removes functional redundancy, results in delayed disassembly of the JDP scaffold. The non-
1318 targeting control siRNA (siScrambled) and depletion of HSF-1 (see section on HSF-1 mediated
1319 assembly of DNAJA-DNAJB1 scaffold) are used as controls for RNAi. Nuclei stained with
1320 DAPI (magenta). Scale bar 20 µm (n = 3). **b,** Quantification of the PLA signals from (**a**). Data
1321 are mean +/- s.e.m. **c,** Cells tune the activation of DNAJA1-DNAJB1 scaffold according to
1322 the level of protein damage sustained after HS. Heat stress at 39 ˚C *vs* 42 ˚C for 2h mimics
1323 mild-moderate and high fever, respectively. PLA signal in yellow. Quantification of PLA
1324 signal reported in Fig 1d. The nuclei stained with DAPI (magenta). Scale bar 20 µm (n = 3).
1325
1326 **Supplementary Data Figure 5. Resolution of different heat-induced aggregates/SGs in**
1327 **cells. a,** Detection of heat-induced ubiquitin (Ub) positive protein aggregates. 1% NP-40
1328 insoluble aggregates were isolated at indicated time points during heat stress recovery using a
1329 two-phase fractionation approach and probed with antibody against ubiquitin (n = 3).
1330 Immunoblots show the clearance of Ub-positive protein aggregates in HeLa cells before 6h
1331 post-HS. GAPDH, loading control. **b,** Resolution of TIA-1-GFP containing stress granules
1332 (SGs; yellow) also occurs in HeLa cells before 6h post-HS. Nuclei stained with DAPI
1333 (magenta) (n = 3).
1334

1335 **Supplementary Data Figure 6. Heat-induced aggregate solubilization after inhibition of**
1336 **Hsp70 with VER-155008. a,** Resolution of heat-induced aggregates in cells +/- Hsp70
1337 inhibitor VER-155008. Top: Schematic diagram illustrating the decoration of heat induced
1338 aggregates by the yeast HSP104^{DWB}-GFP. Hsp70-JDP chaperone system facilitates the loading
1339 of the inactive mutant of Hsp104 onto aggregate surface. Bottom: HS triggered the formation
1340 and solubilization of Hsp104^{DWB}-GFP positive aggregates (cyan; punctated fluorescent signal
1341 pointed by white arrows) in HeLa cells. U denotes unstressed cells. Heat shock (HS) in red.
1342 Scale bar 20 µm (n = 3). Below: Visualization of assembly and disassembly of the DNAJA1-
1343 DNAJB1 scaffold (PLA; yellow) in HeLa cells recovering from heat shock (HS). The inhibitor
1344 was added to cells 5h after HS. DMSO, vehicle control for VER-155008. Nuclei in magenta.
1345 Scale bar 20 µm (n = 3). Quantification of Hsp104^{DWB}-GFP positive aggregate levels in HeLa
1346 cells during HS recovery (see Methods). Data are mean +/- s.e.m. **b,** Inhibition of
1347 disaggregation/refolding of preformed luciferase aggregates by the Hsp70 inhibitor VER-
1348 155008, *in vitro* (n = 3, data are mean +/- s.e.m. ** adjusted $p < 0.01$, one-way ANOVA Tukey
1349 post hoc test).
1350
1351 **Supplementary Data Figure 7. Disaggregation of heat-induced aggregates re-initiates**
1352 **after washing off VER-155008**. **a,** VER-155008 wash-off experimental setup. **b,** Washing off
1353 VER-155008 by cell culture medium change at 12h post-HS results in the resumption of
1354 Hsp104^{DWB}-GFP (cyan) positive aggregate solubilization in HeLa cells recovering from heat
1355 stress. VER-155008 was added to cells at 5h post-HS. DMSO, vehicle control for VER-
1356 155008. Nuclei stained with DAPI (magenta). Aggregates are indicated by white arrows. Scale
1357 bar 20 µm (n = 3). **c,** The assembled DNAJA1-DNAJB1 scaffolds (PLA signal, yellow) support
1358 the resumption of protein disaggregation after washing off the Hsp70 inhibitor. VER-155008
1359 washed off HeLa cells show efficient disassembly of the DNAJA1-DNAJB1 scaffold of the

1360 disaggregase at 24h after HS compared to control with the inhibitor. DMSO, vehicle control
1361 for VER-155008. Nuclei stained with DAPI (magenta). Scale bar 20 µm. (n = 3).
1362
1363 **Supplementary Data Figure 8. Expression of yeast Hsp104 disaggregase in human cells**
1364 **decreases the assembly of DNAJA1-DNAJB1 scaffold of the Hsp70 disaggregase. a,** Yeast
1365 Hsp104 cooperates with human Hsp70-JDP system to target and solubilize preformed
1366 luciferase aggregates more effectively compared to Hsp70-JDP disaggregase alone, *in vitro* (n
1367 = 3, data are mean +/- s.e.m., **** adjusted p value < 0.0001, one-way ANOVA with Tukey
1368 post hoc test). Hsp110 functions as NEF. **b,** Assembly of DNAJA1-DNAJB1 scaffold of the
1369 Hsp70 disaggregase (PLA signal, yellow) is reduced in HeLa cells overexpressing wild-type
1370 Hsp104-GFP (cyan) compared to GFP control. Nuclei stained with DAPI (magenta). Heat
1371 shock (HS) in red. Scale bar = 20 µm (n = 3). Immunoblots show the induction of DNAJA1
1372 and DNAJB1 after HS. GAPDH, loading control. **c,** Rapid solubilization of HNRNPK
1373 aggregates (cyan, indicated by white arrows, see section on endogenous substrates of Hsp70-
1374 DNAJA1-DNAJB1 disaggregase) immediately after heat shock in HeLa cells overexpressing
1375 Hsp104-GFP (yellow). Control cells express GFP alone (yellow). Nuclei stained with DAPI
1376 (magenta). Heat shock (HS) in red. Scale bar = 20 µm (n = 3).
1377
1378 **Supplementary Data Figure 9. Cooperation between DNAJB1 and DNAJA1 is crucial for**
1379 **efficient Hsp70 disaggregase function in cells. a,** The reaction containing class A JDP
1380 binding defective mutant DNAJB1^{RRR} (RRR denotes D4R+E69R+E70R) shows decreased
1381 disaggregation of heat-induced luciferase aggregates, *in vitro* (n = 3, data are mean +/- s.e.m.
1382 ** adjusted p-value < 0.01, one-way ANOVA Tukey post hoc test). **b,** Top: Solubilization of
1383 heat-induced Hsp104^{DWB}-GFP (cyan) positive aggregates in HEK 293 cells recovering from
1384 heat stress. The nuclei stained with DAPI (magenta). Aggregated proteins are indicated by
1385 white arrows. Heat shock (HS) in red. Scale bar 20 µm (n = 3). Bottom: Visualization of the

1386 (dis)assembly dynamics of DNAJA1-DNAJB1 scaffold of the Hsp70 disaggregase (PLA
1387 signal, yellow) in HEK 293 cells recovering from heat shock. Scale bar 20 µm (n = 3). **c,**
1388 Quantification of heat-induced Hsp104^{DWB}-GFP positive protein aggregates from Figure 1h-k
1389 and Supplementary Data Figure 9b (data are mean +/- s.e.m.). **d,** Rapid assembly of DNAJA1-
1390 DNAJB1 scaffold in heat shocked *DNAJB1* KO HEK 293 cells overexpressing DNAJB1 *vs*
1391 wild-type HEK 293 cells (PLA, yellow). Nuclei stained with DAPI (magenta). Scale bar 20
1392 µm (n = 3). **e,** The role of DNAJB1 in Hsp70-mediated disaggregase function cannot be
1393 substituted for by other class A and B JDPs in stress recovering cells. Left: Overexpression
1394 levels of DNAJA1, DNAJA2, DNAJB1 and DNAJB4 tagged with V5 in *DNAJB1* KO HEK
1395 293 cells visualized by immunoblotting. Right: Resolution of heat-induced Hsp104^{DWB}-GFP
1396 positive aggregates (cyan) in *DNAJB1* KO cells ectopically expressing V5-tagged DNAJA1,
1397 DNAJA2, DNAJB1 or DNAJB4. Nuclei stained with DAPI (magenta). Aggregated proteins
1398 are indicated by white arrows. Scale bar 20 µm (n = 3).
1399
1400 **Supplementary Data Figure 10. Heat induced Hsp70 disaggregase is cogged to assemble**
1401 **with DNAJA1-DNAJB1 scaffold. a,** depleting either DNAJA1 or DNAJB1 via RNAi does
1402 not result in unpaired JDPs forming alternative scaffolds with DNAJA2 or DNAJB4. Left:
1403 Levels of DNAJA1-DNAJB1 and DNAJA2-DNAJB1 scaffolds in DNAJA1 depleted HeLa
1404 cells. Right: Levels of DNAJA1-DNAJB1 and DNAJA1-DNAJB4 scaffolds in DNAJB1
1405 depleted HeLa cells. The non-targeting control siRNA (siScrambled) is used as the control for
1406 RNAi. Scale bar 20 µm (n = 3). Corresponding immunoblots show JDP knockdown
1407 efficiencies. GAPDH, loading control. **b,** HS triggered increase in DNAJA1, DNAJA2,
1408 DNAJB1 and DNAJB4 protein levels in recovering HeLa cells measured through multiple
1409 reaction monitoring (MRM, see Methods) mass spectrometry (normalized to tubulin alpha-1A
1410 and unstressed JDP levels). Error bars reflect fold change +/- s.e. of regression (n = 4).
1411

1412 **Supplementary Data Figure 11. Localization of DNAJA1, DNAJA2, DNAJB1 and**
1413 **DNAJB4 in unstressed and heat shocked cells. a,** DNAJA1 is localized in both cytosol and
1414 nucleus in unstressed (U) HeLa cells monitored by immunocytochemistry (yellow). DNAJA1
1415 rapidly localizes into nucleoli immediately after heat shock, and relocates out of nucleoli before
1416 6h post-HS. Nuclei stained with DAPI (magenta). The nucleoli are unstained by DAPI and
1417 appear as dark spots in the nucleus. Line scans across the nucleoli are indicated in white.
1418 Corresponding line scan plots are shown on the right. Scale bar 10 µm (n = 3). (**b-d**), As in (**a**).
1419 (**b**) DNAJA2 shows a predominantly nuclear localization signal in both unstressed and heat
1420 shocked cells. (**c**) DNAJB1 is localized predominantly in the nucleus in unstressed (U) cells
1421 and rapidly localizes into nucleoli immediately after heat shock, and relocates out of nucleoli
1422 before 6h post-HS. (**d**) DNAJB4 displays both cytosolic and nuclear localization and does not
1423 show detectible heat stress induced dynamics in HeLa cells.
1424
1425 **Supplementary Data Figure 12. Identification of aggregated proteins recovered by stress-**
1426 **induced Hsp70 disaggregase activity. a,** Schematic representation of the proteomics
1427 workflow used to identify aggregated proteins rescued by stress-induced Hsp70
1428 disaggregase. The fractions were distinguished by isobaric labeling and proteins that regained
1429 solubility between 6-12h in DMSO, but not in cells treated with VER-155008 were identified
1430 and quantified by LC-MS/MS (see Methods). **b,** Ridge plot showing the distribution of
1431 solubility (pSup) for all proteins during post-HS recovery. **c,** Proteins for which the change in
1432 relative solubility due to the VER-155008 treatment (ΔΔpSup) exceeding 0.26 in at least one
1433 time point were clustered via k-means into four patterns. Mean ΔΔpSup for all proteins in each
1434 cluster is shown, where colored bands represent ± s.d. (n = 4). **d,** Visualization of Hsp70-based
1435 disaggregation of heat aggregated HNRNPK in HeLa cells by immunocytochemistry
1436 (HNRNPK, cyan; DAPI stained nuclei, magenta). Heat-induced Hsp70 disaggregase was
1437 inhibited with VER-155008 +/- cycloheximide (CHX) at 5h after HS. CHX inhibits protein

1438 synthesis. The white arrows indicate HNRNPK aggregated with heat. Aggregate solubilization
1439 is indicated by the disappearance of the punctated fluorescence signal and the appearance of a
1440 diffused signal. DMSO, vehicle control for VER-155008. Heat shock (HS) in red. U denotes
1441 unstressed cells. Scale bar 20 µm (n = 3). **e,** Fluorescence recovery after photobleaching
1442 (FRAP) analysis of heat-induced HNRNPK-containing aggregates shows poor recovery of the
1443 fluorescent signal after photobleaching. GFP-HNRNPK was transiently expressed in HeLa
1444 cells, and FRAP was performed after heat shock. The fluorescence signal of the selected
1445 inclusions was reduced to ~50% by photobleaching with the 488-nm laser (photobleached area
1446 indicated by the white squire), and its recovery was recorded for 40 seconds. The fluorescence
1447 intensity of GFP-HNRNPK after photobleaching was normalized as described in Methods.
1448 Selected images of a cell containing GFP-HNRNPK positive aggregates (green) before
1449 photobleaching and at indicated intervals after photobleaching are shown. The white arrows
1450 indicate GFP-HNRNPK aggregates. Scale bar 2 µm (n = 7).
1451
1452 **Supplementary Data Figure 13. TIA-1 containing stress granules disassembly is not**
1453 **affected in cells depleted of class A and B JDPs.** Depletion of DNAJA1, DNAJA2, DNAJB1,
1454 and DNAJB4 via RNAi has no effect on the resolution of TIA-1 SGs (yellow) in heat stress
1455 recovering HeLa cells. DNAJA1 and DNAJB1, but not DNAJA2 and DNAJB4 knockdown
1456 results in inhibition of HNRNPK (cyan) aggregate solubilization. The inset depicts zoomed out
1457 cells. The non-targeting control siRNA (siScrambled) is used as the control for RNAi. Nuclei
1458 stained with DAPI (magenta). Scale bar 20 µm. Below: Quantification of TIA-1 SGs and
1459 HNRNPK aggregates (n = 3, data are mean +/- s.e.m. * adjusted p-value < 0.05, ** adjusted p-
1460 value < 0.01, ns - not significant, one-way ANOVA LSD post hoc test).
1461
1462 **Supplementary Data Figure 14. Resolution of Hsp104^{DWB}-GFP positive aggregates in**
1463 **VCP depleted/inhibited cells. a,** Resolution of heat-induced Hsp104^{DWB}-GFP positive

1464 aggregates (cyan; punctated fluorescent signal pointed by white arrows) is blocked in HeLa
1465 cells RNAi depleted of VCP. The non-targeting control siRNA (siScrambled). Scale bar 20 µm
1466 (n = 3). Nuclei stained with DAPI (magenta). Heat shock (HS) in red. U denotes unstressed
1467 cells. **b,** Heat-induced Hsp104^{DWB}-GFP positive aggregates do not have a ubiquitin signal.
1468 Colocalization of the immunofluorescence signal from ubiquitin (Ub, yellow) and the
1469 fluorescence signal from Hsp104^{DWB}-GFP (cyan) in HeLa cells recovering from heat shock
1470 (HS) (6h post-HS). Nuclei stained with DAPI (magenta). Line scans are indicated in white.
1471 Corresponding line scan plots are shown on the right. Scale bar 10 µm (n = 3). **c,** Disassembly
1472 of Hsp70 disaggregase is delayed in VCP depleted HeLa cells (PLA signal, yellow). The non-
1473 targeting control siRNA (siScrambled) and depletion of HSF-1 are used as controls for RNAi
1474 (see section on HSF-1 mediated assembly of DNAJA-DNAJB1 scaffold). Nuclei stained with
1475 DAPI (magenta). Heat shock (HS) in red. U denotes unstressed cells. Scale bar 20 µm (n = 3).
1476 **d,** Blocking VCP disaggregase activity with inhibitor NMS-873 (10 µM, high dose) after 5h
1477 post-HS does not inhibit the resolution of Hsp104^{DWB}-GFP positive aggregates by Hsp70-
1478 DNAJA1-DNAJB1 disaggregase. On the contrary, the addition of NMS-873 at 0h post-HS
1479 results in a phenotype similar to the depletion of VCP. DMSO, vehicle control for the inhibitor
1480 (n = 3). Nuclei stained with DAPI (magenta).
1481
1482 **Supplementary Data Figure 15. Cells overexpressing VCP still activate Hsp70-DNAJA1-**
1483 **DNAJB1 disaggregase during heat stress recovery.** The assembly and disassembly
1484 dynamics of DNAJA1-DNAJB1 scaffold of Hsp70 disaggregase is not affected in HeLa cells
1485 overexpressing VCP (PLA signal, yellow; VCP-EGFP signal, cyan). GFP-alone is expressed
1486 as control. Nuclei stained with DAPI (magenta). Scale bar 20 µm (n = 3).
1487
1488 **Supplementary Data Figure 16. Disaggregation of heat-induced Hsp104^{DWB}-GFP positive**
1489 **aggregates requires an intact heat shock response**. **a,** Immunoblots showing changes in

1490 steady-state protein levels of DNAJA1, DNAJB1 and Hsp70 after HS in HeLa cells. **b,**
1491 Induction of DNAJA1 and DNAJB1 mRNA measured by qRT-PCR (log_2 fold (-ΔCt; relative
1492 to GAPDH mRNA) in HeLa cells recovering from HS. s.e.m. calculated from ΔCt value per
1493 experiment. Error bars reflect mean +/- s.e.m. (n = 3). **c,** Inhibition of DNAJA1 and DNAJB1
1494 protein synthesis after HS through HSF-1 depletion blocks DNAJA1-DNAJB1 scaffold
1495 assembly. Left: Immunoblots show HSF-1 knockdown by RNAi and inhibition of JDP
1496 synthesis after HS. GAPDH, loading control. Right: PLA shows a decreased assembly of
1497 Hsp70 disaggregase in HSF-1-depleted cells. The non-targeting control siRNA (siScrambled)
1498 is used as the control for RNAi. Scale bar 20 µm (n = 3). **d,** Disruption of the heat shock
1499 response by depleting HSF-1 blocks solubilization of heat-induced $Hsp104^{DWB}$-GFP (cyan)
1500 positive aggregates in recovering HeLa cells. Aggregated proteins are visualized as punctated
1501 fluorescence signals and indicated by white arrows. Nuclei stained with DAPI (magenta). Line
1502 scans across the nucleoli are indicated in white. Corresponding line scan plots are shown on
1503 the right. Scale bar 10 µm (n = 3).
1504
1505 **Supplementary Data Figure 17. Resolution of different heat-induced aggregate/SG types**
1506 **in cells. a,** The resolution of TIA-1 containing stress granules occurs independent of the heat
1507 shock response. Inactivation of the heat shock response through depletion of HSF-1 does not
1508 affect the disassembly of TIA-1-GFP containing SGs (yellow). In contrast, activation of the
1509 stress signaling pathway is required to solubilize heat-induced HNRNPK aggregates (cyan).
1510 HSF-1 depletion results in inhibition of the disaggregation of HNRNPK aggregates in HeLa
1511 cells. The inset depicts zoomed out cells. The non-targeting control siRNA (siScrambled) is
1512 used as the control for RNAi. Nuclei stained with DAPI (magenta). Scale bar 20 µm. Scale bar
1513 20 µm. Below: Quantification of TIA-1 SGs and HNRNPK aggregates (n = 3, data are mean
1514 +/- s.e.m. * adjusted p-value < 0.05, ** adjusted p-value < 0.01, ns - not significant, one-way
1515 ANOVA LSD post hoc test). **b,** DNAJA1 and DNAJB1 molecules synthesized before HS are

1516 not involved in Hsp70 disaggregase formation. Left: Cycloheximide (CHX) is added to HeLa
1517 cells to block the induction of DNAJA1 and DNAJB1 at specific time points during recovery
1518 from heat stress. DNAJA1 and DNAJB1 induction after heat stress is shown by
1519 immunoblotting. GAPDH, loading control. DMSO, vehicle control for CHX (n = 2). Right:
1520 The newly synthesized DNAJA1 and DNAJB1 molecules are used to assemble the DNAJA1-
1521 DNAJB1 scaffold of Hsp70 disaggregase after heat shock (HS, red). The addition of CHX at
1522 0h after HS, which inhibits the synthesis of new DNAJA1 and DNAJB1 molecules, completely
1523 blocks the assembly of the JDP scaffold (PLA signal, yellow). Treatment of cells with CHX at
1524 2.5h post-HS does not prevent the synthesis of new DNAJA1 and DNAJB1 molecules, and
1525 assembly of the JDP scaffold. Nuclei stained with DAPI (magenta). DMSO, vehicle control for
1526 CHX. Scale bar 20 µm (n = 3).
1527
1528 **Supplementary Data Figure 18. The localization of DNAJA1 and DNAJB1 into nucleoli**
1529 **immediately after heat shock occurs independent of the heat shock response. a,** Cellular
1530 HSF-1 levels after RNAi knockdown are shown by immunoblot. GAPDH, loading control. The
1531 non-targeting control siRNA (siScrambled) is used as the control for RNAi. **b,** DNAJA1
1532 molecules synthesized prior to heat stress rapidly localize into nucleoli immediately after heat
1533 shock (HS, red), and relocate out of nucleoli before 6h post-HS at similar levels in both HSF-
1534 1 depleted and control (siScrambled) HeLa cells. Subcellular localization of DNAJA1 in
1535 unstressed (U) and heat shocked (HS) HeLa cells monitored by immunocytochemistry
1536 (yellow). Nuclei stained with DAPI (magenta). The nucleoli are unstained by DAPI and appear
1537 as dark spots in the nucleus. Line scans across the nucleoli are indicated in white.
1538 Corresponding line scan plots are shown on the right. Scale bar 10 µm (n = 3). **c,** As in (**b**),
1539 DNAJB1 molecules synthesized prior to HS rapidly locate into nucleoli immediately after HS,
1540 and relocates out of nucleoli before 6h post-HS to a similar degree in HSF-1 depleted and
1541 control cells. Scale bar 10 µm (n = 3).

1542

1543 **Supplementary Data Figure 19. Pre-HS synthesized DNAJA1 and DNAJB1 shuttle to**
1544 **nucleoli immediately after heat stress. a,** DNAJA1 molecules predominantly synthesized
1545 before heat stress show similar level of localization into nucleoli immediately after heat shock
1546 (HS, red), and relocate out of the nucleoli before 6h post-HS. Cycloheximide (CHX) was added
1547 to inhibit protein synthesis at 0h after HS. DMSO added at 0h post-HS as vehicle control.
1548 DNAJA1 detected in unstressed cell (U) and heat shocked HeLa cells by immunocytochemistry
1549 (yellow). Nuclei stained with DAPI (magenta). The nucleoli are unstained by DAPI and appear
1550 as dark spots in the nucleus. Line scans across the nucleoli are indicated in white.
1551 Corresponding line scan plots are shown on the right. Scale bar 10 µm (n = 3). **b,** As in (**a**),
1552 Pre-HS synthesized DNAJB1 molecules in CHX treated cells rapidly locate into nucleoli
1553 immediately after HS, and relocate out of nucleoli before 6h post-HS similar to control (DMSO
1554 treated) cells. Scale bar 10 µm (n = 3). **c,** Hsp70 molecules rapidly localize into nucleoli
1555 immediately after heat shock, and relocate out of the nucleoli before 6h post-HS. Scale bar 10
1556 µm (n = 3).

1557

1558 **Supplementary Data Figure 20. Stress-induced Hsp70 disaggregase provides heat**
1559 **tolerance. a,** Simplified scheme of Ultra-Glo rLuciferase-based cytotoxicity assay. Leaked
1560 LDH is detected as a readout for damaged or dying cells. **b,** Assembly of DNAJA1-DNAJB1
1561 scaffold of the Hsp70 disaggregase (PLA, yellow) in cells treated with VER-155008 at 2.5h
1562 after HS. Control, cells without HS. DMSO, vehicle control for VER-155008. The nuclei
1563 stained with DAPI (magenta). Scale bar 20 µm (n = 3). **c,** Disruption of stress-induced Hsp70
1564 disaggregase activity increased heat toxicity in cells. Cytotoxicity level in unstressed (blue)
1565 and HS recovering HeLa cells (red) with and without VER-155008 treatment. DMSO, vehicle
1566 control for the inhibitor. Error bars depicted as s.e.m. (n = 3).

1567

1568 **Supplementary Data Figure 21. Assembly of Hsp70-DNAJA1-DNAJB1 disaggregase is**
1569 **not affected in dermal fibroblasts obtained from young *vs* old human donors. a,** Induction
1570 of the DNAJA1-DNAJB1 scaffold of Hsp70 disaggregase in heat shocked primary dermal
1571 fibroblasts (HDFs) derived from humans of different chronological ages (21 years of age (21y),
1572 26y, 55y, 58y, 70y, and 75y) in cells at passage (P) 3. Nuclei stained with DAPI (magenta). U
1573 denotes unstressed cells. Heat shock (HS) in red. Scale bar 20 µm (n = 3). **b,** The assembly
1574 dynamics of different JDP scaffolds formed between members of class A (DNAJA1 and
1575 DNAJA2) and class B (DNAJB1 and DNAJB4) (PLA signal, yellow) in human dermal
1576 fibroblasts after HS. Nuclei stained with DAPI (magenta). Scale bar 20 µm. (n = 3). **c,** Dermal
1577 fibroblasts undergoing replicative aging show increased senescence-specific β-galactosidase
1578 levels. Detection of senescence-specific β-galactosidase levels in P 6, P 12 and P 18 HDFs
1579 derived from 21-year-old (21y) human donor (see Methods). DIC images show cells at P 12
1580 and P 18 stained positive for senescence-specific β-galactosidase (white arrows). Scale bar 20
1581 µm. (n = 4). **d,** Quantification of senescence-specific β-galactosidase positive cells at P 6, P 12
1582 and P 18. Data are mean +/- s.e.m. **** adjusted p-value < 0.0001, one-way ANOVA Tukey
1583 post hoc test).
1584
1585 **Supplementary Data Figure 22. Hsp70-DNAJA1-DNAJB1 disaggregase activity is one of**
1586 **the earliest PQC functions to collapse during replicative aging of cells. a,** Immunoblot
1587 analysis shows similar induction patterns of HSPA6 chaperone after heat shock (HS) in non-
1588 senescent P 6 and replicative aging P 12 human dermal fibroblasts (HDFs) derived from donors
1589 aged 21, 55 and 75 years indicating that HSR is fully intact in all cells. VCP levels also do not
1590 change in P 6 and P 12 HDFs. GAPDH, loading control, (n = 3). **b,** Nuclear shuttling of ATF-
1591 6 (cyan) required to activate the endoplasmic reticulum unfolded protein response (UPR_{ER}) is
1592 equally active in P 6 and P 12 HDFs. Nuclei stained with DAPI (magenta). U and HS denote
1593 unstressed and heat shocked cells, respectively. HS performed at 44 ˚C for two hours in the

1594 incubator.[53] Line scans across the nuclei are indicated in white. Corresponding line scan plots
1595 are shown on the right. Scale bar 20 µm (n = 3). Insets depict magnified cells. **c,** P 6 and P 12
1596 HDFs show similar proteasome activity (see Methods) immediately after HS. ns – not
1597 significant, one-way ANOVA Tukey post hoc test.
1598
1599 **Supplementary Data Figure 23. Persistence of heat-induced aggregates in aged human**
1600 **dermal fibroblasts. a,** Regardless of chronological age, nonsenescent P 6 cells can efficiently
1601 solubilize heat-induced protein aggregates during recovery. Levels of Hsp104^{DWB}-GFP
1602 positive aggregates (cyan) in unstressed and heat-shocked P 6 dermal fibroblasts derived from
1603 21- and 75-year-old humans. Nuclei stained with Hoechst (magenta). White arrows show
1604 aggregates. U denotes unstressed cells. Heat shock (HS) in red. Scale bar 20 µm (n = 3). Insets
1605 depict magnified cells. **b,** Human dermal fibroblasts undergoing replicative aging (P 12) show
1606 defects in solubilizing heat-induced protein aggregates during recovery. Note that even
1607 unstressed cells (U) show Hsp104^{DWB}-GFP positive aggregates. As in (**a**), Hsp104^{DWB}-GFP
1608 positive aggregates (cyan) in unstressed and heat-shocked P 12 human dermal fibroblasts (21y
1609 and 75y). Nuclei stained with Hoechst (magenta). White arrows show aggregates. Scale bar 20
1610 µm (n = 3). Insets depict magnified cells. P denotes the cell passage.
1611
1612 **Supplementary Data Figure 24. Hsp70-DNAJA1-DNAJB1 disaggregase activity**
1613 **disassembles disease-linked polyQ aggregates in cells. a,** Disassembly of polyQ amyloids
1614 by disaggregation. **b,** Amyloid aggregates formed by HttQ46-GFP can be solubilized by
1615 inducing Hsp70-DNAJA1-DNAJB1 disaggregase activity. Top: The PLA signal (yellow)
1616 shows the induction of Hsp70-DNAJA1-DNAJB1 disaggregase in HeLa cells after heat shock
1617 (HS, red). Bottom: Solubilization of amyloids formed by HttQ-GFP variants with different
1618 lengths of glutamine stretches (HttQ23-GFP, HttQ46-GFP and HttQ119-GFP) after activation
1619 of Hsp70 disaggregase. HttQ23-GFP, a control that does not aggregate. Punctated GFP

1620 fluorescence (cyan) indicates aggregated polyQ (white arrows). Non-aggregating or solubilized
1621 polyQ generates a diffused fluorescence signal. Nuclei stained with DAPI (magenta). **c,** As in
1622 (**b**), inhibition of heat-induced Hsp70 disaggregase activity 5h after HS by adding VER-155008
1623 blocks HttQ46-GFP amyloid disassembly. DMSO, vehicle control for the inhibitor. Cells were
1624 treated with cycloheximide (CHX) at 5h after HS to block the translation of new HttpolyQ
1625 proteins. U denotes unstressed cells. Scale bar 20 µm (n = 3). **d,** Depletion of DNAJA1 or
1626 DNAJB1 inhibits Hsp70-mediated polyQ disassembly. Top: The disassembly of HttQ46-GFP
1627 aggregates is inhibited in DNAJA1 and DNAJB1 depleted HeLa cells. Punctated GFP
1628 fluorescence (cyan) indicates aggregated HttQ46-GFP (white arrows). The solubilized HttQ46-
1629 GFP generates a diffused fluorescence signal. The non-targeting control siRNA (siScrambled)
1630 is used as the control for RNAi. Nuclei stained with DAPI (magenta). Hsp70-DNAJA1-
1631 DNAJB1 disaggregase is activated by HS. CHX was added 5 h after HS to inhibit the synthesis
1632 of new HttQ46-GFP molecules. Bottom: Immunoblot showing knockdown of DNAJA1 and
1633 DNAJB1 in HeLa cells expressing HttQ46-GFP. **e,** Disassembly of HttQ inclusions by heat-
1634 induced Hsp70 disaggregase is masked by high levels of aggregation of newly synthesized
1635 amyloidogenic proteins. Cells treated with +/- CHX with and without VER-155008. CHX was
1636 added 5h after HS to inhibit HttQ-GFP synthesis. VER-155008 was added 5h after HS to inhibit
1637 heat-induced Hsp70 disaggregase activity. DMSO, vehicle control for the inhibitor. GFP
1638 fluorescence (cyan) indicates the aggregated (punctated signal, indicated by white arrows) and
1639 non-aggregated (diffused signal) state of HttQ23-GFP, HttQ46-GFP, and HttQ119-GFP.
1640 HttQ23-GFP, HttQ control that does not aggregate. The nuclei stained with DAPI (magenta).
1641 Scale bar 20 µm (n = 3).
1642
1643 **Supplementary information 1.**
1644 **Disassembly of disease-linked polyQ aggregates by Hsp70-DNAJA1-DNAJB1**
1645 **disaggregase.** For this analysis, we used GFP tagged Huntingtin protein (Htt) exon 1

1646 containing an expanded polyglutamine sequence (polyQ) (Supplementary Data Fig. 24a).
1647 These cytotoxic aggregates could form independently of proteotoxic stresses, such as heat.
1648 PolyQ aggregation was induced in unstressed HeLa cells (cyan foci, Supplementary Data Fig.
1649 24b) by overexpressing Htt exon-1 carrying varying lengths of sequential glutamine stretches
1650 (HttQ46-mEmGFP and HttQ119-GFP; HttQ23-mEmGFP, non-aggregating control). The
1651 Hsp70-DNAJA1-DNAJB1 disaggregase was activated by HS and cycloheximide (CHX) was
1652 added 5h after HS to prevent aggregation of newly synthesized HttpolyQ molecules. CHX
1653 addition at 5h after HS had minimal effects on the induction of Hsp70-DNAJA1-DNAJB1
1654 disaggregase. We observed the solubilization of pre-existing HttQ46-mEmGFP aggregates
1655 (disappearance of fluorescent puncta and appearance of a diffuse signal 12h after HS) with
1656 induction of the disaggregase (Supplementary Data Fig. 24b). Adding the Hsp70 inhibitor with
1657 CHX 5h after HS (Supplementary Data Fig. 24c) or knocking down DNAJA1 and DNAJB1
1658 using RNAi (Supplementary Data Fig. 24d), completely abrogated amyloid solubilization.
1659 Together, these results indicate that Hsp70-DNAJA1-DNAJB1 disaggregase also has the
1660 ability to target amyloid aggregates in cells. Interestingly, the omission of CHX treatment from
1661 the experimental regime prevented the previously observed decrease in the steady-state level
1662 of HttQ46-mEmGFP aggregates (Supplementary Data Fig. 24e) despite the induction of Hsp70
1663 disaggregase. Given the highly aggregate-prone nature of HttpolyQ species, we presume that
1664 the aggregation rate of newly synthesized HttQ46-mEmGFP monomers was faster than the
1665 disaggregation rate of the Hsp70-DNAJA1-DNAJB1 chaperone machine. In contrast, the
1666 amyloids formed by Htt exon-1 with a longer Q stretch (HttQ119-GFP) were completely
1667 resistant to the action of Hsp70-DNAJA1-DNAJB1 disaggregase even after blocking the
1668 aggregation of newly synthesized proteins using CHX (Supplementary Data Fig. 24b, e). These
1669 observations highlight important functional boundaries associated with the inherent capacity
1670 of this disaggregase to modulate amyloid load in cells.
1671

1672 **References (Supplementary)**

1673 67 Newcombe, E. A. *et al.* Tadpole-like conformations of huntingtin exon 1 are
1674 characterized by conformational heterogeneity that persists regardless of
1675 polyglutamine length. *J. Mol. Biol.* **430**, 1442-1458 (2018).

1676 68 Green, M. R. & Sambrook, J. *Molecular cloning: a laboratory manual*. 4 edn, (Cold
1677 spring harbor laboratory press, 2014).

1678 69 Hageman, J. & Kampinga, H. H. Computational analysis of the human
1679 HSPH/HSPA/DNAJ family and cloning of a human HSPH/HSPA/DNAJ expression
1680 library. *Cell Stress Chaperones* **14**, 1-21 (2009).

1681 70 Song, B. *et al.* Neural differentiation of patient specific iPS cells as a novel approach
1682 to study the pathophysiology of multiple sclerosis. *Stem Cell Res* **8**, 259-273,
1683 doi:10.1016/j.scr.2011.12.001 (2012).

1684 71 Bolte, S. & Cordelières, F. P. A guided tour into subcellular colocalization analysis in
1685 light microscopy. *J. Microsc.* **224**, 213-232 (2006).

1686 72 Klickstein, J. A., Mukkavalli, S. & Raman, M. AggreCount: an unbiased image
1687 analysis tool for identifying and quantifying cellular aggregates in a spatially defined
1688 manner. *J. Biol. Chem.* **295**, 17672-17683 (2020).

1689 73 Park, J. *et al.* Misfolded polypeptides are selectively recognized and transported
1690 toward aggresomes by a CED complex. *Nat. Commun.* **8**, 15730,
1691 doi:10.1038/ncomms15730 (2017).

1692 74 Rapsomaniki, M. A. *et al.* easyFRAP: an interactive, easy-to-use tool for qualitative
1693 and quantitative analysis of FRAP data. *Bioinformatics* **28**, 1800-1801 (2012).

1694 75 Hageman, J., van Waarde, M. A., Zylicz, A., Walerych, D. & Kampinga, H. H. The
1695 diverse members of the mammalian HSP70 machine show distinct chaperone-like
1696 activities. *Biochem. J.* **435**, 127-142 (2011).

1697 76 Wessel, D. & Flügge, U. A method for the quantitative recovery of protein in dilute
1698 solution in the presence of detergents and lipids. *Anal. Biochem.* **138**, 141-143 (1984).
1699 77 Escher, C. *et al.* Using iRT, a normalized retention time for more targeted
1700 measurement of peptides. *Proteomics* **12**, 1111-1121, doi:10.1002/pmic.201100463
1701 (2012).
1702 78 Cox, D., Ang, C.-S., Nillegoda, N. B., Reid, G. E. & Hatters, D. M. Hidden
1703 information on protein function in censuses of proteome foldedness. *Nature*
1704 *communications* **13**, 1-14 (2022).
1705 79 Szklarczyk, D. *et al.* STRING v11: protein–protein association networks with
1706 increased coverage, supporting functional discovery in genome-wide experimental
1707 datasets. *Nucleic Acids Res.* **47**, D607-D613 (2019).
1708 80 Shannon, P. *et al.* Cytoscape: a software environment for integrated models of
1709 biomolecular interaction networks. *Genome Res.* **13**, 2498-2504 (2003).
1710 81 Pedregosa, F. *et al.* Scikit-learn: Machine learning in Python. *J Mach Learn Res.* **12**,
1711 2825-2830 (2011).
1712 82 Perez-Riverol, Y. *et al.* The PRIDE database and related tools and resources in 2019:
1713 improving support for quantification data. *Nucleic Acids Res.* **47**, D442-D450 (2019).
1714 83 Sharma, V. *et al.* Panorama Public: A Public Repository for Quantitative Data Sets
1715 Processed in Skyline. *Mol. Cell. Proteomics* **17**, 1239-1244,
1716 doi:10.1074/mcp.RA117.000543 (2018).
1717

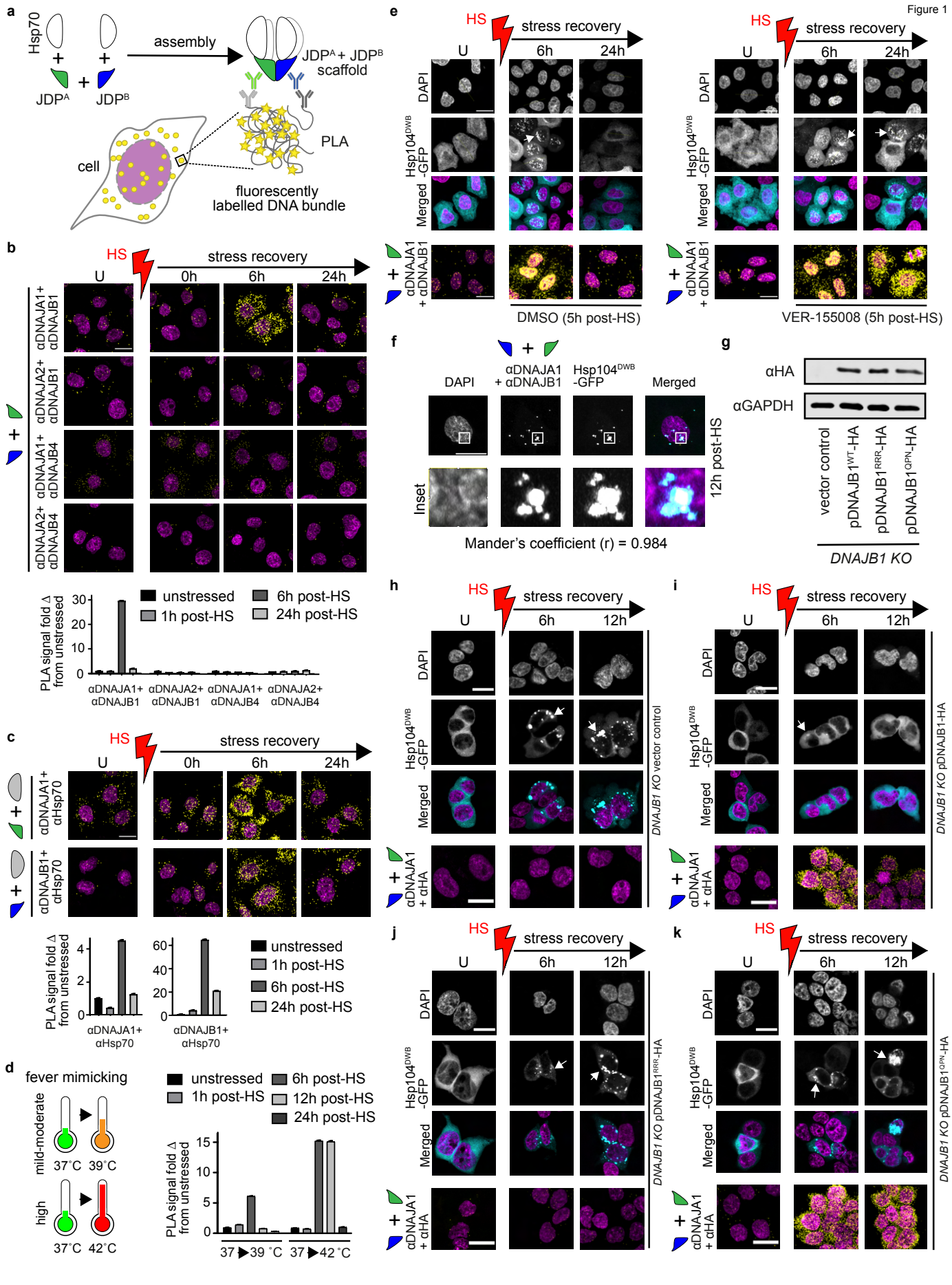
a
Hsp70
JDP^A
JDP^B
assembly
JDP^A + JDP^B scaffold
PLA
cell
fluorescently labelled DNA bundle
b
HS
stress recovery
U
0h
6h
24h
αDNAJA1+ αDNAJB1
αDNAJA2+ αDNAJB1
αDNAJA1+ αDNAJB4
αDNAJA2+ αDNAJB4
PLA signal fold Δ from unstressed
unstressed
1h post-HS
6h post-HS
24h post-HS
c
αDNAJA1+ αHsp70
αDNAJB1+ αHsp70
d
fever mimicking
mild-moderate
37˚C 39˚C
high
37˚C 42˚C
12h post-HS
37 ▶ 39 ˚C
37 ▶ 42 ˚C
e
DAPI
Hsp104^DWB -GFP
Merged
αDNAJA1 + αDNAJB1
DMSO (5h post-HS)
VER-155008 (5h post-HS)
f
αDNAJA1 + αDNAJB1
Hsp104^DWB -GFP
Inset
12h post-HS
Mander's coefficient (r) = 0.984
g
αHA
αGAPDH
vector control
pDNAJB1^WT-HA
pDNAJB1^RRR-HA
pDNAJB1^QPN-HA
DNAJB1 KO
h
12h
αDNAJA1 + αHA
DNAJB1 KO vector control
i
DNAJB1 KO pDNAJB1-HA
j
DNAJB1 KO pDNAJB1^RRR-HA
k
DNAJB1 KO pDNAJB1^QPN-HA

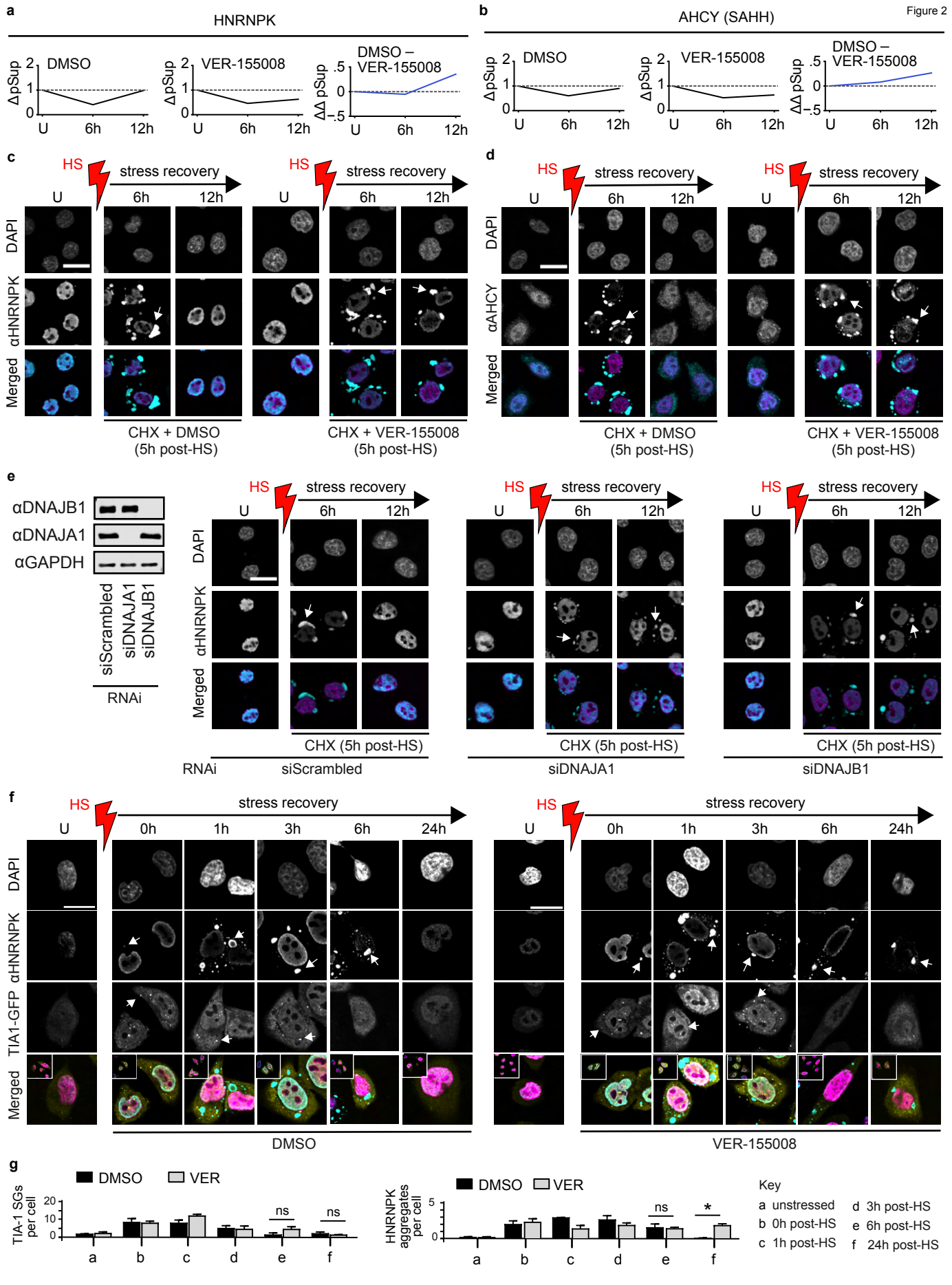
a
HNRNPK
DMSO
VER-155008
DMSO – VER-155008
ΔpSup
ΔΔ pSup
U
6h
12h
b
AHCY (SAHH)
c
HS
stress recovery
DAPI
αHNRNPK
Merged
CHX + DMSO (5h post-HS)
CHX + VER-155008 (5h post-HS)
d
αAHCY
e
αDNAJB1
αDNAJA1
αGAPDH
siScrambled
siDNAJA1
siDNAJB1
RNAi
CHX (5h post-HS)
siDNAJA1
siDNAJB1
f
0h
1h
3h
24h
TIA1-GFP
DMSO
VER-155008
g
DMSO
VER
TIA-1 SGs per cell
HNRNPK aggregates per cell
ns
*
Key
a unstressed
b 0h post-HS
c 1h post-HS
d 3h post-HS
e 6h post-HS
f 24h post-HS

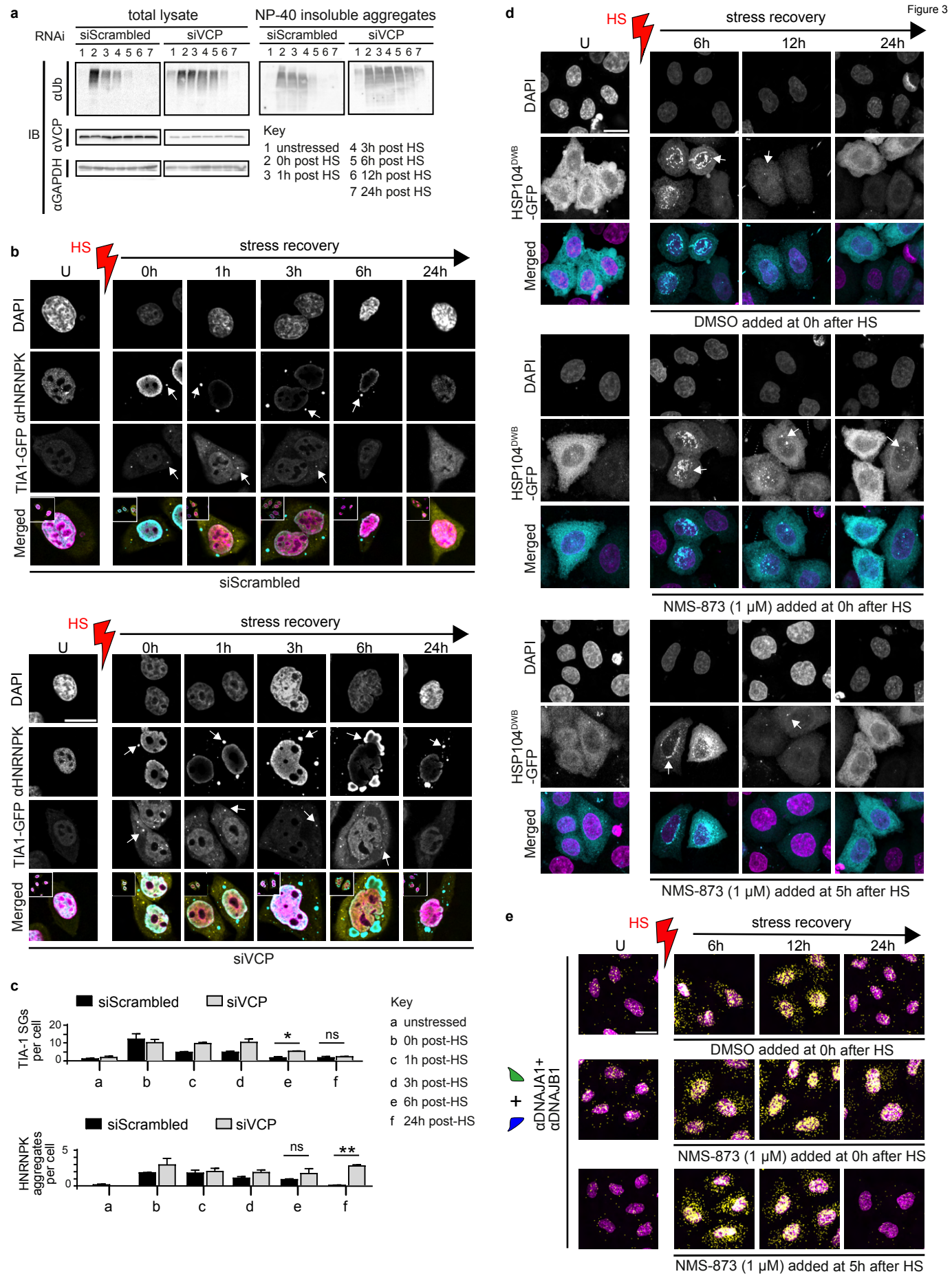
a
total lysate
NP-40 insoluble aggregates
RNAi
siScrambled
siVCP
1 2 3 4 5 6 7
IB
αUb
αVCP
αGAPDH
Key
1 unstressed
2 0h post HS
3 1h post HS
4 3h post HS
5 6h post HS
6 12h post HS
7 24h post HS
b
HS
stress recovery
U
0h
1h
3h
6h
24h
DAPI
αHNRNPK
TIA1-GFP
Merged
siScrambled
siVCP
c
siScrambled
siVCP
TIA-1 SGs per cell
HNRNPK aggregates per cell
ns
*
**
a
b
c
d
e
f
Key
a unstressed
b 0h post-HS
c 1h post-HS
d 3h post-HS
e 6h post-HS
f 24h post-HS
d
HS
stress recovery
U
6h
12h
24h
DAPI
HSP104DWB-GFP
Merged
DMSO added at 0h after HS
NMS-873 (1 μM) added at 0h after HS
NMS-873 (1 μM) added at 5h after HS
e
HS
stress recovery
U
6h
12h
24h
αDNAJA1+
αDNAJB1
DMSO added at 0h after HS
NMS-873 (1 μM) added at 0h after HS
NMS-873 (1 μM) added at 5h after HS

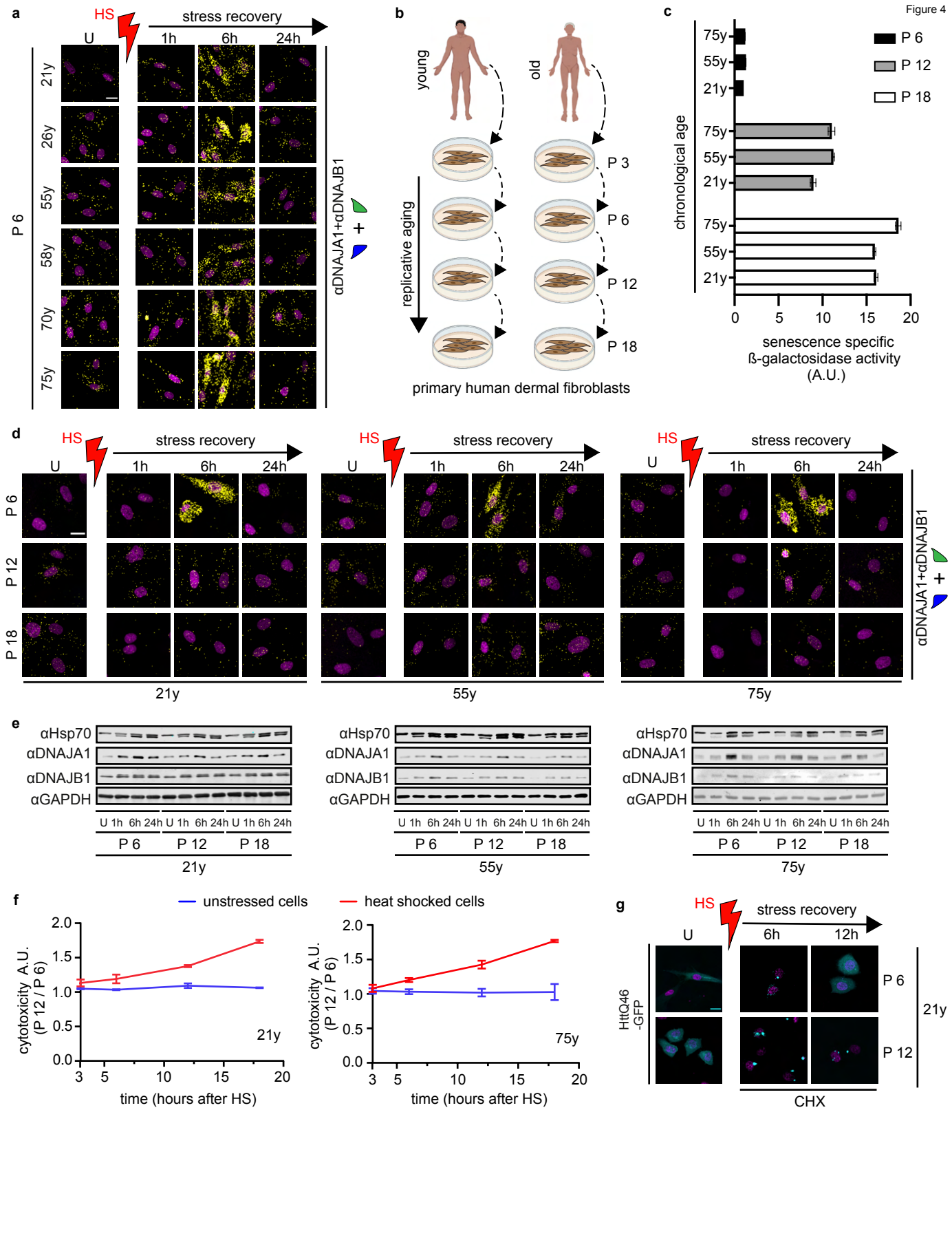
a
HS
stress recovery
U
1h
6h
24h
P 6
21y
26y
55y
58y
70y
75y
αDNAJA1+αDNAJB1
b
young
old
P 3
P 6
P 12
P 18
replicative aging
primary human dermal fibroblasts
c
P 6
P 12
P 18
chronological age
75y
55y
21y
0
5
10
15
20
senescence specific
ß-galactosidase activity
(A.U.)
d
HS
stress recovery
U
1h
6h
24h
P 6
P 12
P 18
αDNAJA1+αDNAJB1
21y
55y
75y
e
αHsp70
αDNAJA1
αDNAJB1
αGAPDH
U 1h 6h 24h U 1h 6h 24h U 1h 6h 24h
P 6
P 12
P 18
21y
55y
75y
f
unstressed cells
heat shocked cells
cytotoxicity A.U.
(P 12 / P 6)
2.0
1.5
1.0
0.5
0.0
3
5
10
15
20
time (hours after HS)
21y
75y
g
HS
stress recovery
U
6h
12h
HttQ46
-GFP
P 6
P 12
21y
CHX

a

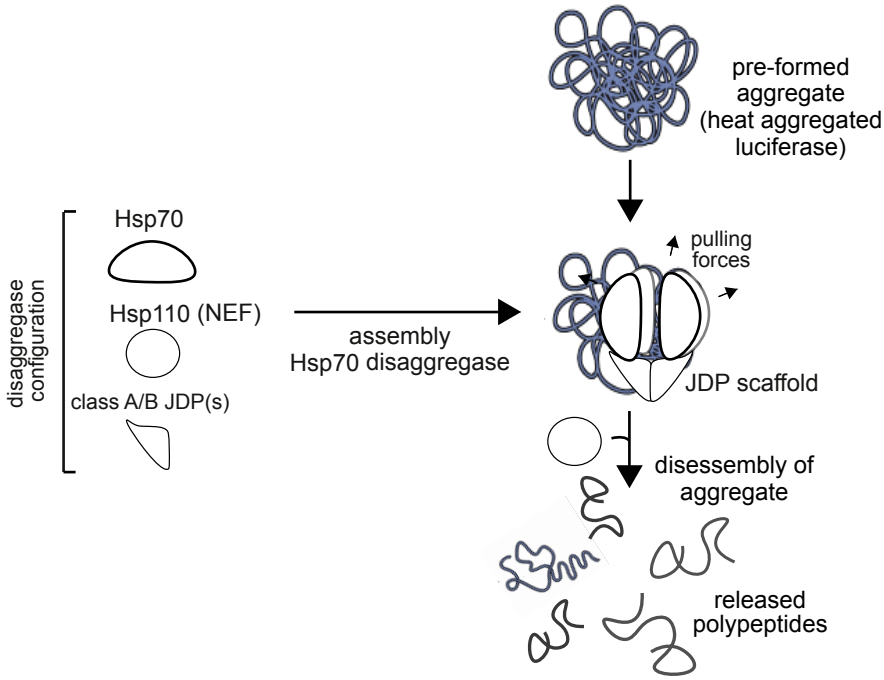
pre-formed aggregate (heat aggregated luciferase)
disaggregase configuration
Hsp70
Hsp110 (NEF)
class A/B JDP(s)
assembly Hsp70 disaggregase
pulling forces
JDP scaffold
disessembly of aggregate
released polypeptides

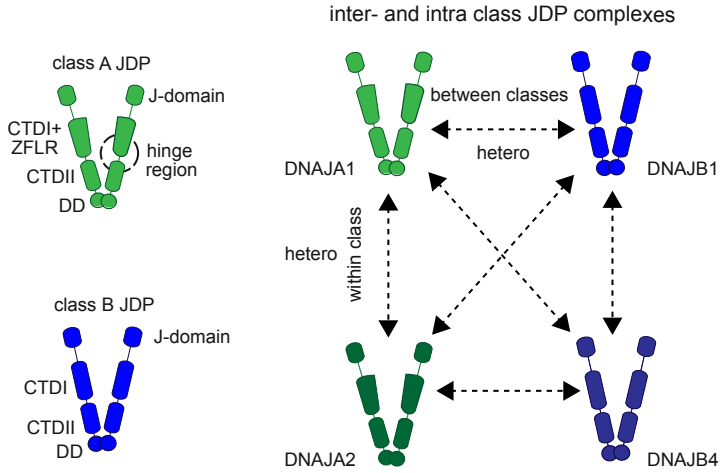
inter- and intra class JDP complexes
class A JDP
J-domain
CTDI+ ZFLR
hinge region
CTDII
DD
class B JDP
J-domain
CTDI
CTDII
DD
between classes
hetero
within class
hetero
DNAJA1
DNAJB1
DNAJA2
DNAJB4

b

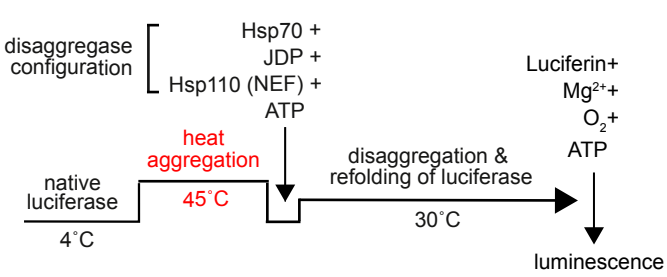
disaggregase configuration
Hsp70 +
JDP +
Hsp110 (NEF) +
ATP
heat aggregation
native luciferase
45˚C
4˚C
disaggregation & refolding of luciferase
30˚C
Luciferin+
Mg2+ +
O2 +
ATP
luminescence

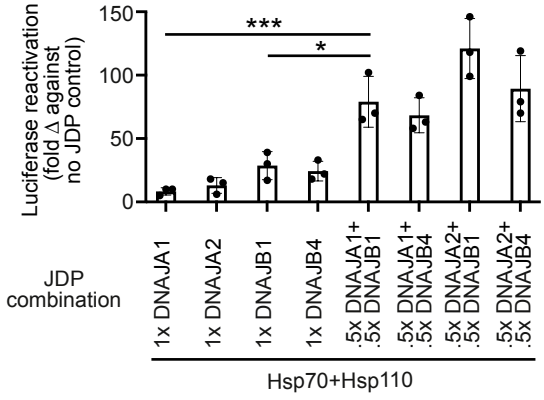
Luciferase reactivation (fold Δ against no JDP control)
150
100
50
0
***
*
JDP combination
1x DNAJA1
1x DNAJA2
1x DNAJB1
1x DNAJB4
.5x DNAJA1+ .5x DNAJB1
.5x DNAJA1+ .5x DNAJB4
.5x DNAJA2+ .5x DNAJB1
.5x DNAJA2+ .5x DNAJB4
Hsp70+Hsp110

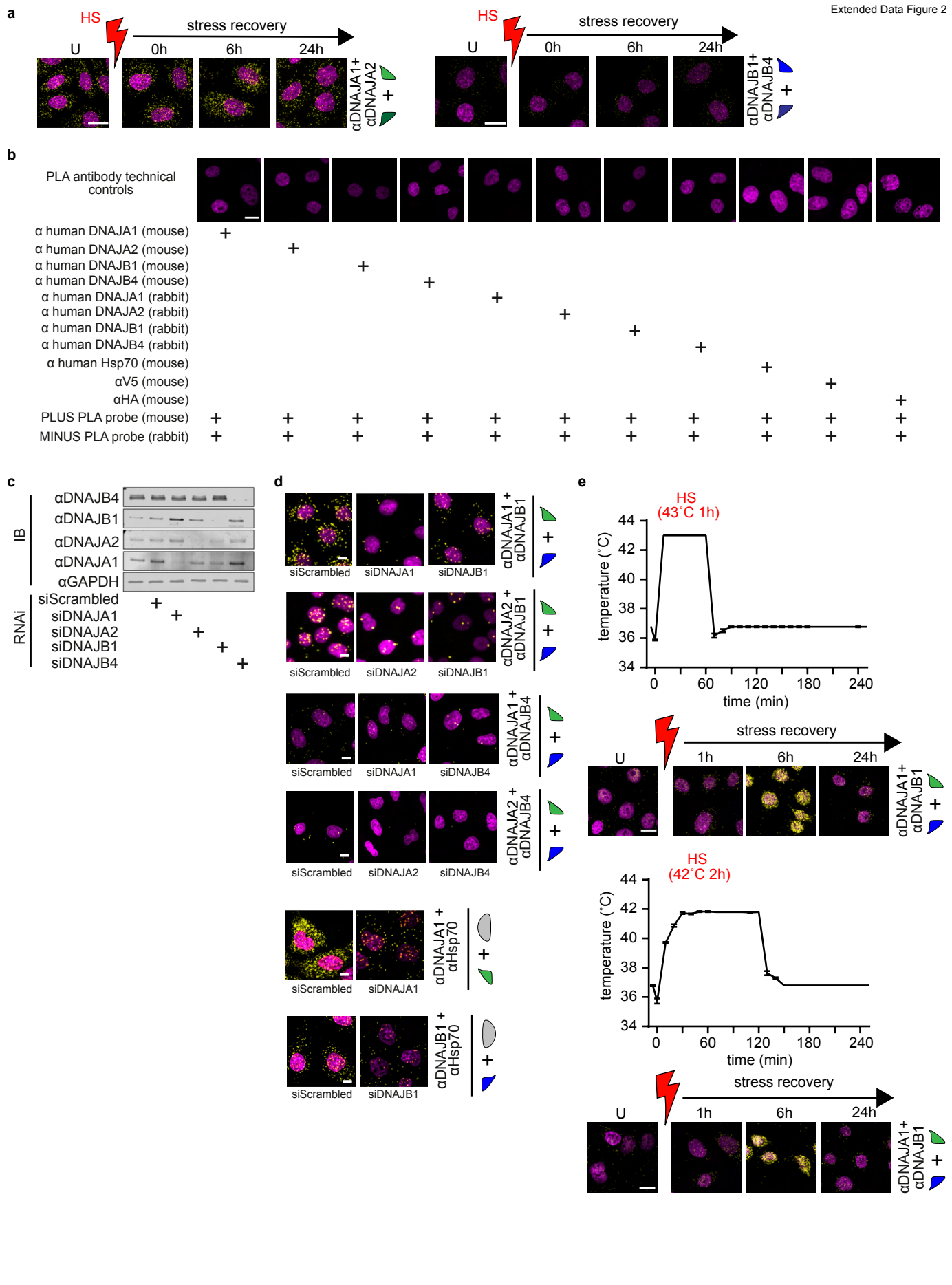
a
HS
stress recovery
U
0h
6h
24h
αDNAJA1+
αDNAJA2
+
HS
stress recovery
U
0h
6h
24h
αDNAJB1+
αDNAJB4
+
b
PLA antibody technical controls
α human DNAJA1 (mouse)
α human DNAJA2 (mouse)
α human DNAJB1 (mouse)
α human DNAJB4 (mouse)
α human DNAJA1 (rabbit)
α human DNAJA2 (rabbit)
α human DNAJB1 (rabbit)
α human DNAJB4 (rabbit)
α human Hsp70 (mouse)
αV5 (mouse)
αHA (mouse)
PLUS PLA probe (mouse)
MINUS PLA probe (rabbit)
c
IB
αDNAJB4
αDNAJB1
αDNAJA2
αDNAJA1
αGAPDH
RNAi
siScrambled
siDNAJA1
siDNAJA2
siDNAJB1
siDNAJB4
d
siScrambled
siDNAJA1
siDNAJB1
αDNAJA1 +
αDNAJB1
siScrambled
siDNAJA2
siDNAJB1
αDNAJA2 +
αDNAJB1
siScrambled
siDNAJA1
siDNAJB4
αDNAJA1 +
αDNAJB4
siScrambled
siDNAJA2
siDNAJB4
αDNAJA2 +
αDNAJB4
siScrambled
siDNAJA1
αDNAJA1 +
αHsp70
siScrambled
siDNAJB1
αDNAJB1 +
αHsp70
e
HS
(43˚C 1h)
temperature (˚C)
time (min)
stress recovery
U
1h
6h
24h
αDNAJA1+
αDNAJB1
+
HS
(42˚C 2h)
temperature (˚C)
time (min)
stress recovery
U
1h
6h
24h
αDNAJA1+
αDNAJB1
+

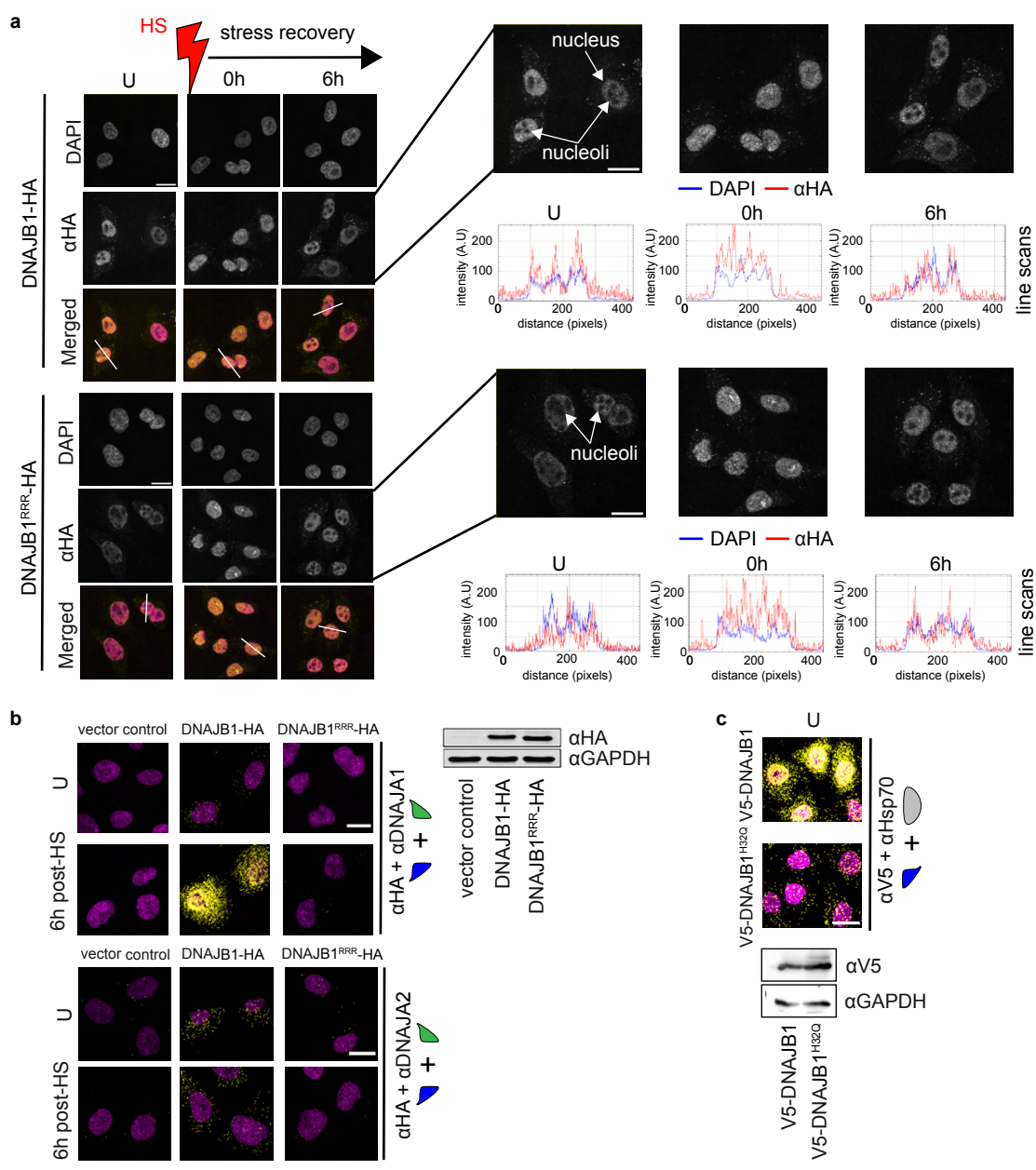
a
HS
stress recovery
U
0h
6h
DNAJB1-HA
DAPI
αHA
Merged
nucleus
nucleoli
DAPI αHA
intensity (A.U)
distance (pixels)
line scans
DNAJB1RRR-HA
b
vector control
DNAJB1-HA
DNAJB1RRR-HA
U
6h post-HS
αHA + αDNAJA1
αHA + αDNAJA2
αHA
αGAPDH
c
V5-DNAJB1
V5-DNAJB1H32Q
αV5 + αHsp70
αV5
αGAPDH

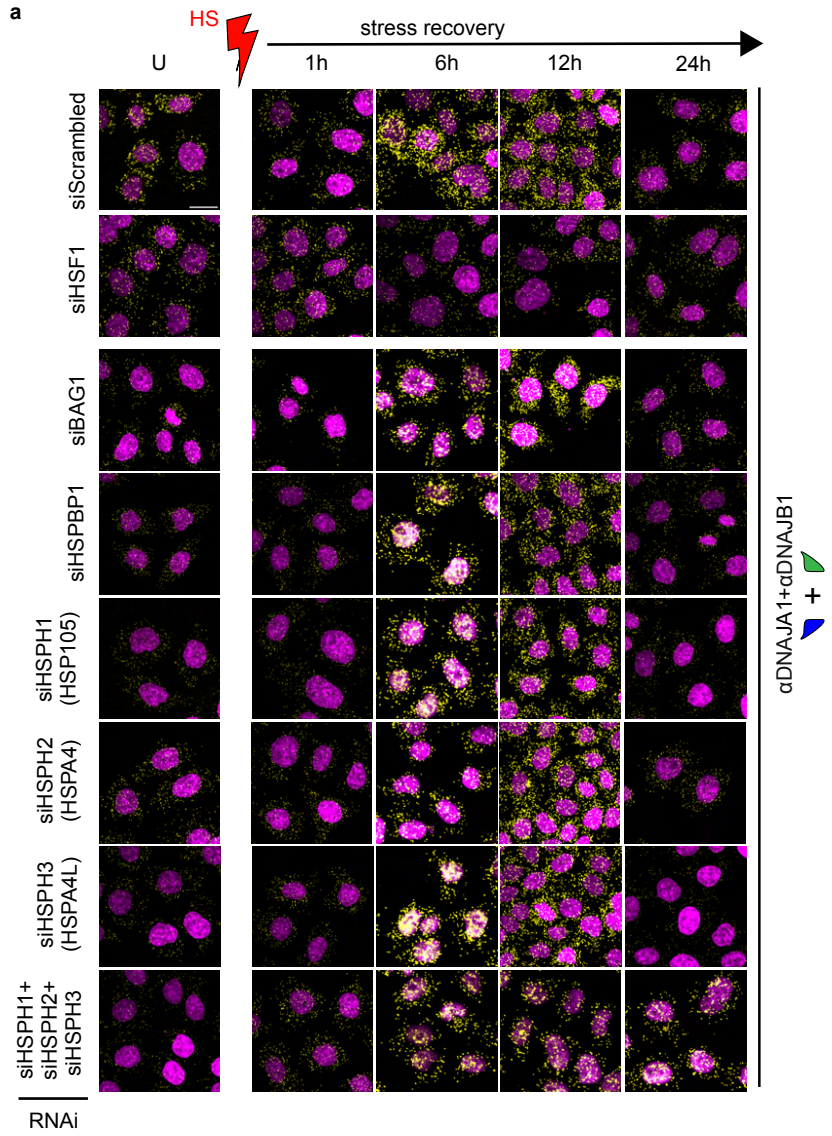
a
HS
stress recovery
U
1h
6h
12h
24h
siScrambled
siHSF1
siBAG1
siHSPBP1
siHSPH1 (HSP105)
siHSPH2 (HSPA4)
siHSPH3 (HSPA4L)
siHSPH1+ siHSPH2+ siHSPH3
RNAi
αDNAJA1+αDNAJB1
+

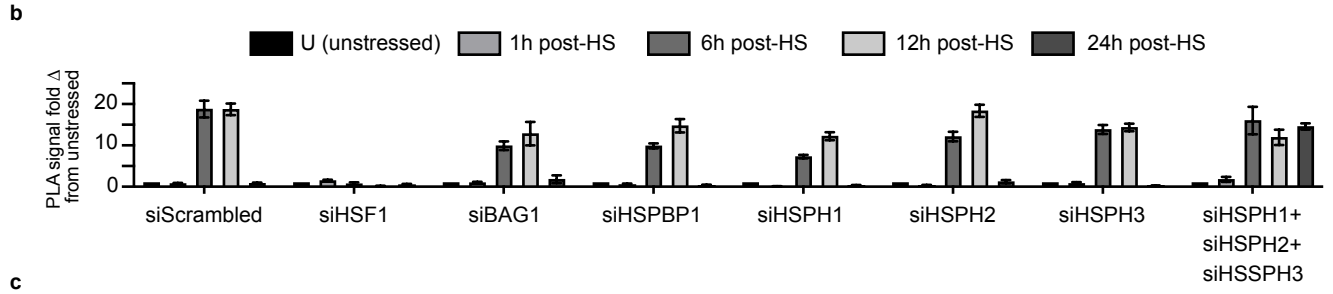
b
U (unstressed)
1h post-HS
6h post-HS
12h post-HS
24h post-HS
PLA signal fold Δ from unstressed
20
10
0
siScrambled
siHSF1
siBAG1
siHSPBP1
siHSPH1
siHSPH2
siHSPH3
siHSPH1+ siHSPH2+ siHSSPH3

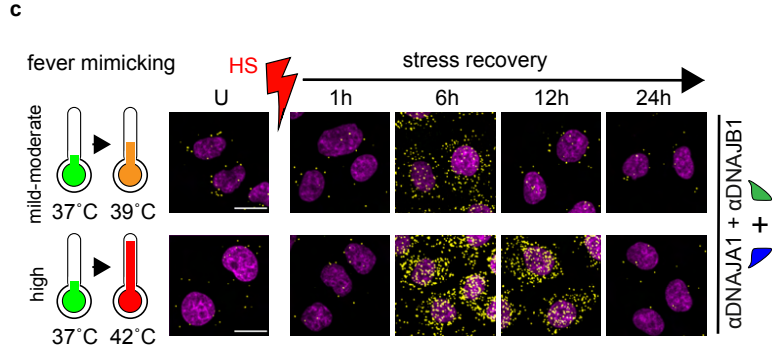
c
fever mimicking
HS
stress recovery
U
1h
6h
12h
24h
mild-moderate
37˚C
39˚C
high
37˚C
42˚C
αDNAJA1 + αDNAJB1
+

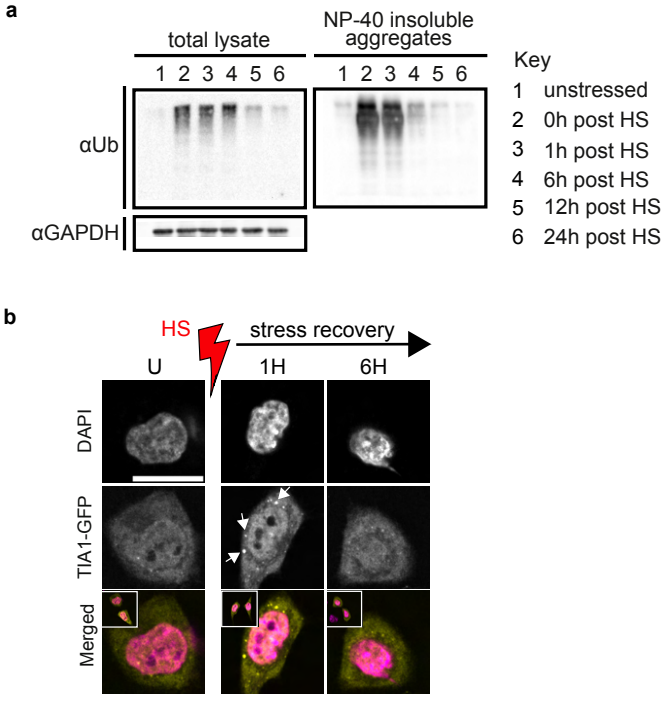
a
total lysate
NP-40 insoluble aggregates
1 2 3 4 5 6
1 2 3 4 5 6
αUb
αGAPDH
Key
1 unstressed
2 0h post HS
3 1h post HS
4 6h post HS
5 12h post HS
6 24h post HS
b
HS
stress recovery
U
1H
6H
DAPI
TIA1-GFP
Merged

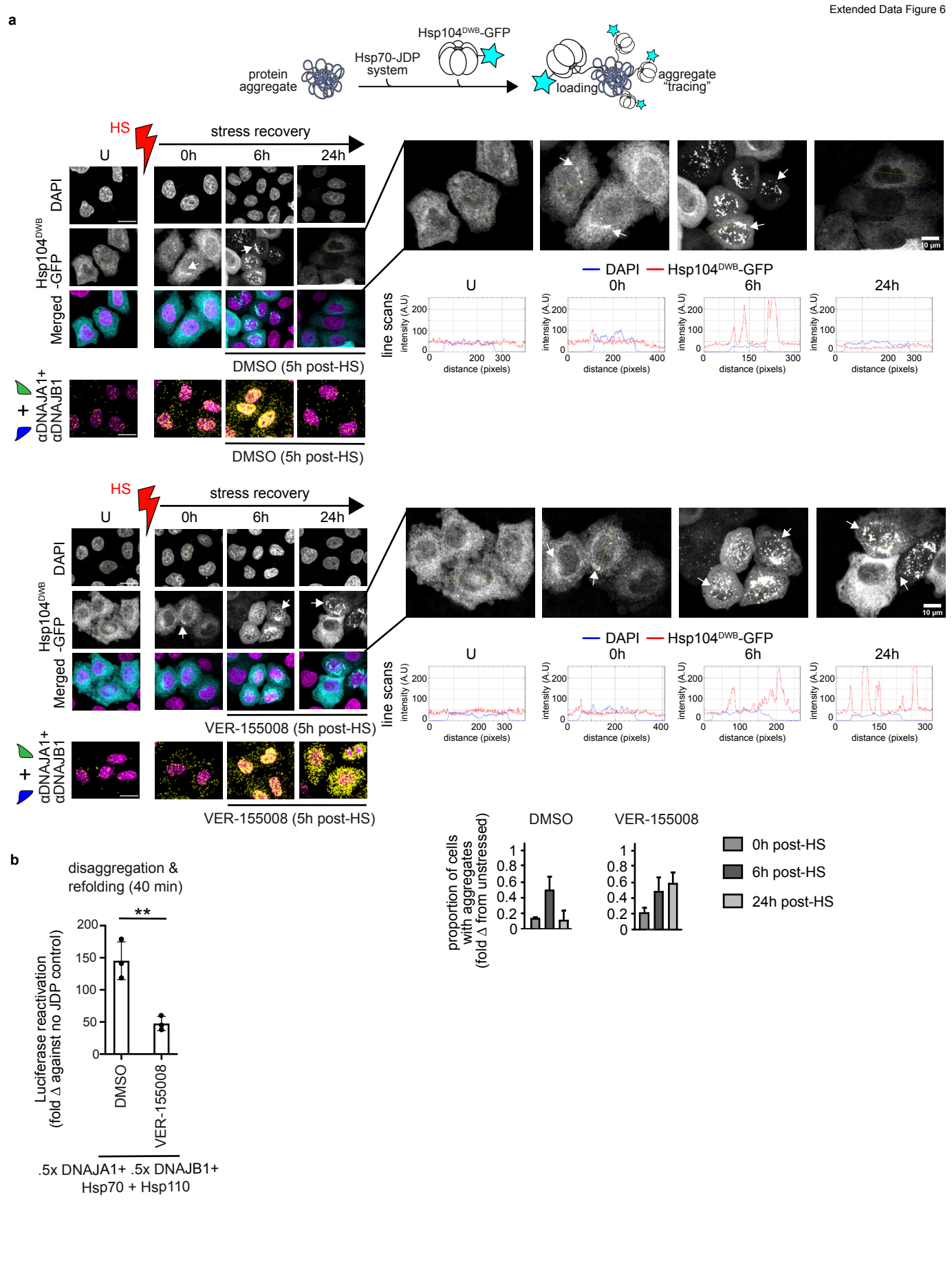
a
protein aggregate
Hsp70-JDP system
Hsp104DWB-GFP
loading
aggregate "tracing"
HS
stress recovery
U
0h
6h
24h
DAPI
Hsp104DWB -GFP
Merged
DMSO (5h post-HS)
αDNAJA1+ αDNAJB1
10 µm
DAPI
Hsp104DWB-GFP
line scans
intensity (A.U)
distance (pixels)
VER-155008 (5h post-HS)
b
disaggregation & refolding (40 min)
Luciferase reactivation (fold Δ against no JDP control)
**
DMSO
VER-155008
.5x DNAJA1+ .5x DNAJB1+ Hsp70 + Hsp110
proportion of cells with aggregates (fold Δ from unstressed)
0h post-HS
6h post-HS
24h post-HS

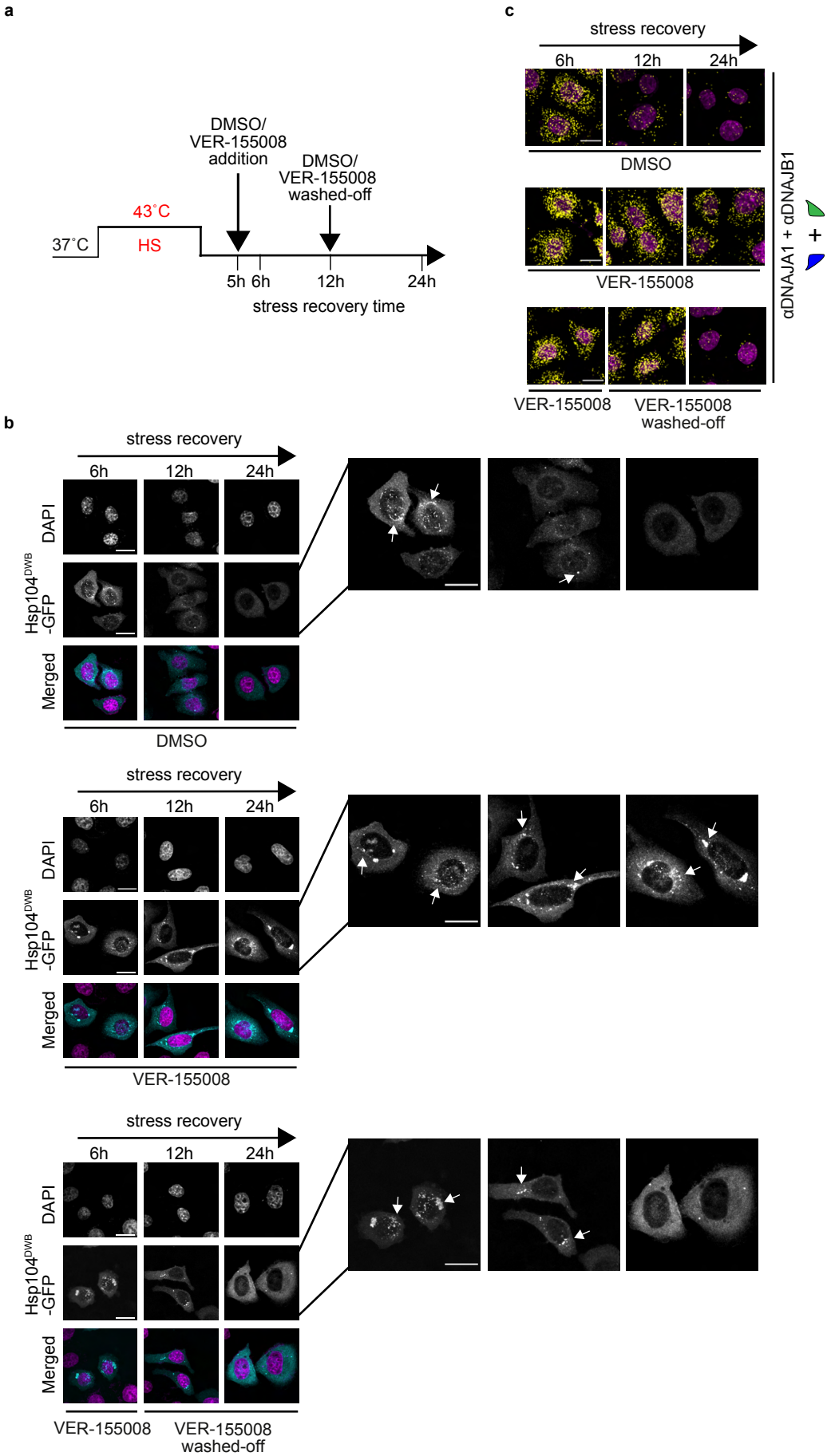
a
DMSO/
VER-155008
addition
DMSO/
VER-155008
washed-off
43˚C
37˚C
HS
5h 6h
12h
24h
stress recovery time
c
stress recovery
6h
12h
24h
DMSO
VER-155008
VER-155008
VER-155008
washed-off
αDNAJA1 + αDNAJB1
b
stress recovery
6h
12h
24h
DAPI
Hsp104DWB
-GFP
Merged
DMSO
VER-155008
VER-155008
VER-155008
washed-off

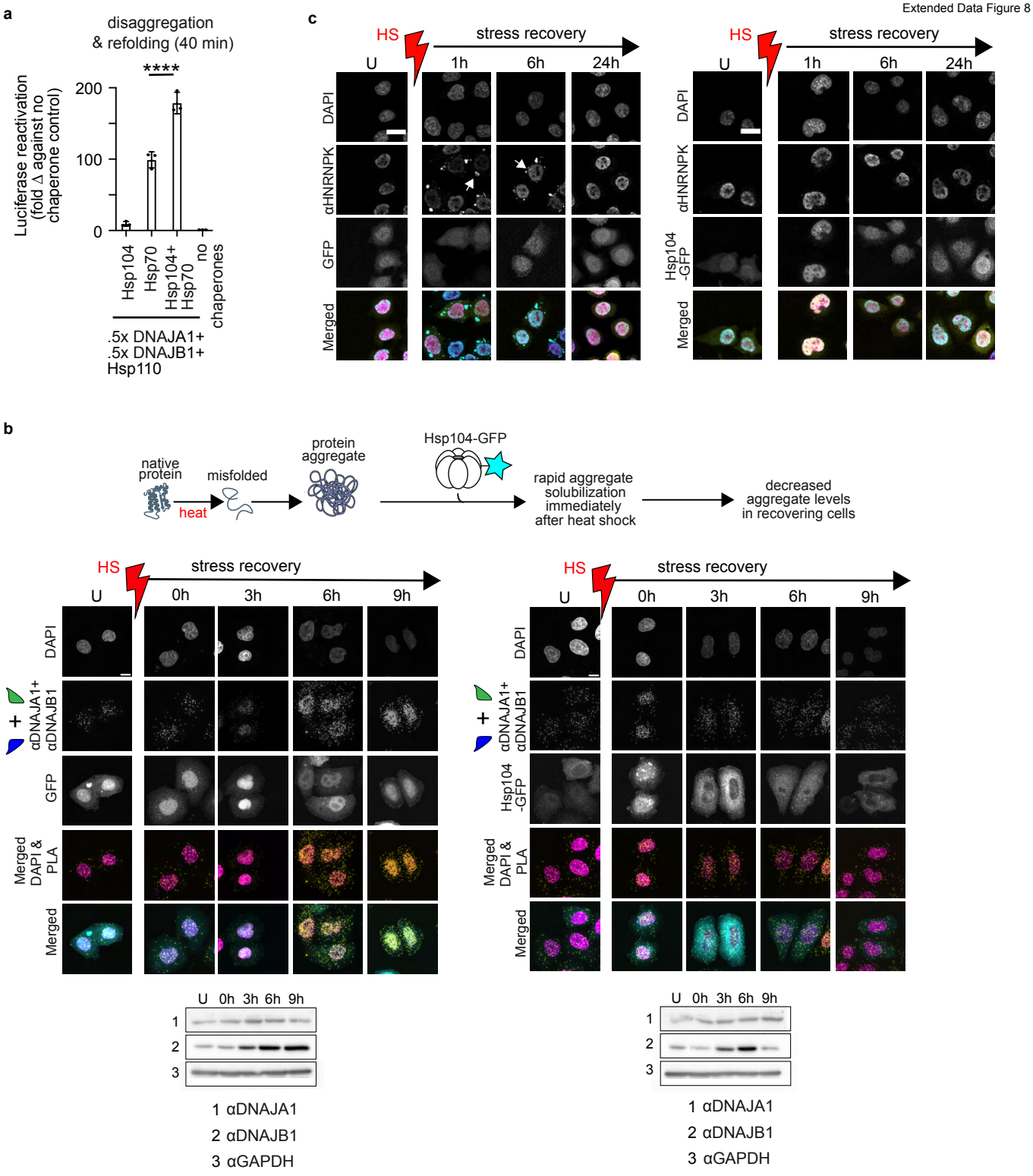
a
disaggregation
& refolding (40 min)
****
Luciferase reactivation
(fold Δ against no
chaperone control)
200
100
0
Hsp104
Hsp70
Hsp104+
Hsp70
no
chaperones
.5x DNAJA1+
.5x DNAJB1+
Hsp110
c
HS
stress recovery
U
1h
6h
24h
DAPI
αHNRNPK
GFP
Merged
Hsp104
-GFP
b
native
protein
misfolded
heat
protein
aggregate
Hsp104-GFP
rapid aggregate
solubilization
immediately
after heat shock
decreased
aggregate levels
in recovering cells
0h
3h
9h
αDNAJA1+
αDNAJB1
Merged
DAPI &
PLA
1 αDNAJA1
2 αDNAJB1
3 αGAPDH

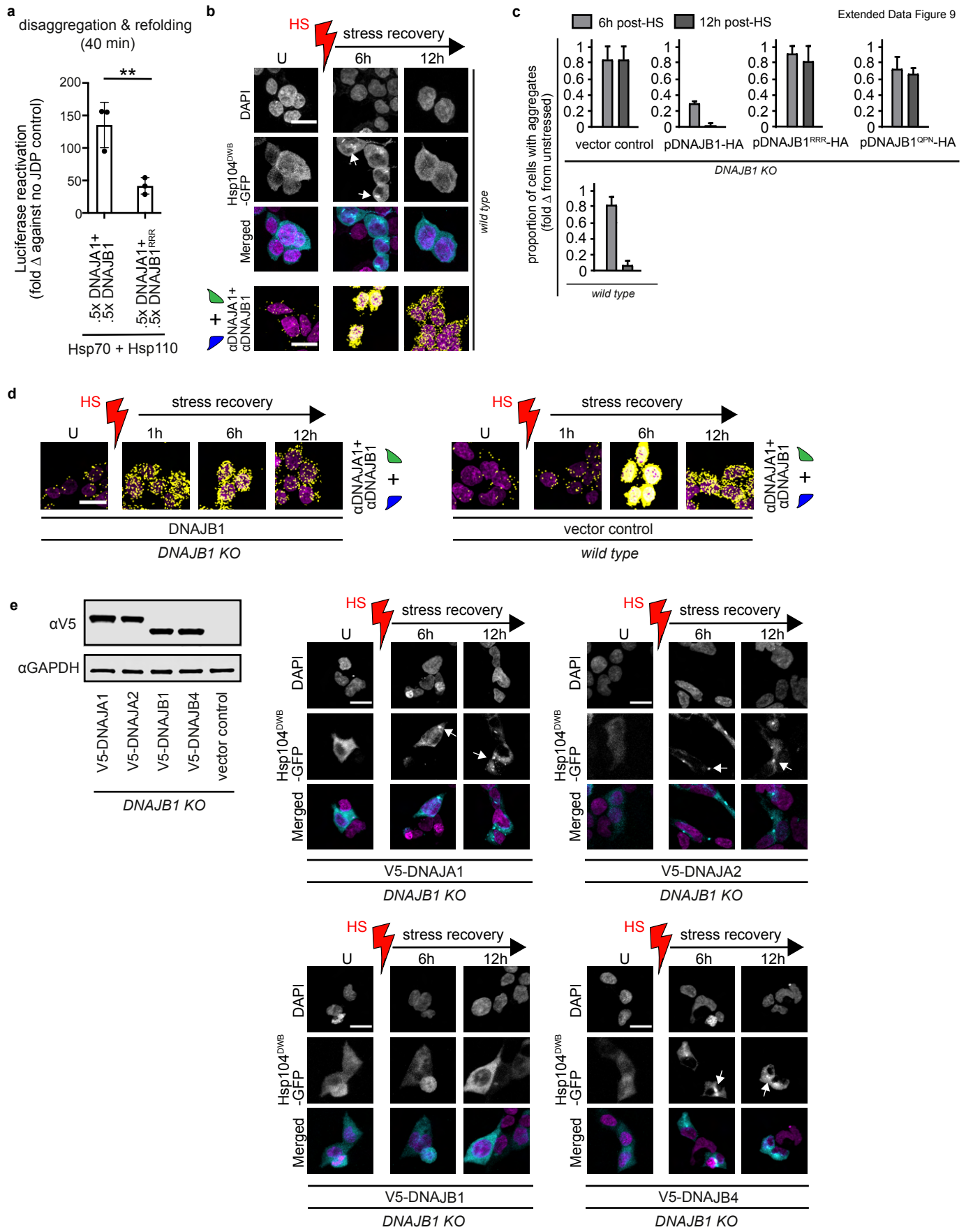
a
disaggregation & refolding
(40 min)
**
Luciferase reactivation
(fold Δ against no JDP control)
200
150
100
50
0
.5x DNAJA1+
.5x DNAJB1
.5x DNAJA1+
.5x DNAJB1RRR
Hsp70 + Hsp110
b
HS
stress recovery
U
6h
12h
DAPI
Hsp104DWB
-GFP
Merged
αDNAJA1+
αDNAJB1
wild type
c
6h post-HS
12h post-HS
proportion of cells with aggregates
(fold Δ from unstressed)
vector control
pDNAJB1-HA
pDNAJB1RRR-HA
pDNAJB1QPN-HA
DNAJB1 KO
wild type
d
HS
stress recovery
U
1h
6h
12h
αDNAJA1+
αDNAJB1
DNAJB1
DNAJB1 KO
vector control
wild type
e
αV5
αGAPDH
V5-DNAJA1
V5-DNAJA2
V5-DNAJB1
V5-DNAJB4
vector control
DNAJB1 KO
V5-DNAJA1
V5-DNAJA2
V5-DNAJB1
V5-DNAJB4

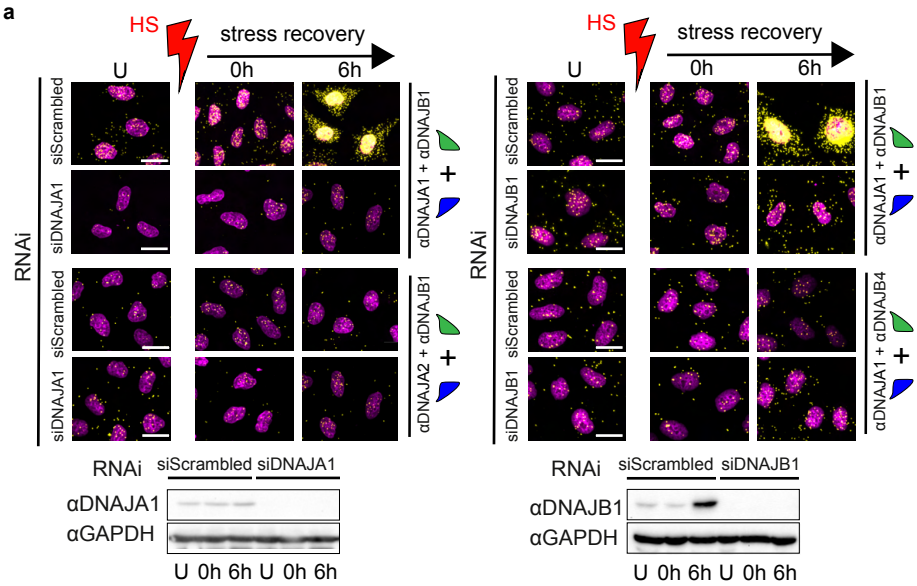
a
HS
stress recovery
U
0h
6h
RNAi
siScrambled
siDNAJA1
siDNAJB1
siDNAJA2
siDNAJB4
αDNAJA1 + αDNAJB1
αDNAJA2 + αDNAJB1
αDNAJA1 + αDNAJB4
+
αDNAJA1
αDNAJB1
αGAPDH
U 0h 6h U 0h 6h

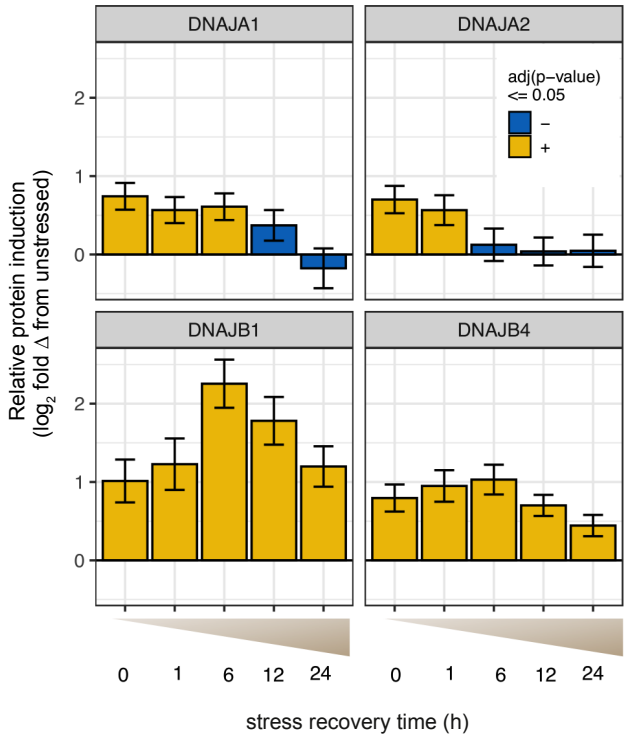
b
DNAJA1
DNAJA2
DNAJB1
DNAJB4
adj(p−value)
<= 0.05
−
+
Relative protein induction
(log2 fold Δ from unstressed)
0
1
2
0 1 6 12 24
stress recovery time (h)

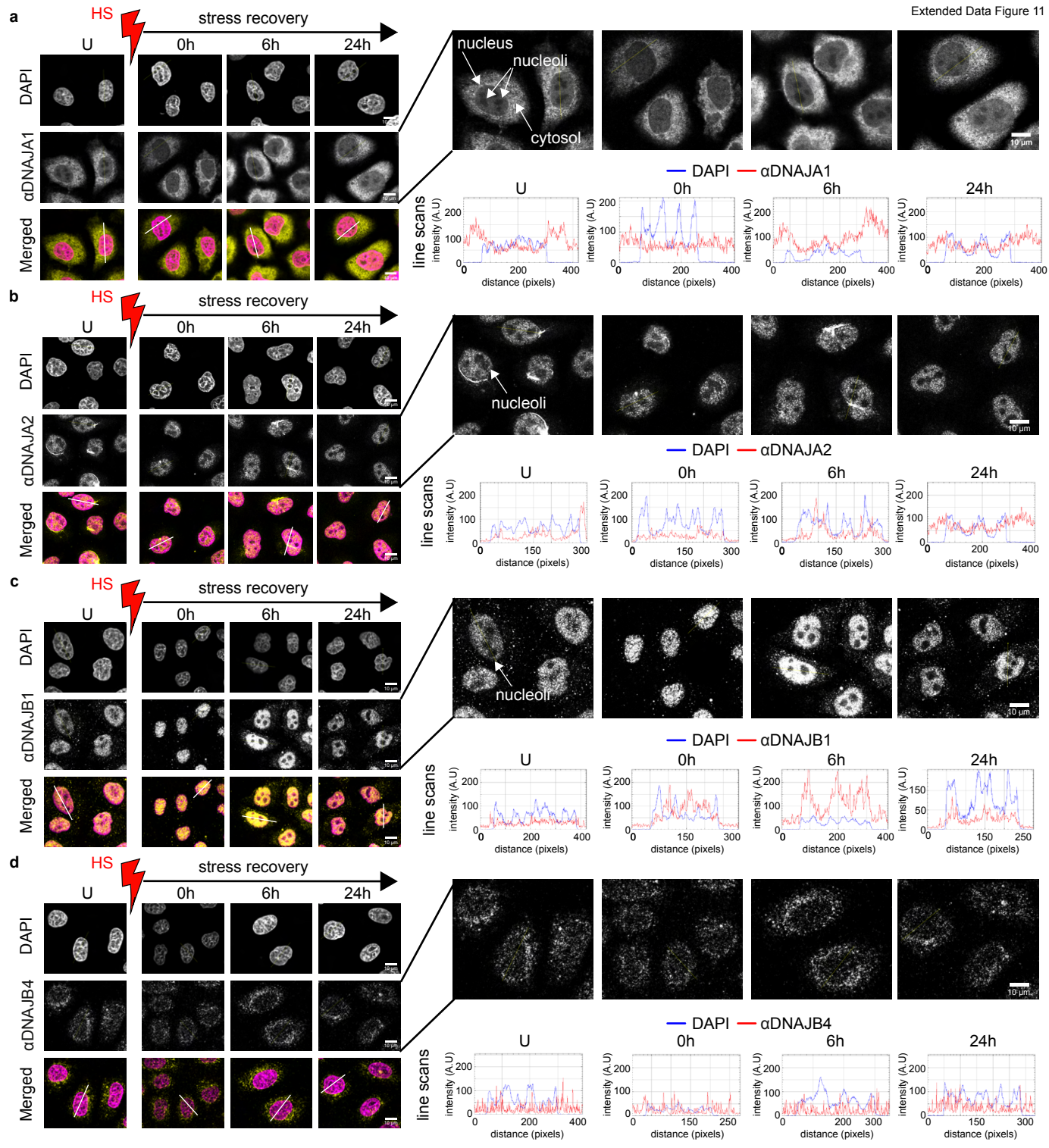
a
HS
stress recovery
U
0h
6h
24h
DAPI
αDNAJA1
Merged
nucleus
nucleoli
cytosol
10 µm
DAPI
αDNAJA1
line scans
intensity (A.U)
distance (pixels)
b
αDNAJA2
nucleoli
αDNAJA2
c
αDNAJB1
αDNAJB1
d
αDNAJB4
αDNAJB4

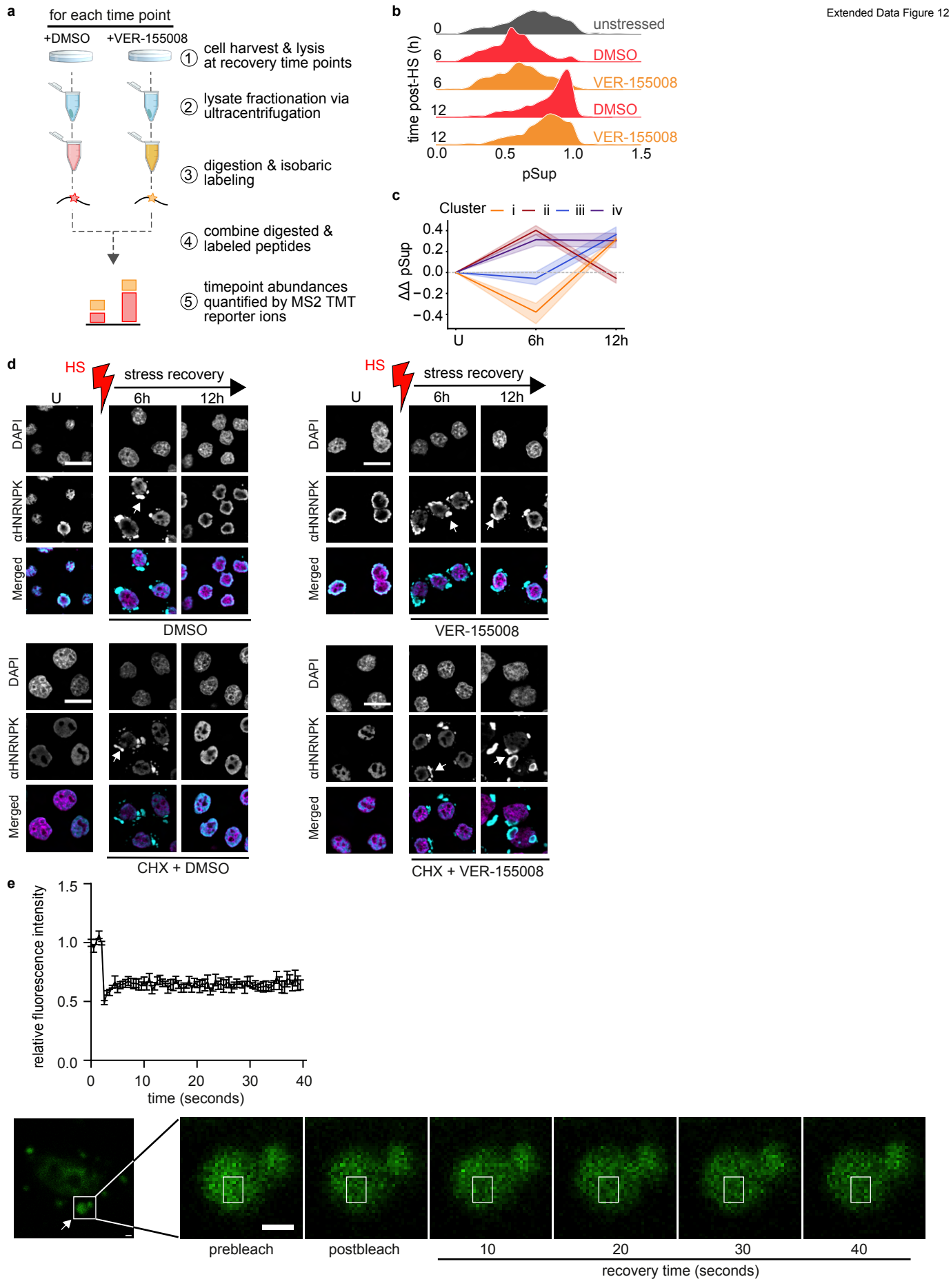
a
for each time point
+DMSO
+VER-155008
① cell harvest & lysis at recovery time points
② lysate fractionation via ultracentrifugation
③ digestion & isobaric labeling
④ combine digested & labeled peptides
⑤ timepoint abundances quantified by MS2 TMT reporter ions
b
time post-HS (h)
0
unstressed
6
DMSO
6
VER-155008
12
DMSO
12
VER-155008
0.0
0.5
1.0
1.5
pSup
c
Cluster i ii iii iv
ΔΔ pSup
0.4
0.2
0.0
−0.2
−0.4
U
6h
12h
d
HS
stress recovery
U
6h
12h
DAPI
αHNRNPK
Merged
DMSO
VER-155008
CHX + DMSO
CHX + VER-155008
e
relative fluorescence intensity
1.5
1.0
0.5
0.0
0
10
20
30
40
time (seconds)
prebleach
postbleach
10
20
30
40
recovery time (seconds)

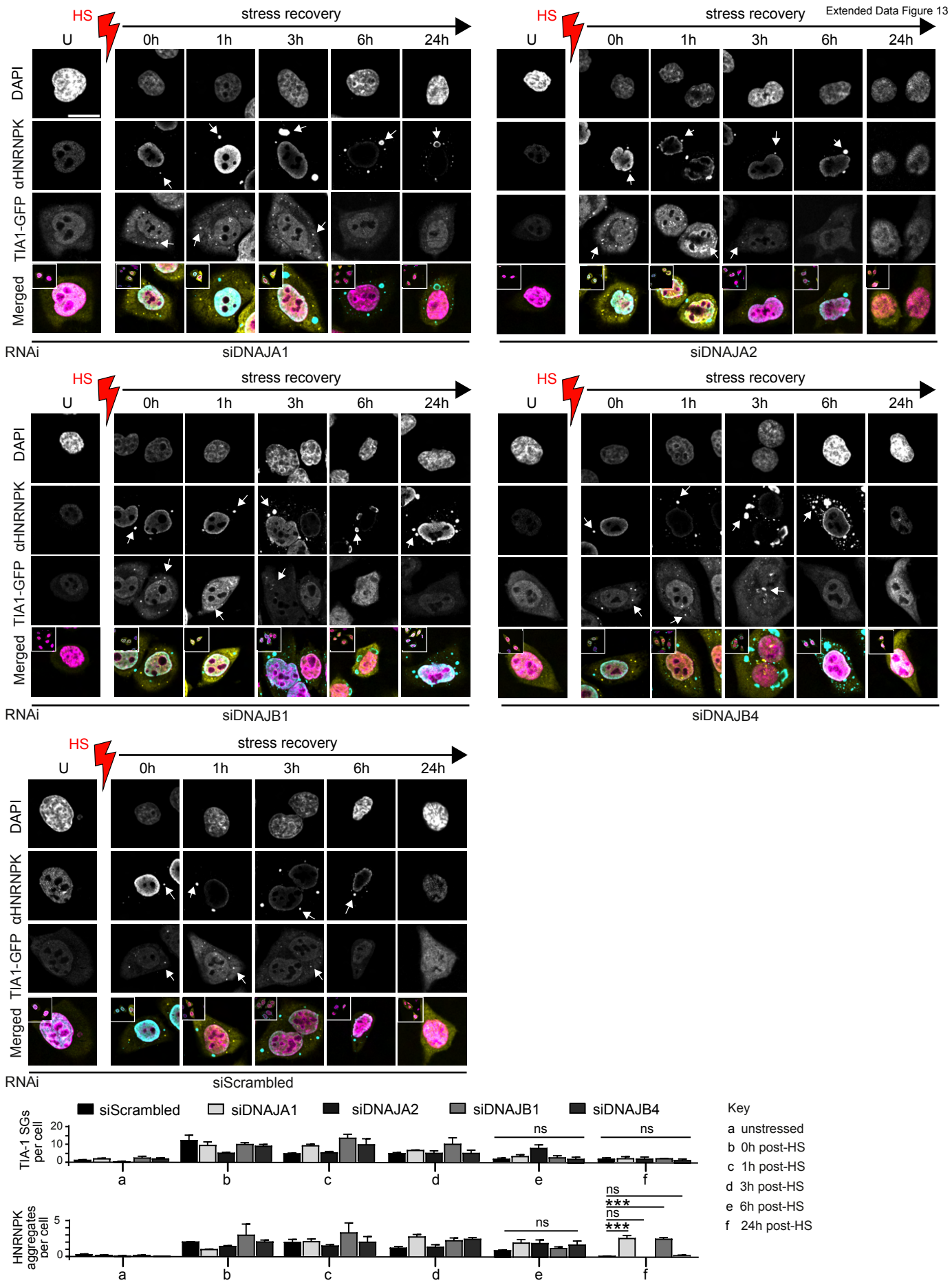
HS
stress recovery
U
0h
1h
3h
6h
24h
DAPI
αHNRNPK
TIA1-GFP
Merged
RNAi
siDNAJA1
siDNAJA2
siDNAJB1
siDNAJB4
siScrambled
TIA-1 SGs per cell
HNRNPK aggregates per cell
ns
***
a
b
c
d
e
f
Key
a unstressed
b 0h post-HS
c 1h post-HS
d 3h post-HS
e 6h post-HS
f 24h post-HS

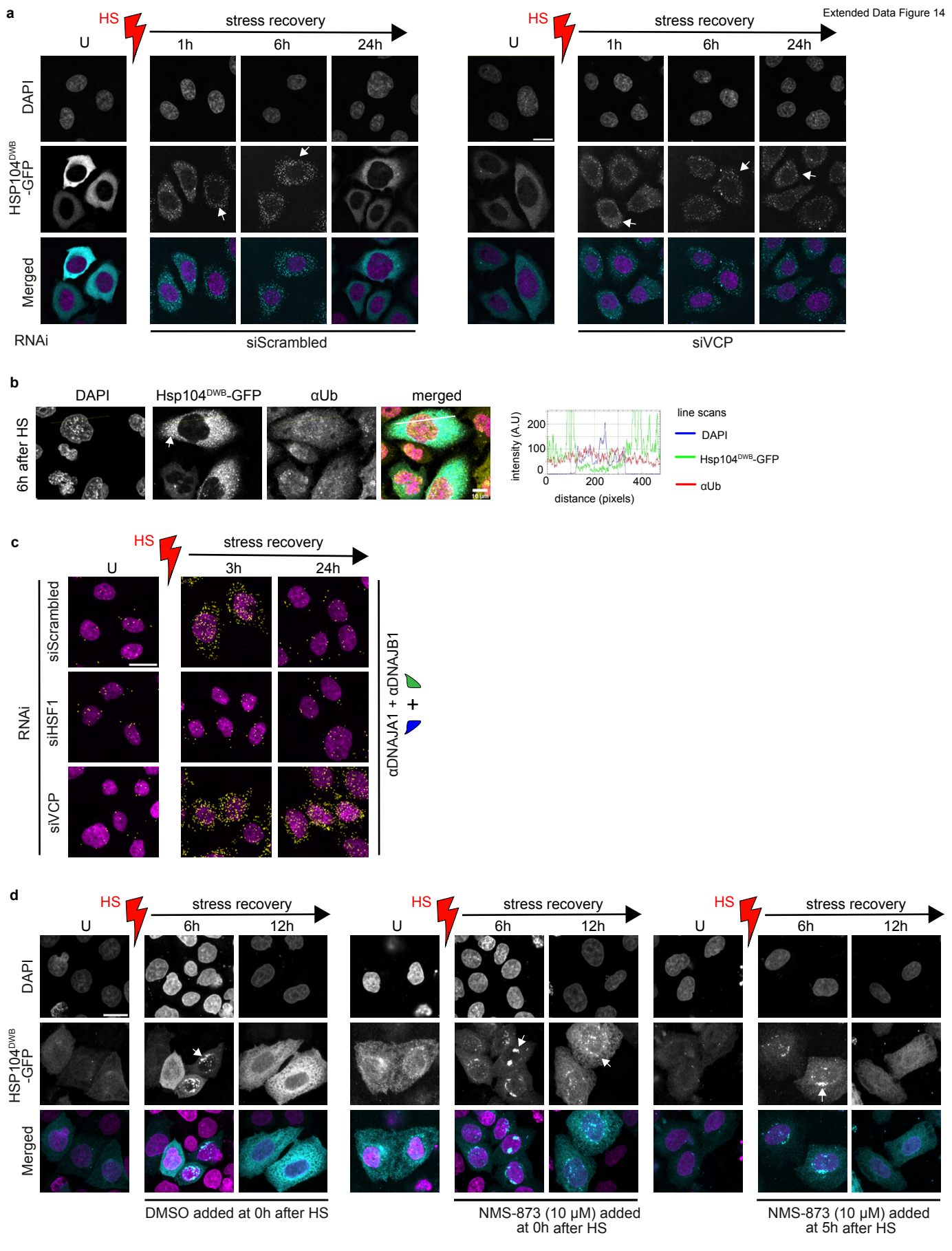
a
HS
stress recovery
U
1h
6h
24h
DAPI
HSP104DWB-GFP
Merged
RNAi
siScrambled
siVCP
b
DAPI
Hsp104DWB-GFP
αUb
merged
6h after HS
intensity (A.U)
200
100
0
0
200
400
distance (pixels)
line scans
DAPI
Hsp104DWB-GFP
αUb
c
3h
siScrambled
siHSF1
siVCP
αDNAJA1 + αDNAJB1
d
DMSO added at 0h after HS
NMS-873 (10 μM) added at 0h after HS
NMS-873 (10 μM) added at 5h after HS

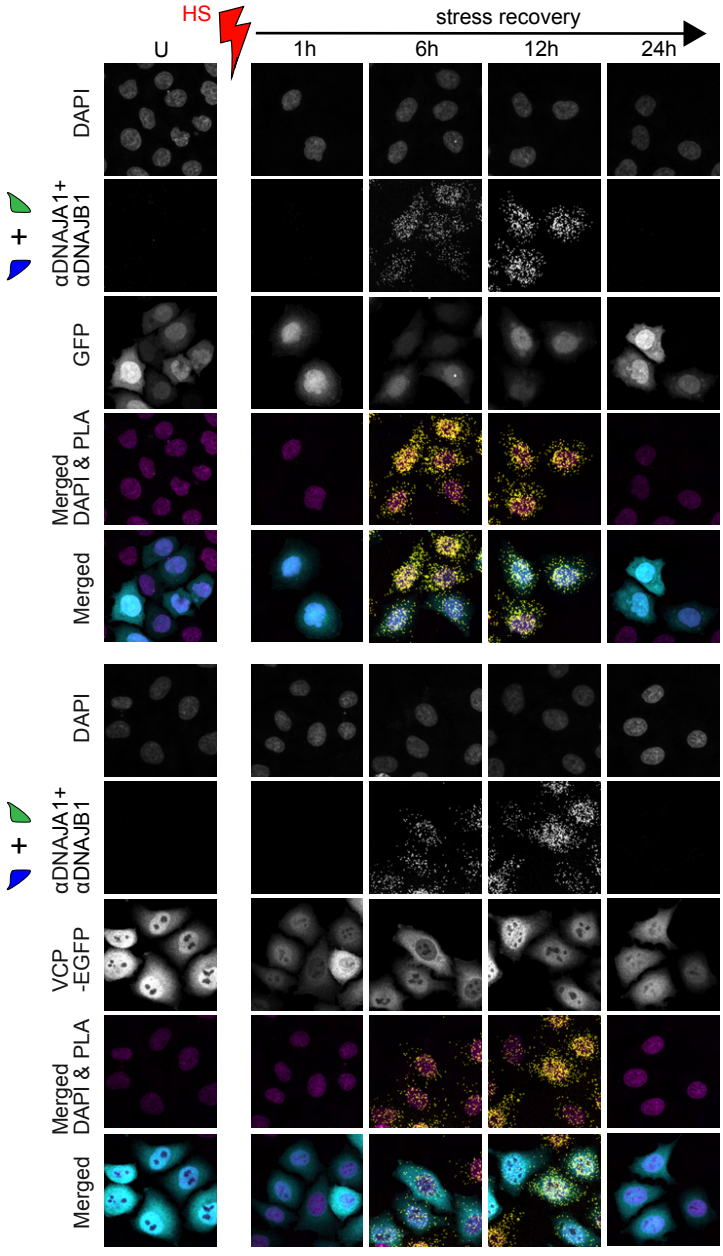
HS
stress recovery
U
1h
6h
12h
24h
DAPI
αDNAJA1+
αDNAJB1
GFP
Merged
DAPI & PLA
Merged
DAPI
αDNAJA1+
αDNAJB1
VCP
-EGFP
Merged
DAPI & PLA
Merged

a

Key

1 unstressed
2 0h post-HS
3 1h post-HS
4 6h post-HS
5 12h post-HS
6 24h post-HS

αDNAJA1
αDNAJB1
αGAPDH
IB

1 2 3 4 5 6

1 unstressed
2 1h post-HS
3 6h post-HS
4 24h post-HS

αHsp70
αGAPDH
IB

1 2 3 4

b

DNAJA1 mRNA

Relative mRNA induction (log_2 fold Δ from ΔΔCt)

8 4 0 -4

a b c d e f

DNAJB1 mRNA

Relative mRNA induction (log_2 fold Δ from ΔΔCt)

8 4 0 -4

a b c d e f

Key

a 30min HS
b 0h post-HS
c 1h post-HS
d 3h post-HS
e 6h post-HS
f 24h post-HS

c

RNAi

siScrambled siHSF-1

U 0h 6h U 0h 6h

IB

αHSF1
αDNAJA1
αDNAJB1
αGAPDH

HS stress recovery

U 0h 6h

RNAi

siScrambled
siHSF-1

αDNAJA1 + αDNAJB1

d

HS stress recovery

U 0h 6h 24h

DAPI
Hsp104^{DWB}-GFP
Merged

siScrambled

10 µm

DAPI — Hsp104^{DWB}-GFP

line scans

U 0h 6h 24h

intensity (A.U)

distance (pixels)

HS stress recovery

U 0h 6h 24h

DAPI
Hsp104^{DWB}-GFP
Merged

siHSF-1

10 µm

DAPI — Hsp104^{DWB}-GFP

line scans

U 0h 6h 24h

intensity (A.U)

distance (pixels)

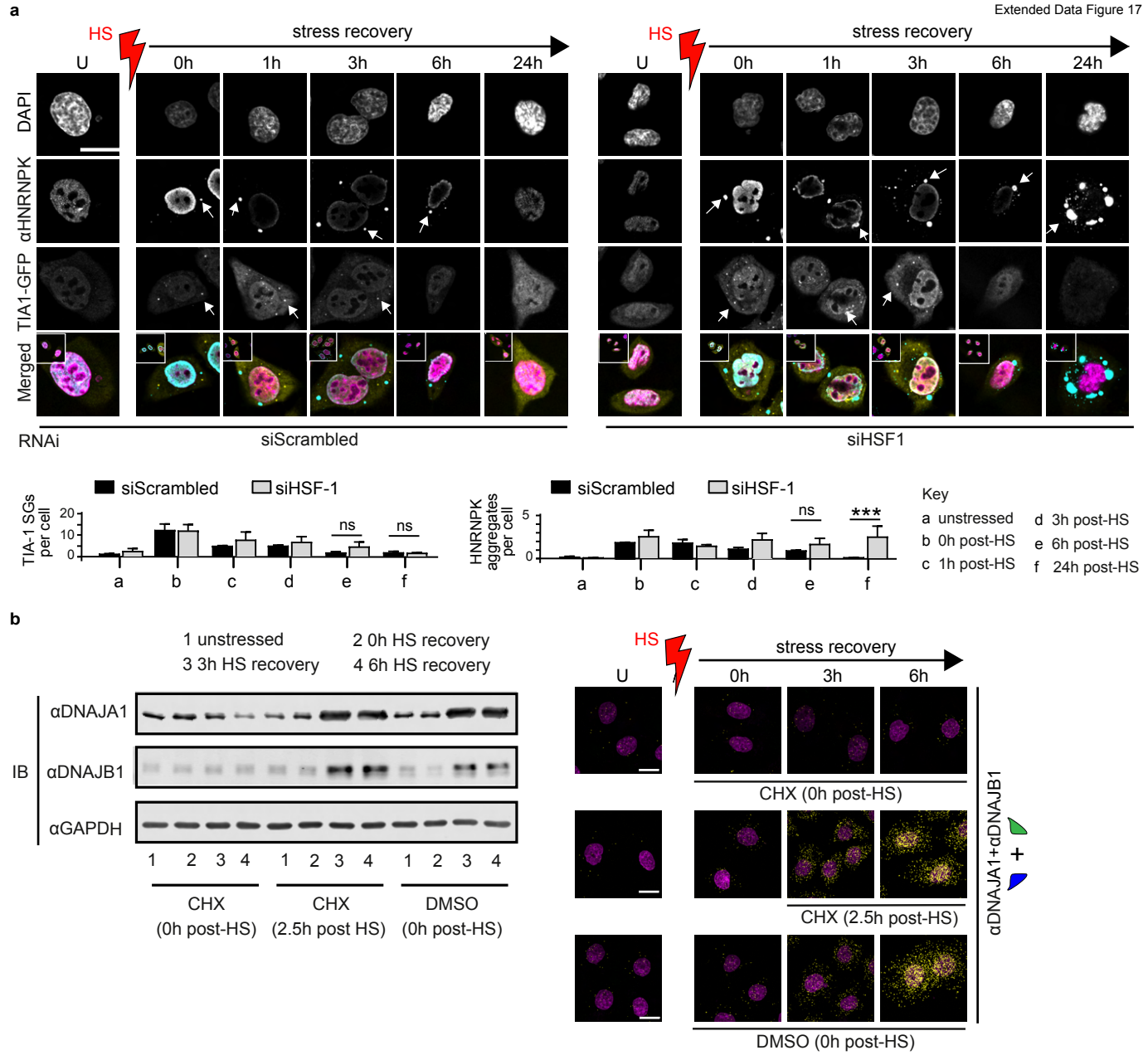
a
HS
stress recovery
U
0h
1h
3h
6h
24h
DAPI
αHNRNPK
TIA1-GFP
Merged
RNAi
siScrambled
siHSF1
siScrambled
siHSF-1
TIA-1 SGs per cell
HNRNPK aggregates per cell
ns
***
a
b
c
d
e
f
Key
a unstressed
b 0h post-HS
c 1h post-HS
d 3h post-HS
e 6h post-HS
f 24h post-HS
b
1 unstressed
2 0h HS recovery
3 3h HS recovery
4 6h HS recovery
IB
αDNAJA1
αDNAJB1
αGAPDH
CHX (0h post-HS)
CHX (2.5h post HS)
DMSO (0h post-HS)
CHX (0h post-HS)
CHX (2.5h post-HS)
DMSO (0h post-HS)
αDNAJA1+αDNAJB1

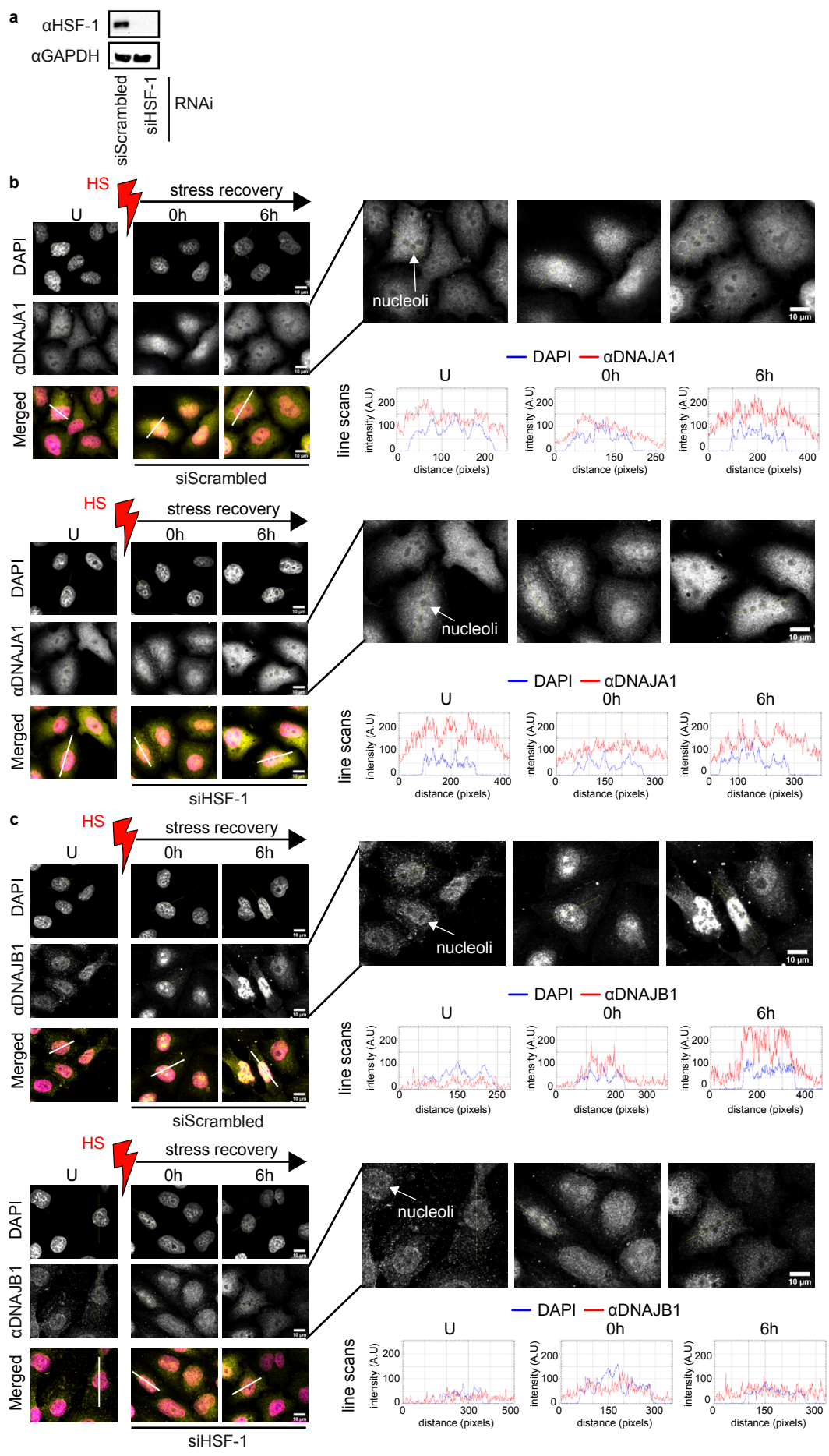
a
αHSF-1
αGAPDH
siScrambled
siHSF-1
RNAi
b
HS
stress recovery
U
0h
6h
DAPI
αDNAJA1
Merged
siScrambled
nucleoli
10 µm
DAPI
αDNAJA1
line scans
intensity (A.U)
distance (pixels)
siHSF-1
c
αDNAJB1
siScrambled
siHSF-1

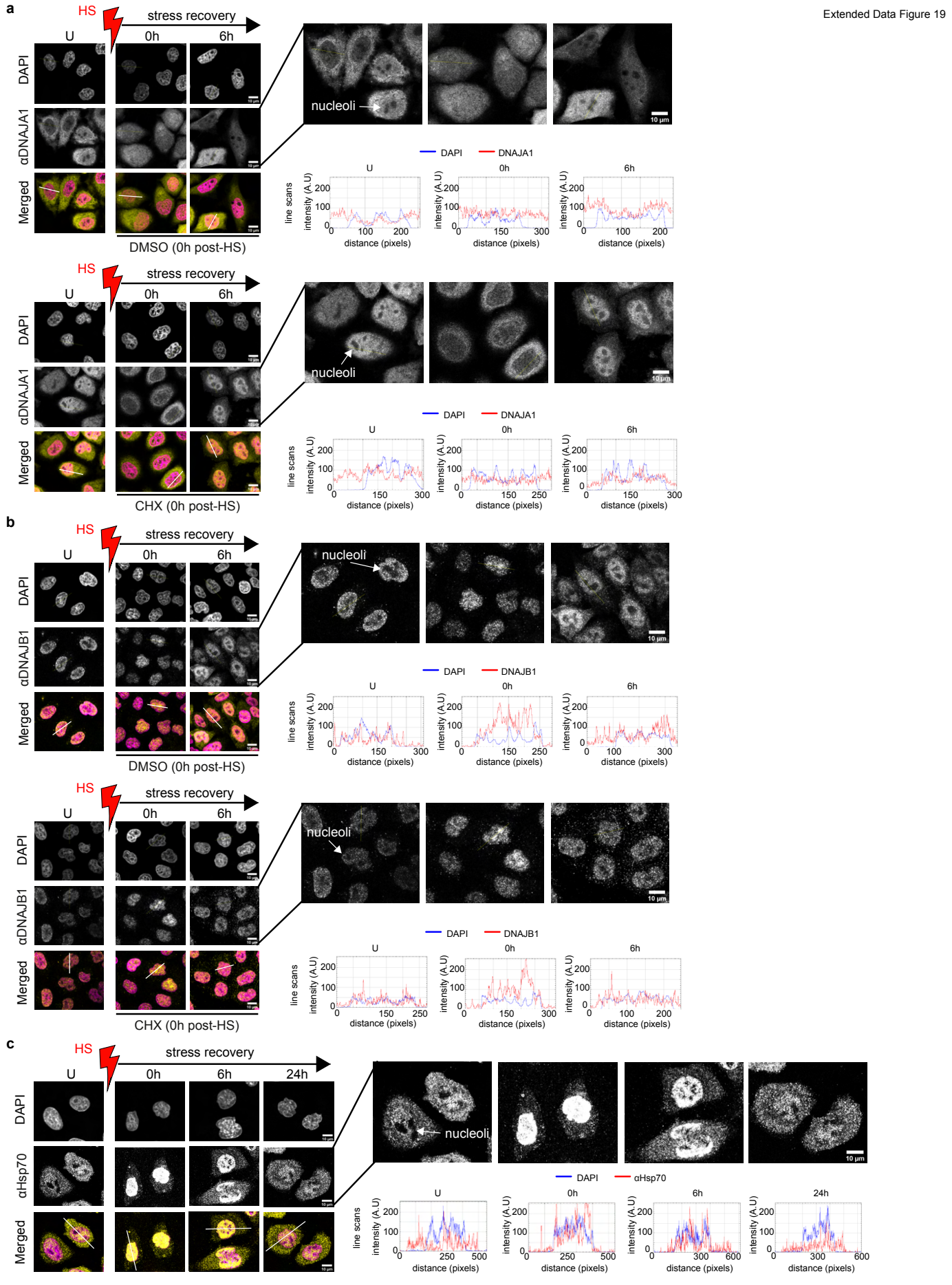
a
HS
stress recovery
U
0h
6h
DAPI
αDNAJA1
Merged
nucleoli
10 µm
DMSO (0h post-HS)
CHX (0h post-HS)
DAPI
DNAJA1
line scans
intensity (A.U)
distance (pixels)
b
αDNAJB1
DNAJB1
c
24h
αHsp70

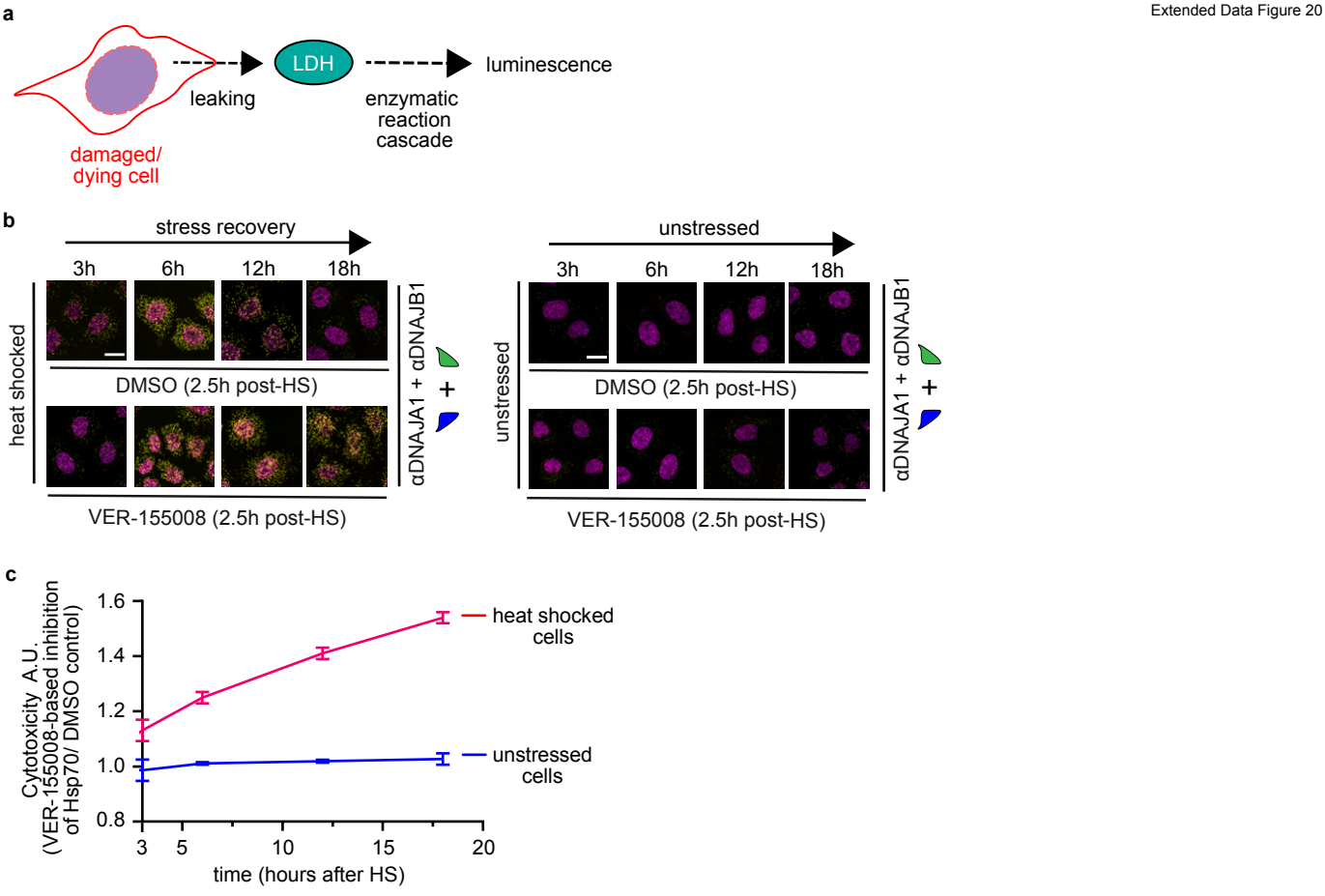
a
LDH
leaking
luminescence
enzymatic reaction cascade
damaged/ dying cell
b
stress recovery
3h
6h
12h
18h
heat shocked
DMSO (2.5h post-HS)
VER-155008 (2.5h post-HS)
αDNAJA1 + αDNAJB1
+
unstressed
c
Cytotoxicity A.U. (VER-155008-based inhibition of Hsp70/ DMSO control)
1.6
1.4
1.2
1.0
0.8
3
5
10
15
20
time (hours after HS)
heat shocked cells
unstressed cells

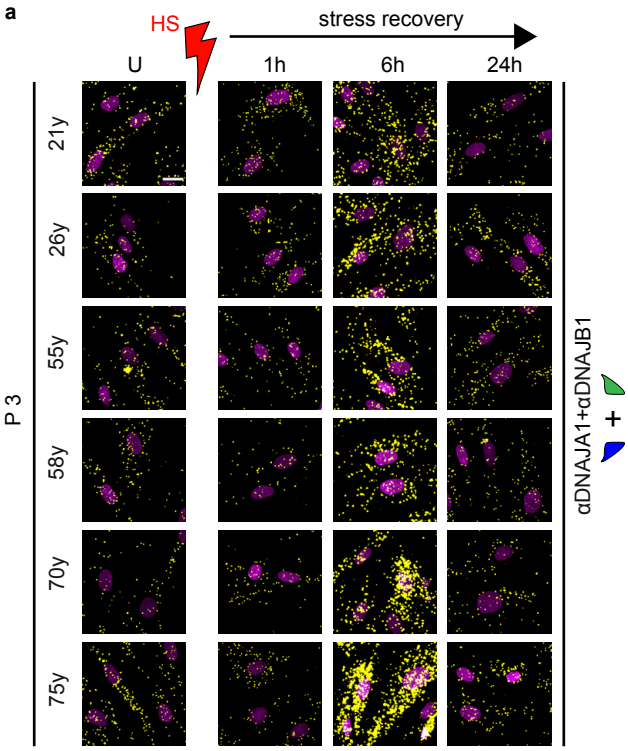
a
HS
stress recovery
U
1h
6h
24h
P 3
21y
26y
55y
58y
70y
75y
αDNAJA1+αDNAJB1

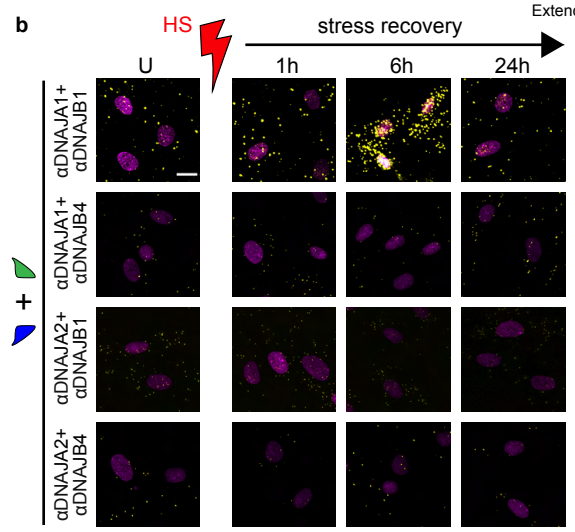
b
HS
stress recovery
U
1h
6h
24h
αDNAJA1+
αDNAJB1
αDNAJA1+
αDNAJB4
αDNAJA2+
αDNAJB1
αDNAJA2+
αDNAJB4

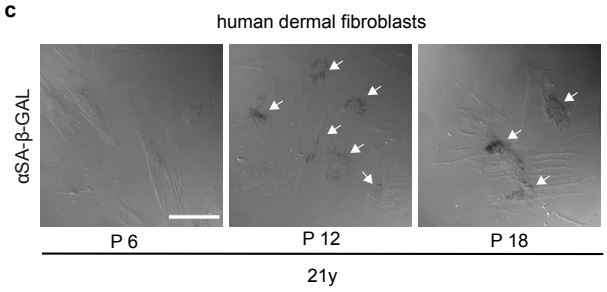
c
human dermal fibroblasts
αSA-β-GAL
P 6
P 12
P 18
21y

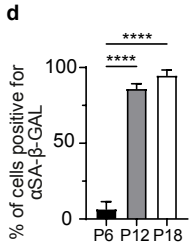
d
% of cells positive for
αSA-β-GAL
100
50
0
****
****
P6
P12
P18

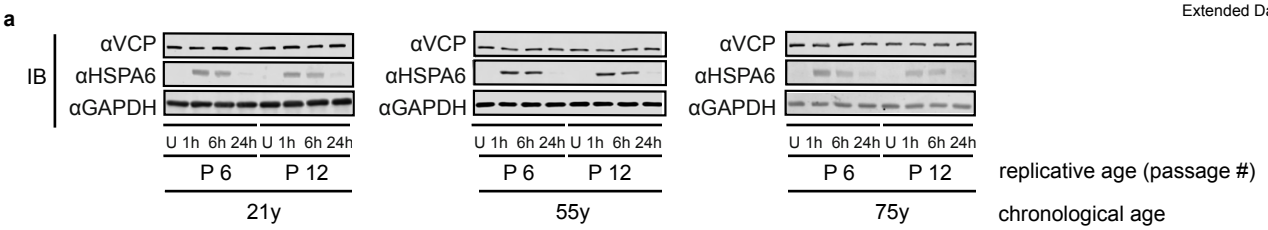
a
IB
αVCP
αHSPA6
αGAPDH
U 1h 6h 24h U 1h 6h 24h
P 6
P 12
21y
55y
75y
replicative age (passage #)
chronological age

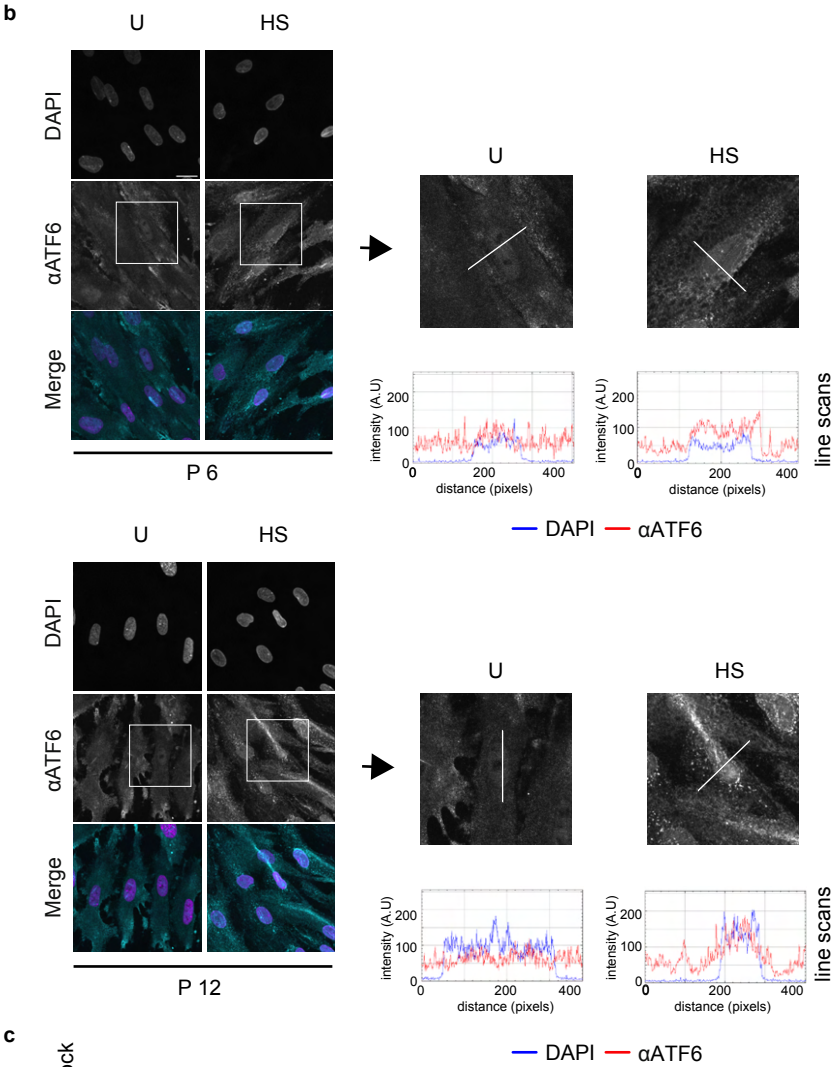
b
U
HS
DAPI
αATF6
Merge
P 6
P 12
intensity (A.U)
distance (pixels)
line scans
DAPI
αATF6

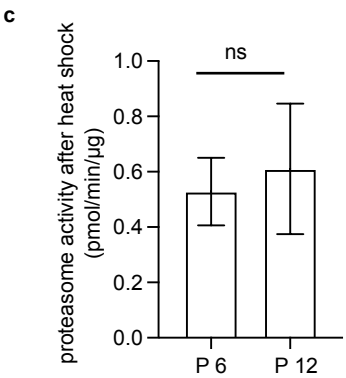
c
ns
proteasome activity after heat shock (pmol/min/µg)
1.0
0.8
0.6
0.4
0.2
0.0
P 6
P 12

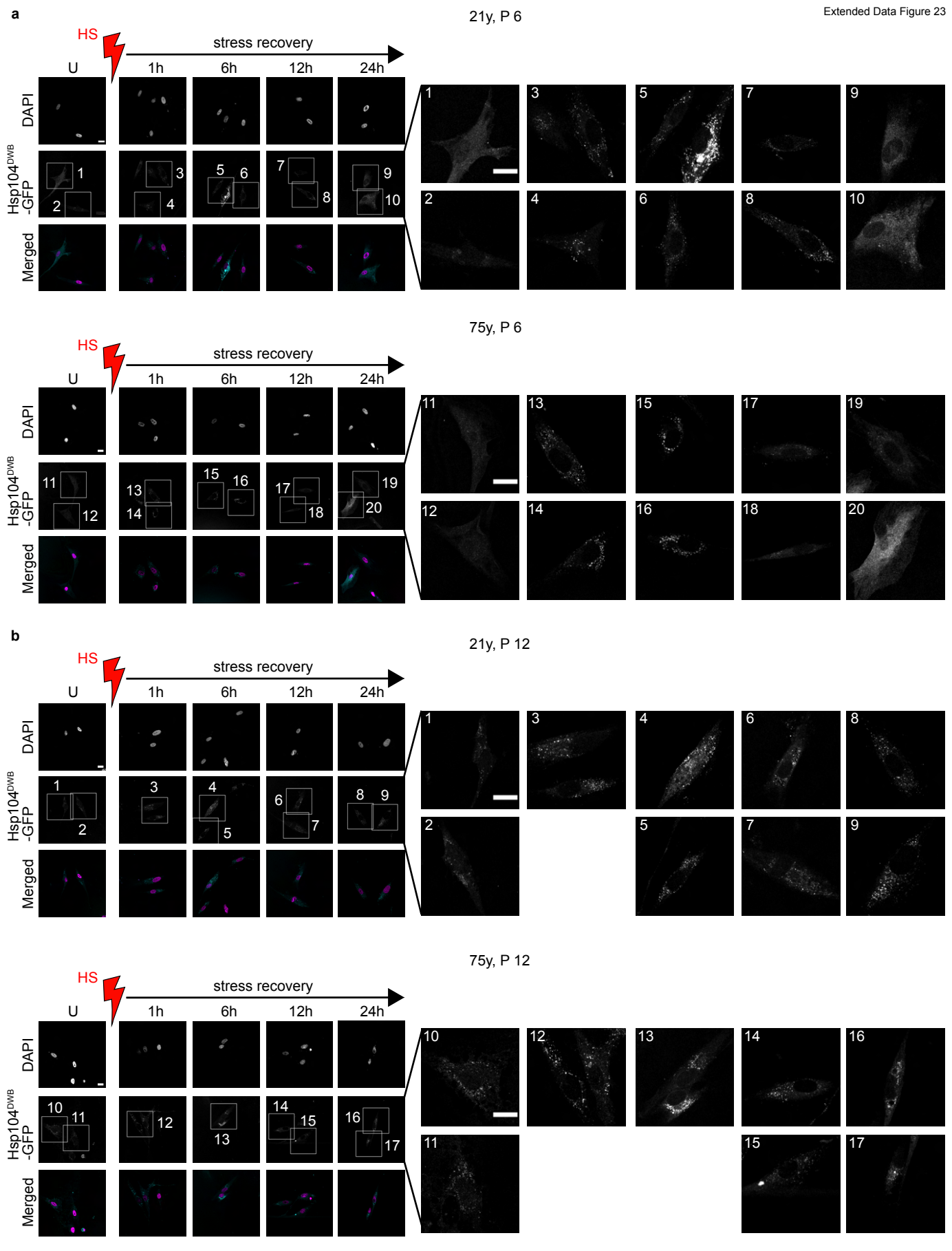
a
21y, P 6
HS
stress recovery
U
1h
6h
12h
24h
DAPI
Hsp104DWB-GFP
Merged
75y, P 6
b
21y, P 12
75y, P 12

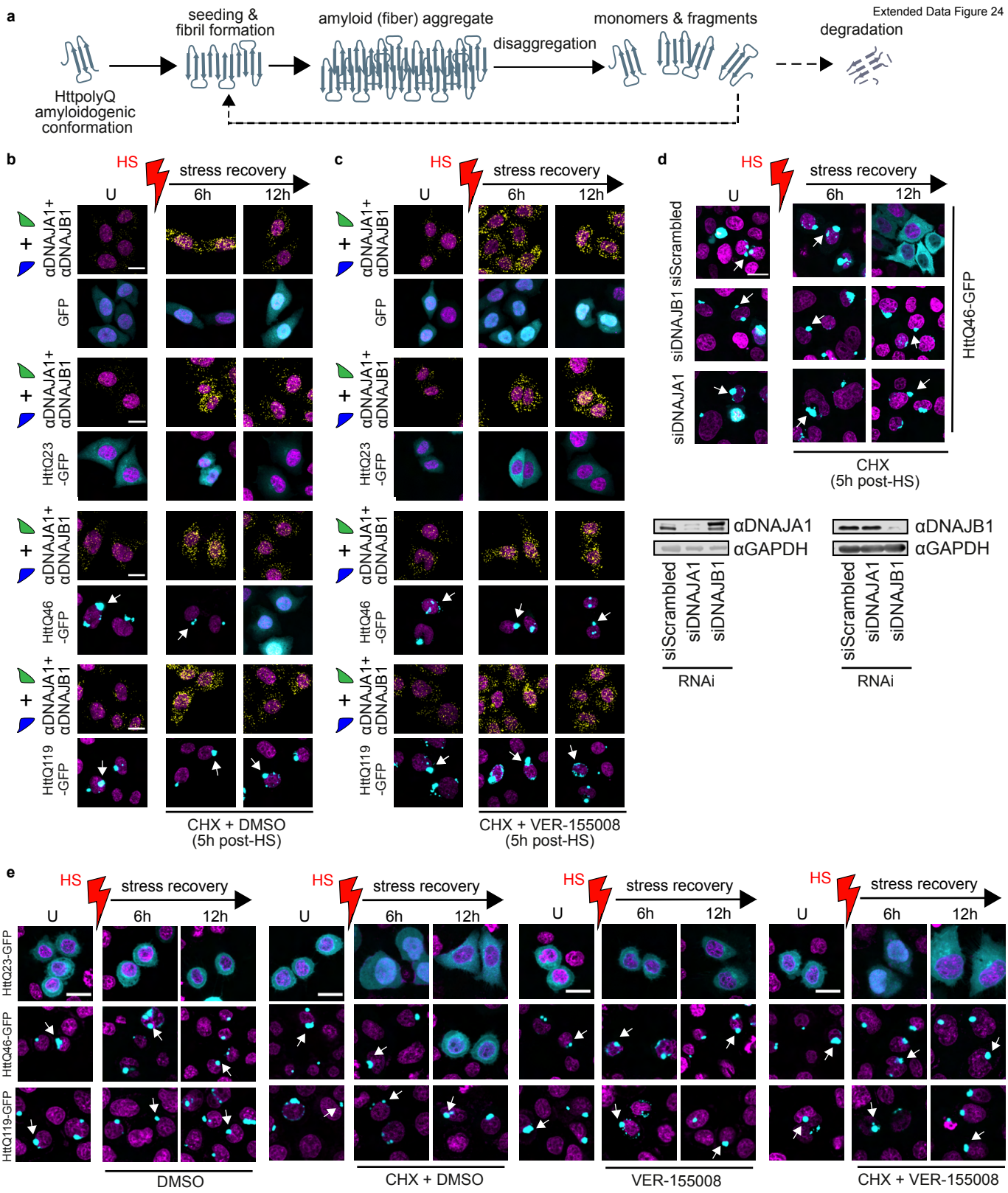
a
seeding & fibril formation
amyloid (fiber) aggregate
disaggregation
monomers & fragments
degradation
HttpolyQ amyloidogenic conformation
b
HS
stress recovery
U
6h
12h
αDNAJA1+ αDNAJB1
GFP
HttQ23 -GFP
HttQ46 -GFP
HttQ119 -GFP
CHX + DMSO (5h post-HS)
c
CHX + VER-155008 (5h post-HS)
d
siScrambled
siDNAJB1
siDNAJA1
HttQ46-GFP
CHX (5h post-HS)
αDNAJA1
αGAPDH
αDNAJB1
RNAi
e
HttQ23-GFP
HttQ46-GFP
HttQ119-GFP
DMSO
CHX + DMSO
VER-155008
CHX + VER-155008